NASA Technical Paper 3132

1992

Comparison of a Two-Dimensional Adaptive-Wall Technique With Analytical Wall Interference Correction Techniques

Raymond E. Mineck
Langley Research Center
Hampton, Virginia

NASA
National Aeronautics and Space Administration
Office of Management
Scientific and Technical Information Program

Summary

Two wind tunnel investigations have been conducted to compare different correction techniques to account for wall interference: adaptive test section walls and classical analytical corrections. A common airfoil model has been tested in the adaptive-wall test section of the NASA Langley 0.3-Meter Transonic Cryogenic Tunnel (0.3-m TCT) and in the ventilated test section of the National Aeronautical Establishment (NAE) Two-Dimensional High Reynolds Number Facility (HRNF). The model has a 9-in. chord and a CAST 10-2/DOA 2 airfoil section. The 0.3-m TCT adaptive-wall test section has four solid walls with flexible top and bottom walls. The ratio of the 0.3-m TCT test section height to the model chord is 1.4. The HRNF has porous top and bottom walls and solid sidewalls. The ratio of the HRNF test section height to the model chord is 6.7. The Mach number for the tests ranged from 0.3 to 0.8 at chord Reynolds numbers of 10×10^6, 15×10^6, and 20×10^6. The angle-of-attack range was from about -2° up to stall.

Wall interference in the test results from the 0.3-m TCT has been accounted for by the movement of the adaptive walls, whereas the results from the HRNF have been corrected for top and bottom wall interference by classical analytical techniques. These results are in good agreement. The comparisons indicate that small residual errors remain in the Mach number and angle of attack. Correcting the results from both tests for the sidewall interference after correcting the results for top and bottom wall interference did not significantly change the agreement. Correcting the results with a unified four-wall correction technique improved the agreement of the results with Navier-Stokes calculations.

Introduction

The artificial constraint of wind tunnel test section walls on the flow field about an airfoil model can introduce errors in the simulation of "free air" conditions. In the past, corrections have been applied to wind tunnel results to account for the presence of the walls. These corrections are relatively simple for tests in closed test sections at low subsonic speeds. However, the corrections become more complex and difficult to apply for tests in ventilated test sections at high subsonic speeds because of difficulties with mathematically modeling and experimentally measuring the flow field at the wall. The high-speed, digital computer has facilitated the development of sophisticated wall correction techniques for tests in ventilated test sections at high subsonic speeds. These techniques often depend on extensive measurements taken on or near the test section boundaries. Several examples of these techniques are presented in reference 1. The high-speed, digital computer has also facilitated the development of adaptive-wall test sections that have the potential of removing the wall interference at its source. Free air results can be approached with a posttest wall correction technique, a real-time adaptive-wall test section technique, or some combination of the two techniques.

The National Aeronautical Establishment (NAE) of Canada and the National Aeronautics and Space Administration (NASA) have a cooperative agreement to develop and validate methods for correcting and/or eliminating wall interference in transonic two-dimensional wind tunnel testing. The NAE uses an analytical wall correction technique for airfoil data from its Two-Dimensional High Reynolds Number Facility (HRNF), whereas NASA uses the adaptive-wall test section technique for airfoil data from the Langley 0.3-Meter Transonic Cryogenic Tunnel (0.3-m TCT). Both organizations desired to validate wall interference correction methods for airfoil data obtained at high subsonic speeds and high Reynolds numbers. To do this, one model was tested in both wind tunnels. The results could then be compared to determine how well they agree with each other.

Under the agreement, the NAE designed and fabricated a CAST 10-2/DOA 2 airfoil model with a 9-in. chord. This airfoil profile was chosen because its aerodynamic characteristics are sensitive to changes in Mach number and Reynolds number. The airfoil model was first tested in the HRNF. The test Mach number ranged from 0.3 to 0.8 at chord Reynolds numbers of $10 \times 10^6, 15 \times 10^6$, and 20×10^6. The angle of attack ranged from about -2° to stall. This facility, described in references 2 and 3, has a 60-in-tall by 15-in-wide test section with perforated top and bottom walls. The ratio of the HRNF test section height to the model chord was 6.7 for this experiment. The relatively large value of this ratio was expected to lead to moderate levels of wall interference. The results from the HRNF tests, presented in reference 4, were corrected for top and bottom wall interference with the method in reference 5.

The same model was subsequently tested in the 0.3-m TCT with the two-dimensional, adaptive-wall test section. Details of the tunnel may be found in reference 6 and a description of the test section may be found in reference 7. The test section is 13 in. tall and 13 in. wide at the entrance. It has four solid walls with flexible top and bottom walls. The ratio of the 0.3-m TCT test section height to

the model chord was 1.4. This small ratio leads to large levels of wall interference unless the flexible walls are properly positioned. The model was tested over the same Mach number and Reynolds number ranges used in the HRNF tests, but the minimum and maximum angles of attack were limited by the wall positioning hardware for some of the test conditions. The test results are presented in reference 8. The top and bottom wall interference was reduced in the 0.3-m TCT results by the movement of the adaptive walls. The wall adaptation technique used for this investigation is described in reference 9.

The purpose of this investigation is to determine how well the results from each tunnel agree with each other and to determine if additional corrections can improve the agreement. The published or baseline results are compared with each other first. Comparisons of the published integrated force and moment coefficients from the 0.3-m TCT and HRNF tests are presented in this report. Additional comparisons of the slopes of the section normal-force curves, the drag rise with Mach number, and the mean and the difference in the pressure coefficient at the quarter-chord are also presented in an attempt to quantify the differences between the baseline results. Three comparisons of the data from both wind tunnels with different corrections applied to the published results are made to determine if the agreement can be improved. These comparisons are limited to the slopes of the section normal-force curves and to the drag rise with Mach number. Comparisons of the chordwise pressure distributions at nearly the same normal-force coefficient and Mach number are presented in a "Supplement to NASA TP-3132." The supplement is available upon request and a request form is included at the back of this paper.

Symbols and Abbreviations

BLC	boundary-layer control
$\overline{C}_{p,25c}$	mean of upper- and lower-surface pressure coefficients at quarter-chord
$C_{p_{te}}$	pressure coefficient at trailing edge
c	model chord, in.
c_d	section drag coefficient, measured on tunnel centerline
c_m	section pitching-moment coefficient
c_n	section normal-force coefficient
c_{n_α}	slope of section normal-force-coefficient curve, deg^{-1}
D	diameter
GN_2	gaseous nitrogen
LN_2	liquid nitrogen
M_∞	free-stream Mach number
NAE	National Aeronautical Establishment
R_c	free-stream Reynolds number based on model chord
TSDE	Transonic small disturbance equation
WIAC	Wall Interference Assessment/Correction
x	chordwise position, measured aft from leading edge, in.
x_s	chordwise position of shock, measured aft from leading edge, in.
y	spanwise position, measured from tunnel centerline, in.
z	normal position, measured from airfoil reference line, in.
α	geometric angle of attack, deg
$\Delta C_{p,25c}$	difference between upper- and lower-surface pressure coefficients at quarter-chord
ΔM_∞	correction to free-stream Mach number because of wall interference
$\Delta\alpha$	correction to angle of attack because of top- and bottom-wall interference, deg

Wind Tunnels

NAE Two-Dimensional High Reynolds Number Facility

The NAE 5-ft by 5-ft Blowdown Wind Tunnel has two interchangeable test sections, one for three-dimensional model testing and the other for two-dimensional model testing. The tunnel was configured as the Two-Dimensional High Reynolds Number Facility (HRNF) for the test results reported herein. Details of the 5-ft by 5-ft Blowdown Wind Tunnel and of the HRNF may be found in references 2 and 3. The tunnel with the two-dimensional test section typically operates at stagnation pressures up to about 10 atm and at stagnation temperatures near room temperature. The test section Mach number can be varied from about 0.10 to 0.95. These test conditions provide a test envelope of chord Reynolds numbers up to 50×10^6 based on a model chord of 12 in. A sketch of the two-dimensional test section is presented in figure 1. The test section is 15 in. wide and 60 in. high at the entrance and is 141 in. long. The sidewalls are solid and parallel. The top and bottom walls are porous and parallel. The porous walls

are covered with a 30-mesh, 40-percent open screen to reduce the edge-tone noise. The resulting overall porosity of the top and bottom walls is 8.4 percent. The static pressures near the top and bottom walls are measured with a 1-in-diameter static pipe located on the centerline of each porous wall. There are 40 pressure orifices extending from 80.9 in. upstream to 47.1 in. downstream of the model center of rotation. The center of rotation is located on the centerline (30 in. from the floor) and 94 in. downstream of the start of the test section. The model is mounted on a turntable within an 18- by 24-in. porous panel covered with a woven wire sheet. The porous panel is connected to a suction box to control the boundary layer in the vicinity of the model. The level of suction is moderate. It is not intended to remove the boundary layer completely but to control the adverse growth of the boundary layer from the pressure distribution imposed on the sidewall by the model and to prevent premature separation of the boundary layer in regions of adverse pressure gradient. For these tests, the normal velocity because of suction at the sheet, nondimensionalized by the free-stream velocity, was nominally 0.0085.

The model was positioned on the turntable with the center of rotation 4 in. aft of the model leading edge. A total head probe rake was mounted 21 in. downstream of the center of the turntable. For the 9-in-chord airfoil used in this investigation, this location corresponds to 1.78 chords downstream of the trailing edge. The drag data reported herein were computed using the measurements from the total head probe on the tunnel centerline and from the test section free-stream static pressure. The wake rake was automatically controlled to traverse completely through the wake. The spacing of the rake steps was reduced for those parts of the wake in which the total pressure gradient was large.

The flow angularity in the HRNF is very small. Measurements taken before the latest improvements to the facility indicate that there is a slight downwash up to about 0.05°. The current flow angularity after the modifications has not been measured, but it is expected to be smaller. No correction to the angle of attack for test section flow angularity has been applied to the results.

NASA Langley 0.3-Meter Transonic Cryogenic Tunnel

The Langley 0.3-m TCT with the 13- by 13-in. two-dimensional adaptive-wall test section installed in the circuit was used for the NASA tests. A sketch of the tunnel is presented in figure 2 and a photograph of the upper leg of the tunnel circuit is presented in figure 3. The 0.3-m TCT is a fan-driven, cryogenic pressure tunnel that uses nitrogen as a test gas. It is capable of operating at stagnation temperatures from 80 to 327 K and at stagnation pressures from 1.2 to 6.0 atm. The fan speed is variable so that the empty test section Mach number can be varied from about 0.20 to 0.95. This combination of test conditions provides a test envelope of chord Reynolds numbers up to about 100×10^6 based on a model chord of 12 in. Additional details of the tunnel may be found in reference 6.

A sketch of the adaptive-wall test section with the test section plenum sidewall removed is presented in figure 4. The test section is 13 in. tall by 13 in. wide at the entrance. All four walls are solid. The sidewalls are rigid and parallel, whereas the top and bottom walls are flexible and movable. The usable portion of the test section is 55.8 in. long. The flexible walls are anchored at the upstream end. The shape of each wall is determined by 21 independent jacks. Pressure orifices are located at each jack position on each flexible wall centerline. The model is supported between two turntables centered 30.7 in. downstream of the test section entrance. Although the tunnel has provisions for a sidewall boundary-layer control system, the system was not used for these tests. Additional details of the test section may be found in reference 7.

The model was positioned on the turntable with the center of rotation 4 in. aft of the model leading edge, the same location relative to the turntable used in the HRNF tests. A total head probe rake was installed at 17.5 in. downstream of the center of the turntables. This location was 1.2 chords downstream of the model trailing edge. The drag data reported herein were computed with the measurements from the total head probe on the tunnel centerline and the average of eight static pressures on the test section sidewall opposite the rake tubes. No traditional model upright and inverted tests of flow angularity and no empty test section tests with a flow angularity probe have been conducted. No corrections to the angle of attack for flow angularity were made.

Model

The model used in these tests had a 9-in. chord and a CAST 10-2/DOA 2 airfoil section. This early supercritical airfoil section is nominally 12 percent thick and has a design lift coefficient of about 0.6 at a Mach number of 0.765. The design and the measured model ordinates are presented in table 1. A sketch of the airfoil shape is presented in figure 5. A photograph of the model prior to installation in the 0.3-m TCT is presented in figure 6. The model had a

15-in. span to fit the HRNF test section. Because the 0.3-m TCT test section is 13 in. wide, the outer 1 in. on each end of the model extended into the model mounting blocks. With this arrangement, the model centerline and the test section centerline coincided. The model chord was defined as the line passing through the center of the leading and trailing edges. This line was rotated 0.88° nose up relative to the reference line used to define the airfoil shape. For these tests, the angle of attack was referenced to the model chord line, not the airfoil reference line.

The model had 45 static pressure orifices in a chordwise row on the upper surface and 23 in a chordwise row on the lower surface. A sketch of the orifice layout is presented in figure 5. The orifices were staggered about the model centerline to minimize interference on the neighboring orifices. The orifice diameter was 0.014 in. for all orifices except those on the forward 22 percent of the airfoil chord, where the diameter was 0.010 in. The smaller diameter orifices would reduce any orifice size effects where the pressure gradients could be large.

Test Program

The test conditions were selected to emphasize the high subsonic Mach numbers and the high Reynolds numbers possible in the two facilities. The test conditions are listed in table 2. The primary goal of the tests was to compare wall interference correction techniques. Previous tests (ref. 10) of a CAST 10-2/DOA 2 airfoil section in the ONERA T2 adaptive-wall tunnel in Toulouse, France, indicate that the shock location differs significantly for fixed and free boundary-layer transition at a chord Reynolds number of 13×10^6. At the Reynolds numbers planned for these tests, the tunnel turbulence levels would influence the boundary-layer characteristics and the shock location. Since the primary purpose of these tests was to evaluate two different techniques to treat wall interference utilizing two different wind tunnels, it was desirable to remove the effect of test section turbulence on boundary-layer transition and shock location. Therefore, both tests were conducted with transition strips placed on both surfaces of the model. The grit size was determined from the method presented in reference 11 for a Reynolds number of 10×10^6. Carborundum grit no. 320 with an average grit size of 0.0011 in. was used for both tests. The transition strip was located at the 5-percent-chord location and was nominally 0.1 in. wide.

The model was tested at Mach numbers from 0.3 to 0.8 at chord Reynolds numbers of 10×10^6, 15×10^6, and 20×10^6. The angle of attack was varied from about $-2°$ through the stall angle. Limitations of the wall positioning hardware of the 0.3-m TCT prevented successful wall adaptation at some test conditions so that data could not be acquired to match the HRNF results. Initially, the angle of attack for tests in the 0.3-m TCT used the same angle of attack measured in the HRNF tests. The measured section normal-force coefficients were slightly different. Subsequently, the angles of attack chosen for the 0.3-m TCT tests were selected to obtain data at nearly the same normal-force coefficients obtained in the HRNF tests.

Wall Adaptation Technique for 0.3-m TCT Tests

Proper movement of the adaptive walls reduced interference effects of the top and bottom walls in the results from the 0.3-m TCT tests. The wall adaptation technique of Wolf and Goodyer, described in reference 9, was used for these tests. This technique positions the top and bottom walls along free air streamlines so that they do not interfere with the flow about the model. To accomplish this, the flow field is represented by two regions: a "real" flow field inside a control surface and an exterior (the term "imaginary" is used in ref. 9) flow field extending from the control surface to infinity. The control surface is the physical wall position that is adjusted for the displacement thickness of the boundary layer. The control surface is a streamline if two independent flow-field parameters are matched there. The wind tunnel produces the real flow field. The wall position and the wall pressures are measured to determine the real flow-field velocity magnitude and direction at the control surface. Potential flow theory is used to produce the exterior flow field. The flow at the wall is assumed to be irrotational and inviscid so potential flow theory with linearized compressibility effects can be used. The boundary condition for the potential flow solution is the measured wall position. The difference between the measured and the computed flow magnitudes is used to compute several wall streamlining criteria. If all the criteria are satisfied, the wall shape is considered to be a streamline. If they are not, the velocity differences along the boundary are used to predict a new wall position for another iteration.

Analytical Wall Interference Corrections

Several different techniques have been used to correct the results from the two wind tunnel tests for wall interference. Three types of corrections were applied to the HRNF results. The first technique corrected the measured (uncorrected) results for top- and bottom-wall interference. These corrected results are referred to as the HRNF baseline results.

The second technique corrected the HRNF baseline results for sidewall interference. These results are referred to as the HRNF four-wall corrected results. The third technique corrected the HRNF measured (uncorrected) results for interference from all four walls with a unified approach. These results are referred to as the HRNF unified four-wall corrected results.

Similarly, three types of corrections were applied to the 0.3-m TCT results. The 0.3-m TCT measured results had no analytical corrections and are referred to as the TCT baseline results. The first technique applied to the data should account for any residual top- and bottom-wall interference. The technique used was different from that used on the HRNF results because the HRNF technique was not designed to treat nonplanar boundary measurements. These results are referred to as the TCT two-wall corrected results. The second and third correction techniques used for the 0.3-m TCT results were the same as those used for the HRNF tests. These results are referred to accordingly as the TCT four-wall and the TCT unified four-wall corrected results.

The identification of the different data sets is summarized in chart 1. A short description of each correction technique is presented in subsequent sections of this paper.

Two-Wall Analytical Correction Technique for HRNF Tests

The results from the HRNF tests were corrected for the interference from the top and bottom walls with the analytical technique of Mokry and Ohman. Details of the technique may be found in reference 5. The correction technique assumes that the flow field near the test section boundaries can be represented by potential flow theory with linearized (Prandtl-Glauert) compressibility effects. A rectangular control surface is defined with the corners coincident with the most upstream and downstream pressure orifices on the top- and bottom-wall static pipes. The streamwise disturbance velocity induced by the walls satisfies the Laplace equation within the control surface. The streamwise disturbance velocity on the control surface can be determined from the pressure distribution on the control surface, the model lift, and the model thickness. Since there are no measured pressures on the upstream and downstream faces of the control surface, the pressures there are determined by linear interpolation. The Laplace equation and wall-induced disturbance velocities on the control surface form a Dirichlet problem that can be solved by the Fourier method. The solution provides the wall-induced streamwise and normal velocities at any point within the control surface. The correction to the angle of attack is computed from the wall-induced normal velocity at the model quarter-chord. The correction to the Mach number is computed from the wall-induced streamwise velocity at the model quarter-chord. The corrections computed for this test for three Mach numbers are presented in figure 7(a). The magnitude of the correction to the angle of attack increases with normal-force coefficient, as expected. The correction to the Mach number is dependent on both the Mach number and the normal-force coefficient.

Chart 1

Identification	Description
TCT baseline	Published results from TCT with wall interference accounted for by movement of the adaptive walls; no analytical corrections.
HRNF baseline	Published results from the HRNF with corrections for top- and bottom-wall interference from the method of reference 5.
TCT two wall	Results from TCT with analytical corrections for top- and bottom-wall interference from the method of reference 12.
TCT four wall	Results from TCT with analytical corrections for top- and bottom-wall interference from the method of reference 12 followed by corrections for sidewall interference from the method of reference 13.
HRNF four wall	Published results from the HRNF with corrections for sidewall interference from the method of reference 13.
TCT unified four wall	Published results from TCT with corrections for all four walls applied from the method of reference 14.
HRNF unified four wall	Uncorrected results from the HRNF with corrections for all four walls applied from the method of reference 14.

Two-Wall Analytical Correction Technique for 0.3-m TCT Tests

For an adaptive-wall test section, the finite test section length, the sidewall boundary layer, and the

imperfections in the wall shape can lead to residual interference effects. The residual interference from the top and bottom walls for the 0.3-m TCT tests was computed by applying Cauchy's integral formula to a closed contour. Details of the implementation are described in reference 12. Potential flow theory with linearized compressibility is used to represent the flow field. The contour used for the integration is defined by the upper and lower walls and the entrance and exit of the test section. The normal and streamwise disturbance velocities on the top and bottom surfaces of the contour are determined from the measured wall shape and pressures. The disturbance velocities on the entrance and exit of the test section are determined by linear interpolation. The normal and streamwise disturbance velocities are treated as a complex disturbance velocity. The complex disturbance velocity is divided into model and wall components. The wall component of the complex disturbance velocity can be determined at an arbitrary point within the contour by integrating around the contour. The wall component of the complex disturbance velocity at the model quarter-chord is used to determine the corrections to the angle of attack and Mach number. A sample of the corrections to the Mach number and angle of attack for the top- and bottom-wall interference is presented in figure 7(b). The residual correction to the angle of attack is generally less than 0.05°; the residual correction to the Mach number is generally below 0.002 for most of the data points. The angle of attack and Mach number residual corrections do not vary smoothly with normal-force coefficient because they depend primarily on the top- and bottom-wall shapes, which are determined by the iterative wall adaptation process.

Sequentially Determined Sidewall Interference Corrections

Residual interference remains in both sets of results from the change in blockage caused by the change in the sidewall boundary-layer thickness. The method of Murthy, described in reference 13, was used to compute the corrections for the test section sidewalls. The Murthy correction is an extension of the Barnwell-Sewall sidewall correction of reference 15. The extension replaces the linear variation of cross-flow velocity with a nonlinear variation. The cross-flow velocity between the sidewall and the test section centerline is represented by the flow between a wavy wall and a straight wall. With this flow model, the correction to the Mach number can be determined from the undisturbed sidewall boundary-layer characteristics, the test section Mach number, and the airfoil model aspect ratio. The correction to the Mach number for each of the tests is presented in figure 8.

The sidewall correction was applied to the data after corrections for the top and bottom walls were applied. This application of the full sidewall correction implies that the pressure measured at the top and bottom walls did not contain a component from the change in the sidewall boundary-layer displacement thickness. The change in blockage from the sidewall boundary layer near the model should not have been sensed at the top and bottom walls for the HRNF tests because of the large ratio of semiheight to semiwidth of the HRNF test section (4.0). It is possible that the change in blockage from the sidewall boundary layer would have been partly sensed at the top and bottom walls for the 0.3-m TCT tests because of the much smaller ratio of semiheight to semiwidth of the 0.3-m TCT test section (1.0). Because the part of the sidewall correction removed by the adaptive walls is not known or easily computed, the full correction is computed and applied.

Unified Four-Wall Interference Correction Technique

A unified, posttest wall interference assessment/correction (WIAC) procedure for transonic conditions has been developed to account for interference from the top and bottom walls as well as from the sidewalls. The WIAC procedure can treat either adaptive-solid or porous-planar top and bottom walls, so it can be used on both the 0.3-m TCT and the HRNF test results. Details about the procedure and its use can be found in references 14, 16, and 17. The WIAC procedure simulates the flow field with a two-dimensional transonic small disturbance equation (TSDE) and has several options to account approximately for the interference from the sidewall boundary layers. For these tests, the Murthy sidewall boundary-layer approximation is used. The WIAC procedure involves a global iteration, each pass of which involves three solutions to the TSDE. First, the tunnel geometry is modeled and the Mach number is adjusted according to the Murthy sidewall boundary-layer approximation while the TSDE is solved in an inverse fashion with measured model and wall pressures used as boundary conditions. This solution deduces an effective inviscid body shape that approximates the model and all viscous effects (including separation and shock interaction with the boundary layers) on the model and all four tunnel walls. Also required for this solution is an estimate of the upwash angle at the inflow face, which is assumed to be measured in the tunnel. The second TSDE solution uses the effective inviscid body shape

from the first step as the inner boundary condition, while the outer free air boundary condition varies as the Mach number and the angle of attack are perturbed from the measured conditions. This solution determines the free-stream Mach number and angle of attack for which the calculated free air pressure coefficient distribution of the effective inviscid body best matches the measured pressure coefficient distribution on the model. The third TSDE solution uses the free-stream conditions determined from the second step (Mach number and angle of attack) and a source-sink-doublet representation of the effective inviscid body shape from the first step for the model boundary conditions. This solution, together with the first solution, allows the "classical-like" interference field to be determined. When the upflow angle at the inflow face is not measured, as was the case in the current tests, up to three global iterations or passes of this procedure are required to deduce the velocity distribution across the front boundary face of the test section and to properly align the effective inviscid body with the tested model.

Presentation of Results

The section normal-force coefficients presented were obtained from the integration of the chordwise pressure distribution on the model. The section drag coefficients were determined from the integration of the model wake pressure distribution on the test section centerline. The reference line used to define an angle of attack of 0° passed through the center of the leading edge and trailing edge. A comparison of the results obtained on the CAST 10-2/DOA 2 airfoil model in the HRNF and the 0.3-m TCT is presented as follows:

Discussion of Results

The results from the two wind tunnels are compared to see how well they agree with each other. Both sets of baseline results contain residual interference from different sources, such as the test section sidewalls. Different comparisons are used to estimate the changes in angle of attack and Mach number needed to improve the agreement. The HRNF results, measured in a relatively large test section, were selected as the reference set when describing changes in angle of attack or Mach number needed to improve the agreement. This does not imply that the 0.3-m TCT results have residual errors and the HRNF results do not.

Comparison of 0.3-m TCT and HRNF Baseline Results

The baseline results from the two wind tunnel tests are compared first. No corrections for the effect of flow angularity or for the interference from the sidewall boundary layer have been applied to the results. The comparison of the integrated force and moment coefficients from the two tests is presented in figures 9 to 11. The normal-force curves exhibit the expected behavior. At low normal-force coefficients, the curves are linear. At the higher Mach numbers, the slope begins to increase at small positive angles of attack. The angle of zero normal force, determined from the fairings, is generally about 0.06° more negative for the 0.3-m TCT tests. This difference may be attributable to errors in setting the model to 0° during installation, to residual wall interference, or to flow angularity. The maximum normal-force coefficient is generally greater for the 0.3-m TCT tests than for the HRNF tests for those test conditions at which a comparison is possible. The drag coefficient at a given normal-force coefficient is generally less for the 0.3-m TCT tests than for the HRNF tests.

The slopes of the fairings of the section normal-force curves have been measured at two section normal-force coefficients: 0.2 and 0.4. Whenever possible, the slope of the fairings was determined with a linear least-squares curve fit. However, when the experimental data did not follow a straight line, the slope of the curve was determined from a quadratic least-squares curve fit. For some extreme cases, the quadratic curve fit failed to adequately represent the results, so the slope was determined manually from the fairing of the curve. The section normal-force curve slopes are presented in figure 12 as a function of Mach number. The slopes are similar at the lower Mach numbers. At the higher Mach numbers, the 0.3-m TCT values are generally larger. Both sets of results show the dramatic loss in the section normal-force curve slope at a Mach number near 0.78.

The section drag coefficient at constant values of section normal-force coefficient has also been determined from the fairings of the integrated force coefficient data. The results are plotted in figure 13. As noted previously, the drag is slightly less at a given Mach number and normal-force coefficient in the 0.3-m TCT. The difference is about four counts (0.0004) and is relatively constant up to the beginning of the drag rise. The only other significant difference is for Mach numbers near the drag rise. The drag-rise Mach number was defined as that point on the fairing at which the slope dc_d/dM_∞ was 0.1. The drag-rise Mach number at $R_c = 10 \times 10^6$ was difficult to determine because of the oscillations in the fairings and appears to be slightly higher for the 0.3-m TCT tests. At $R_c = 15 \times 10^6$, the drag-rise Mach number for the 0.3-m TCT results is about 0.010 higher than that determined for the HRNF results and, at $R_c = 20 \times 10^6$, the drag-rise Mach number for the 0.3-m TCT results is about 0.003 higher than that for the HRNF results.

The chordwise pressure distributions often provide information that is masked by the integration used to determine the force coefficients. The test procedures used for the 0.3-m TCT tests attempted to duplicate the normal-force coefficients from the HRNF tests. Comparisons of the chordwise pressure distributions on the model at nearly the same Mach number and normal-force coefficient are presented in the supplement. Examination of these results indicated that they are in reasonable agreement but that there are some subtle differences. The pressure coefficients on the lower surface from the 0.3-m TCT tests are generally more positive (less negative) than those from the HRNF tests. Also, the upper-surface shock locations are slightly different. The small differences in the normal-force coefficient and the Mach number make it difficult to isolate the effects of Mach number and angle of attack. The upper- and lower-surface pressure coefficients at the quarter-chord are used to separate the effects of Mach number and angle of attack. The difference between the upper- and lower-surface pressure coefficients at a chordwise station is primarily dependent on the angle of attack. The mean of the upper- and lower-surface pressure coefficients at a chordwise station is primarily dependent on the Mach number. The differential and mean pressure coefficients at the quarter-chord are used to identify differences in the Mach number and the angle of attack.

The difference in the upper- and lower-surface pressure coefficients at the quarter-chord was determined directly from the measured pressure distributions and the results are presented in figure 14. The differential pressure coefficient increases with angle of attack. The 0.3-m TCT results are generally more positive than the HRNF results at a given angle of attack. The spacing between the two lines increases with angle of attack. This is consistent with the higher normal-force curve slopes measured in the 0.3-m TCT tests. The 0.3-m TCT and HRNF results have been compared at an angle of attack of 0°. Except for the results at a Mach number of 0.73, the agreement would be improved if the angle of attack for the 0.3-m TCT results was increased by about 0.12°.

The mean pressure coefficient at the quarter-chord was determined directly from the measured pressure distribution and the results are presented in figure 15. The mean pressure coefficient takes on a moderate negative value ($\overline{C}_{p,25c} \approx -0.4$) when there is no shock present on the upper surface (lower angles of attack) and a more negative value when there is a shock (higher angles of attack). The 0.3-m TCT results are generally less negative than the HRNF results when there is no shock on the upper surface and more negative than the HRNF results when there is a shock. The analysis of the differential pressure coefficient results suggested a difference of 0.12° in the angle of attack. These mean pressure coefficients have been replotted in figure 16 after shifting the 0.3-m TCT angle of attack 0.12°. This shift improves the agreement at the higher angles of attack, but there is still a small difference at the lower angles of attack. Since the shift was estimated from the results at an angle of attack of 0°, the results have been cross plotted at that angle in figure 17. The cross plot shows that at a constant value of $\overline{C}_{p,25c}$, the 0.3-m TCT Mach number is about 0.007 larger.

The trailing-edge pressure coefficient is a good indicator of separation over the rear portion of the airfoil. These results are presented in figure 18. As expected, before separation, the flow attempts to stagnate at the trailing edge, hence the positive pressure coefficients. As the flow begins to separate from the aft portion of the airfoil, the pressure coefficient decreases. The results are in reasonable agreement with each other, although there are insufficient measurements near stall to determine the angle of attack at which separation begins.

The shock location cannot be determined directly from the pressure measurements because of the smearing of the pressure rise and the spacing of the pressure orifices. The shock location was defined as the chordwise position where the pressure was at the midpoint of the pressure rise across the shock. The results are presented in figure 19. At Mach numbers below 0.765, the shock first appears on the forward part of the airfoil and moves aft with increasing section normal-force coefficient. At a Mach number of 0.765, the shock first appears on the aft portion of the airfoil. As the normal force increases, a second shock similar to that found at the lower Mach numbers appears on the forward portion of the airfoil. At Mach numbers above 0.765, only the shock on the rear portion of the airfoil appears. The shock location from the 0.3-m TCT tests is generally forward of the shock location from the HRNF tests. These results are cross plotted in figure 20 at $c_n = 0.6$. The cross plot indicates that the Mach number for the same shock location is generally higher for the 0.3-m TCT tests. For shock locations aft of $x/c = 0.30$, the Mach number for a given shock location is about 0.004 higher for the 0.3-m TCT test results.

Comparison of 0.3-m TCT Two-Wall Corrected and HRNF Baseline Results

The results from the 0.3-m TCT tests have been corrected for any residual interference from the top and bottom walls with the method described in reference 12. The corrections to the angle of attack were small. Results at $R_c = 10 \times 10^6$ are presented since they cover a wider range of Mach numbers. The slopes of the normal-force curves, presented in figure 21, were determined with the same method used for the baseline results. The agreement of the 0.3-TCT two-wall corrected results with the HRNF baseline results is not as good as the agreement of the 0.3-m TCT baseline results with the HRNF baseline results. (See fig. 12(a).) At $c_n = 0.4$, the two-wall correction drove the normal-force curve slopes apart at Mach numbers of 0.50 and 0.70. The variation of the drag rise with Mach number is presented in figure 22. The correction to the drag is less than one count (0.0001) and the correction to the Mach number is less than 0.003. These corrections have very little effect on the drag correlation.

Comparison of 0.3-m TCT and HRNF Four-Wall Corrected Results

The results from both tests contain residual interference from the test section sidewalls. The 0.3-m TCT two-wall corrected and the HRNF baseline results have then been corrected for the interference from the test section sidewalls with the method of Murthy, described in reference 13. The normal-force curve slopes and the drag have been determined in the same manner used for the two-wall corrected results and have been plotted against the corrected Mach number. The slopes of the corrected normal-force curves are presented in figure 23. The sidewall corrections, shown in figure 8, are larger for the HRNF than for the TCT. The results from both tests are shifted to a lower Mach number and the slope is increased by the correction to the dynamic pressure. The correlation of the four-wall corrected results is slightly poorer than that of the baseline results. Since the correction was applied to the 0.3-m TCT two-wall corrected results, the same difference at Mach numbers of 0.50 and 0.70 occurs. The corrected drag rise is presented in figure 24. The sidewall correction shifted both curves to a lower Mach number and a slightly higher drag. Again, the correlation of the four-wall corrected results is slightly poorer than that of the baseline results. Applying only part of the 0.3-m TCT sidewall correction, because of partial correction from the adaptation of the top and bottom walls, would only further increase the difference between the curves.

Comparison of 0.3-m TCT and HRNF Unified Four-Wall Corrected Results

Different correction techniques have been applied to the 0.3-m TCT and the HRNF results. A common correction technique that can treat either a porous wall or a nonplanar solid-wall boundary was selected to correct the 0.3-m TCT baseline results and the HRNF uncorrected results. The technique accounts for the interference from both the top and bottom walls and the sidewalls. A set of uncorrected results at the same nominal Mach number was input into the correction technique. The uncorrected Mach number of the uncorrected set of results seldom deviated from the average Mach number of the set by more than 0.002. The corrected Mach number typically deviated up to 0.005 from the average, with several values differing by more than 0.010. The scatter made

it more difficult to determine the section normal-force curve slopes and the drag rise with Mach number. The corrected normal-force curve slopes are presented in figure 25 and the corrected drag rise with Mach number is presented in figure 26. The agreement of the drag level and the drag-rise Mach number is slightly better for the corrected results than for the baseline results. The value of the normal-force curve slope is significantly larger for both sets of the corrected results. The section normal-force curve slopes are in good agreement except at the highest Mach numbers at a section normal-force coefficient of 0.4. The baseline results are in good agreement with each other and the corrected results are in good agreement with each other. However, the corrected results are not in good agreement with the baseline results. From the information provided, it is not known if the unified four-wall corrected results or the baseline results are closer to the ideal, free air results.

Navier-Stokes calculations for the CAST 10-2/DOA 2 airfoil can provide a third set of results to compare with the baseline and unified four-wall corrected results. The Navier-Stokes solver that was used for these calculations was developed by Swanson and Turkel (ref. 18). The algorithm uses a modified, five-stage Runge-Kutta scheme to advance the solution in time to a steady state. Artificial dissipation terms are added to the difference equations to allow shock capturing without oscillations. The computations were performed on a C-grid with 320 streamwise points and 64 normal points, with a normal mesh spacing at the surface of 1×10^{-5} chord. Results from the Navier-Stokes calculations are compared with the baseline and with the unified four-wall corrected results in reference 19 for several Mach numbers. A sample of the comparisons at a Mach number of 0.75 is presented in figure 27. The Navier-Stokes computed results agree better with the corrected results than with the baseline results. Since the corrected results agree better with the Navier-Stokes calculations, the corrected results are probably closer to free air results than the baseline results are.

Concluding Remarks

A two-dimensional airfoil model has been tested in the adaptive-wall test section of the NASA Langley 0.3-Meter Transonic Cryogenic Tunnel (0.3-m TCT) and in the National Aeronautical Establishment (NAE) Two-Dimensional High Reynolds Number Facility (HRNF). The model has a 9-in. chord and a CAST 10-2/DOA 2 airfoil section. The primary goal of the tests was to compare different techniques to account for wall interference: adaptive test section walls and classical analytical corrections. The test results have been corrected with several different techniques. These studies indicated the following:

1. The baseline results from the two tests corrected with the standard techniques used at each tunnel were in good agreement. Both the adaptive-wall and the analytical correction techniques do an adequate job correcting for the top- and bottom-wall interference.

2. The 0.3-m TCT baseline results generally had a larger normal-force curve slope, a more negative angle of zero lift, a larger maximum normal-force coefficient, and a lower drag coefficient at a constant normal-force coefficient compared with the HRNF results. The shock location on the upper surface was more forward for the 0.3-m TCT tests than for the HRNF tests.

3. An analysis of the baseline results indicates that there was a residual error in the Mach number and angle of attack. If the HRNF results were treated as the baseline, then the drag rise, the mean pressure coefficient at the quarter-chord, and the upper-surface shock location indicated that the agreement would have been improved if the 0.3-m TCT Mach number was reduced between 0.003 to 0.010. The differential pressure coefficient data and the angle of zero lift indicated that the 0.3-m TCT angle of attack should have been increased between 0.06° and 0.12°.

4. Correcting the 0.3-m TCT results for residual top- and bottom-wall interference did not improve the correlation of the normal-force curve slopes and the drag rise.

5. Correcting the results from both tunnels for side-wall interference in a sequential mode did not improve the correlation.

6. Correcting the results from both tunnels for all four walls in a unified mode improved the correlation of the experimental results with Navier-Stokes calculations.

NASA Langley Research Center
Hampton, VA 23665-5225
January 23, 1992

References

1. Mokry, M.; Chan, Y. Y.; and Jones, D. J.: *Two-Dimensional Wind Tunnel Wall Interference.* AGARD-AG-281, Nov. 1983. (Available from DTIC as AD A138 964.)

2. Brown, D., ed.: *Information for Users of the National Research Council's 5-Foot × 5-Foot Blowdown Wind Tunnel at the National Aeronautical Establishment,* Third ed. LTR-HA-6, National Aeronautical Establ., National Research Council of Canada, Sept. 1977.

3. Ohman, L. H., ed.: *The NAE High Reynolds Number 15 In. × 60 In. Two-Dimensional Test Facility. Part 1. General Information.* LTR-HA-4-PT-1, National Aeronautical Establ., National Research Council of Canada, Apr. 1970.

4. Chan, Y. Y.: *Wind Tunnel Investigation of CAST-10-2/DOA-2 12% Supercritical Airfoil Model.* LTR-HA-5x5/0162, National Aeronautical Establ., National Research Council of Canada, May 1986.

5. Mokry, M.; and Ohman, L. H.: Application of Fast Fourier Transform to Two-Dimensional Wind Tunnel Wall Interference. *J. Aircr.*, vol. 17, no. 6, June 1980, pp. 402–408.

6. Ray, Edward J.; Ladson, Charles L.; Adcock, Jerry B.; Lawing, Pierce L.; and Hall, Robert M.: *Review of Design and Operational Characteristics of the 0.3-Meter Transonic Cryogenic Tunnel.* NASA TM-80123, 1979.

7. Mineck, Raymond E.: *Hardware and Operating Features of the Adaptive Wall Test Section for the Langley 0.3-Meter Transonic Cryogenic Tunnel.* NASA TM-4114, 1989.

8. Mineck, Raymond E.: *Wall Interference Tests of a CAST 10-2/DOA 2 Airfoil in an Adaptive-Wall Test Section.* NASA TM-4015, 1987.

9. Wolf, Stephen W. D.; and Goodyer, Michael J.: *Predictive Wall Adjustment Strategy for Two-Dimensional Flexible Walled Adaptive Wind Tunnel—A Detailed Description of the First One-Step Method.* NASA CR-181635, 1988.

10. Seraudie, Alain; Blanchard, Alain; and Breil, Jean-Francoise: *Rapport d'Essais du Profil CAST 10, en Transition Déclenchée, Effectués dans la Soufflerie Transsonique Cryogénique T2 en Présence de Parois Auto-Adaptables.* R.T. OA 63/1685 AND, ONERA, CERT (Toulouse, France), Aug. 1985.

11. Braslow, Albert L.; and Knox, Eugene C.: *Simplified Method for Determination of Critical Height of Distributed Roughness Particles for Boundary-Layer Transition at Mach Numbers From 0 to 5.* NACA TN 4363, 1958.

12. Murthy, A. V.: *Residual Interference Assessment in Adaptive Wall Wind Tunnels.* NASA CR-181896, 1989.

13. Murthy, A. V.: *Effect of Aspect Ratio on Sidewall Boundary-Layer Influence in Two-Dimensional Airfoil Testing.* NASA CR-4008, 1986.

14. Green, Lawrence Lee Richard: Wall Interference Assessment and Corrections for Transonic Adaptive Wall Airfoil Data. M.S. Thesis, George Washington Univ., Apr. 1988.

15. Sewall, William G.: The Effects of Sidewall Boundary Layers in Two-Dimensional Subsonic and Transonic Wind Tunnels. *AIAA J.*, vol. 20, no. 9, Sept. 1982, pp. 1253–1256.

16. Green, Lawrence L.; and Newman, Perry A.: *Wall-Interference Assessment and Corrections for Transonic NACA 0012 Airfoil Data From Various Wind Tunnels.* NASA TP-3070, 1991.

17. Kemp, William B., Jr.: *TWINTN4: A Program for Transonic Four-Wall Interference Assessment in Two-Dimensional Wind Tunnels.* NASA CR-3777, 1984.

18. Swanson, R. C.; and Turkel, Eli: A Multistage Time-Stepping Scheme for the Navier-Stokes Equations. AIAA-85-0035, Jan. 1985.

19. Mineck, Raymond E.; and Green, Lawrence L.: Wall Interference Assessment/Correction (WIAC) for Transonic Airfoil Data From Porous and Shaped Wall Test Sections. AIAA-90-1406, June 1990.

Table 1. Airfoil Model Ordinates

Upper surface			Lower surface		
x/c	z/c, design	z/c, measured	x/c	z/c, design	z/c, measured
0.0000	0.0034	0.0034	0.0001	0.0034	0.0034
.0003	.0062	.0063	.0004	.0004	.0004
.0015	.0094	.0093	.0014	−.0021	−.0021
.0033	.0124	.0123	.0031	−.0043	−.0043
.0063	.0159	.0158	.0061	−.0066	−.0065
.0140	.0217	.0217	.0096	−.0081	−.0081
.0195	.0250	.0251	.0153	−.0099	−.0099
.0247	.0279	.0279	.0273	−.0127	−.0128
.0356	.0331	.0332	.0339	−.0141	−.0142
.0470	.0376	.0377	.0470	−.0169	−.0169
.0654	.0432	.0433	.0673	−.0205	−.0206
.0846	.0478	.0478	.0874	−.0238	−.0238
.1179	.0536	.0536	.1148	−.0277	−.0277
.1519	.0580	.0580	.1562	−.0328	−.0329
.2139	.0633	.0633	.2741	−.0446	−.0447
.2764	.0665	.0665	.3366	−.0492	−.0492
.3321	.0681	.0681	.3919	−.0520	−.0520
.3949	.0689	.0689	.4539	−.0532	−.0532
.4576	.0686	.0685	.5161	−.0520	−.0520
.5132	.0673	.0672	.5714	−.0489	−.0488
.5757	.0645	.0644	.6340	−.0436	−.0436
.6376	.0601	.0600	.6967	−.0373	−.0374
.6925	.0542	.0541	.7525	−.0316	−.0317
.7539	.0453	.0452	.8149	−.0255	−.0257
.8152	.0338	.0337	.8775	−.0204	−.0206
.8763	.0203	.0202	.9189	−.0177	−.0178
.9172	.0106	.0105	.9468	−.0162	−.0164
.9511	.0024	.0024	.9743	−.0151	−.0152
.9782	−.0042	−.0042	1.0000	−.0145	−.0146
1.0000	−.0095	−.0095			

Table 2. Test Conditions Used in HRNF and TCT Tests

M_∞	Tests run at R_c of—		
	10×10^6	15×10^6	20×10^6
0.300	Both	HRNF	Neither
.500	Both	HRNF	HRNF
.600	Both	HRNF	Both
.700	Both	Both	Both
.730	Both	Both	Both
.750	Both	Both	Both
.765	Both	Both	Both
.780	Both	Both	Both
.790	Both	HRNF	HRNF
.800	Both	HRNF	Both

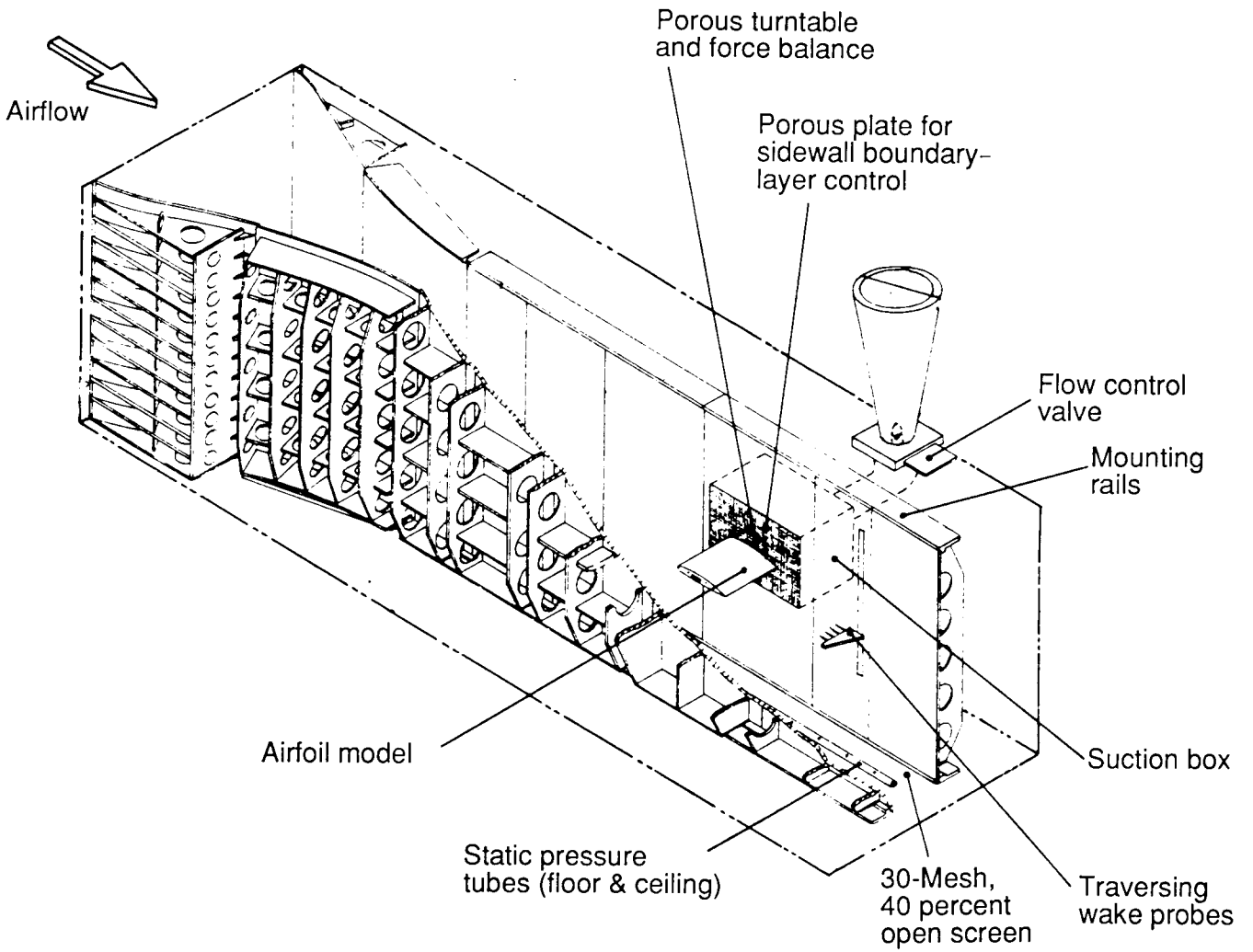

Figure 1. Details of NAE Two-Dimensional High Reynolds Number Facility.

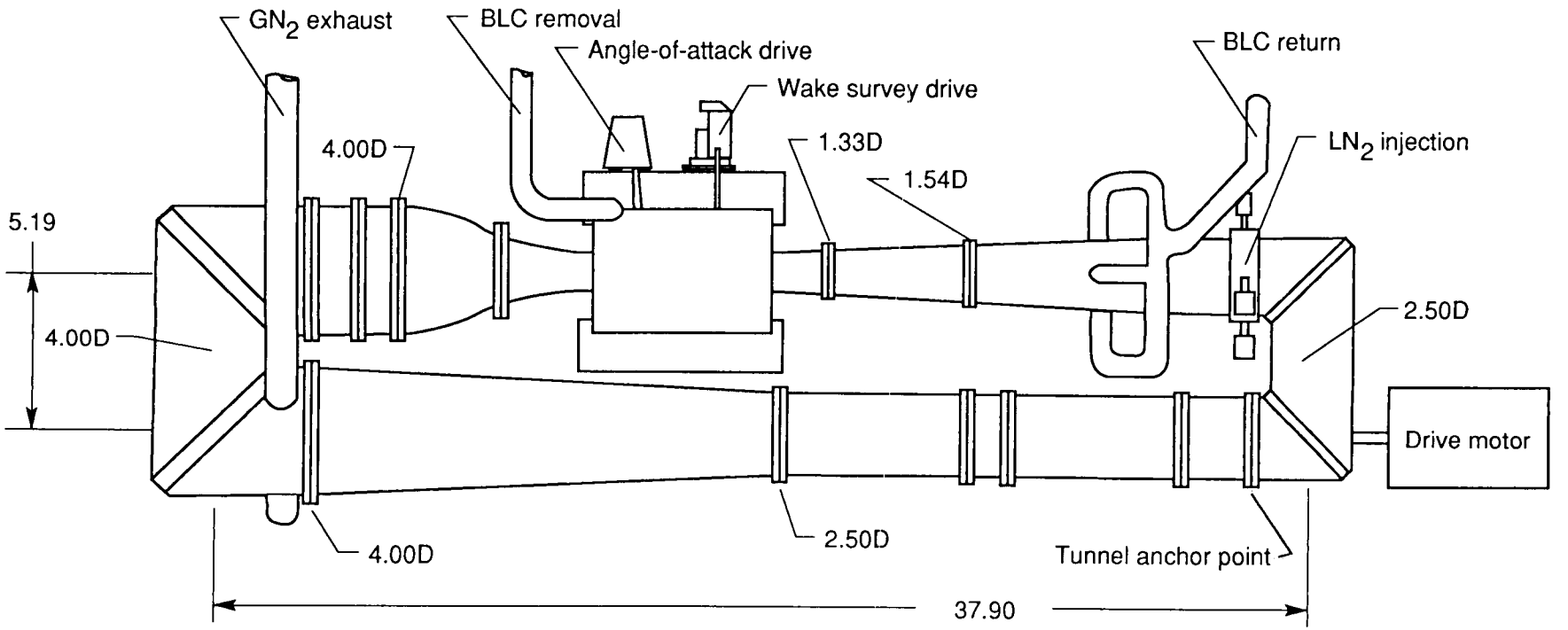

Figure 2. Sketch of 0.3-m TCT circuit with 13- by 13-in. adaptive-wall test section. Dimensions are in feet.

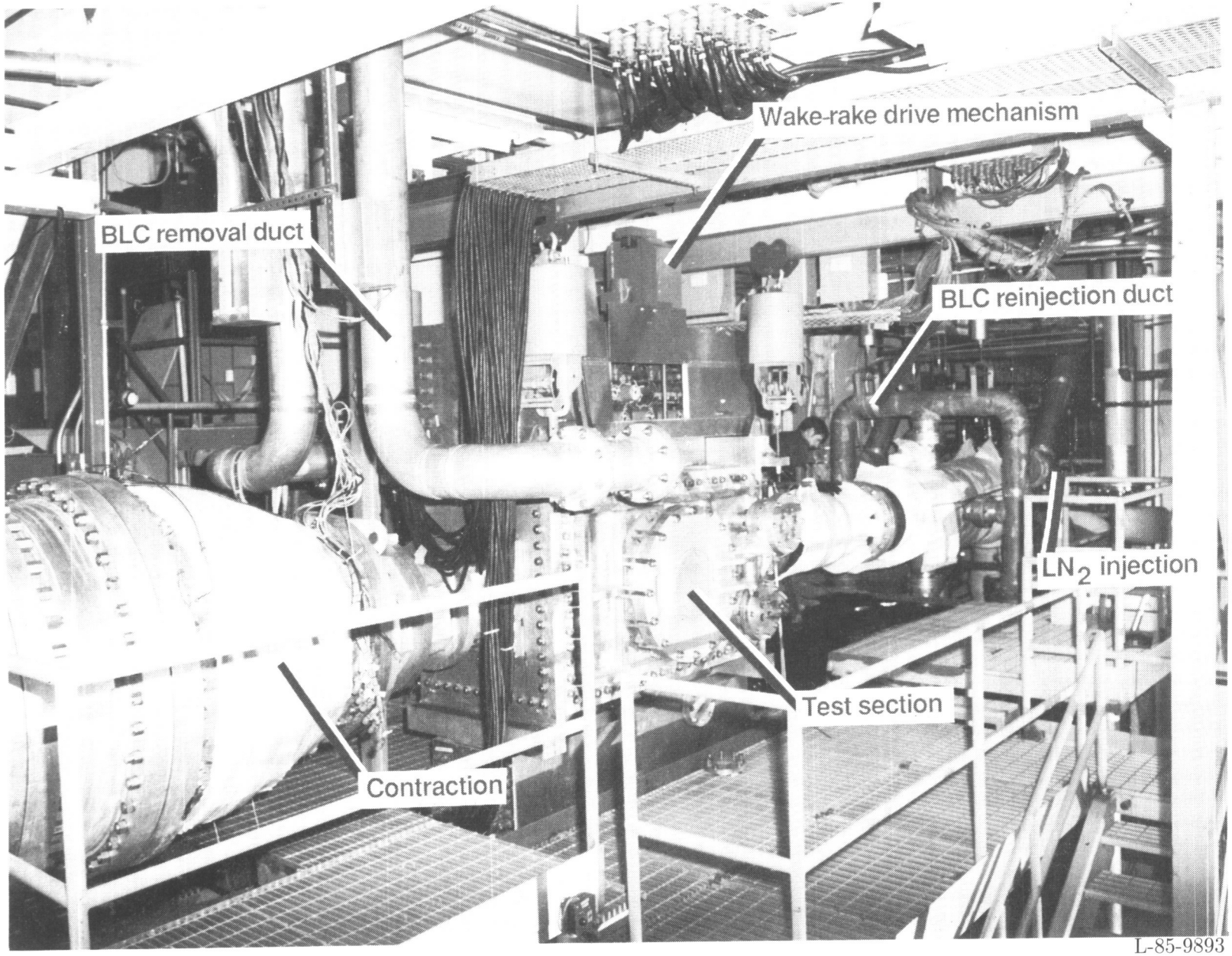

Figure 3. Photograph of upper leg of Langley 0.3-Meter Transonic Cryogenic Tunnel with 13- by 13-in. adaptive-wall test section.

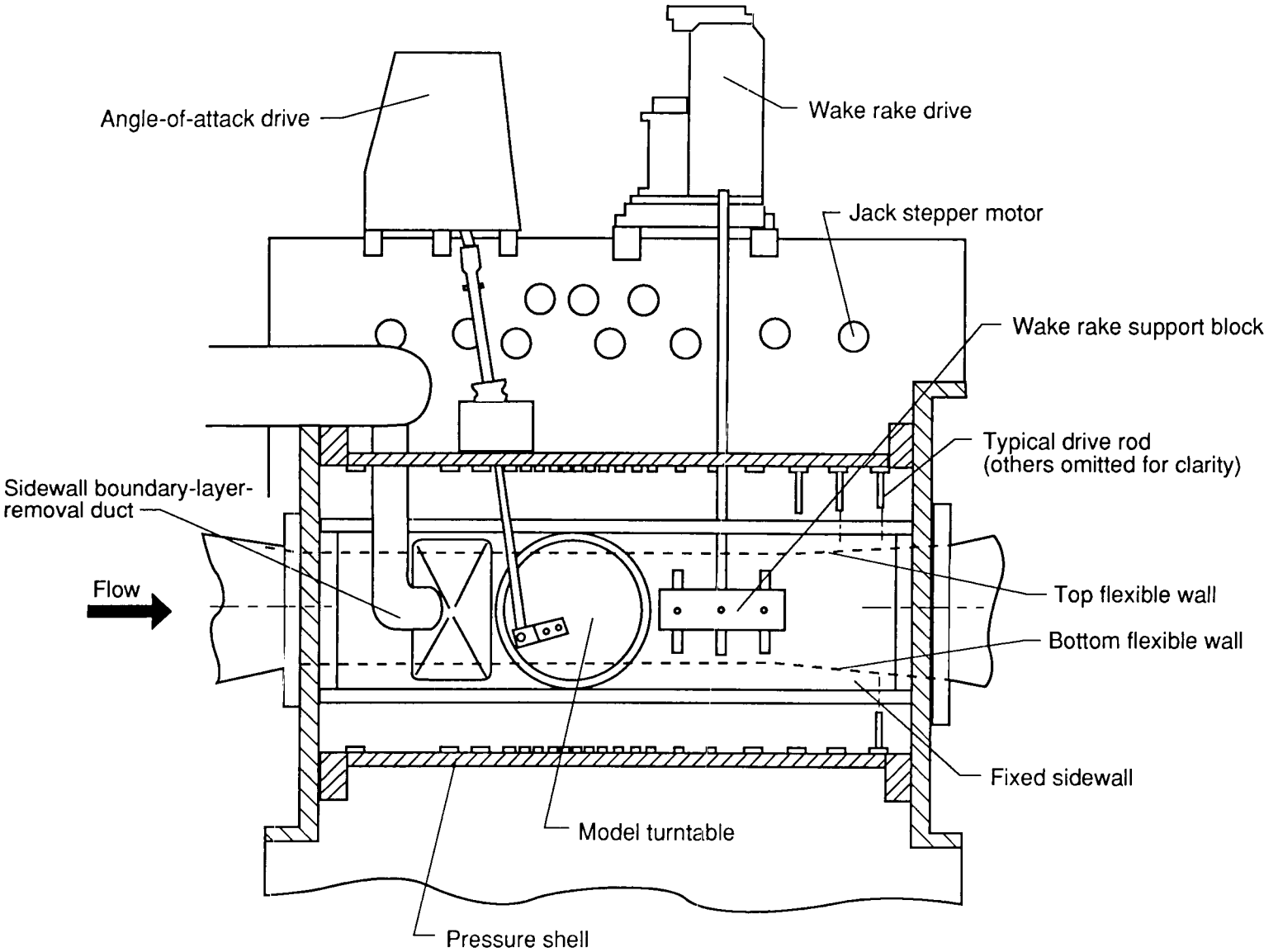

Figure 4. Layout of 13- by 13-in. adaptive-wall test section with plenum sidewall removed.

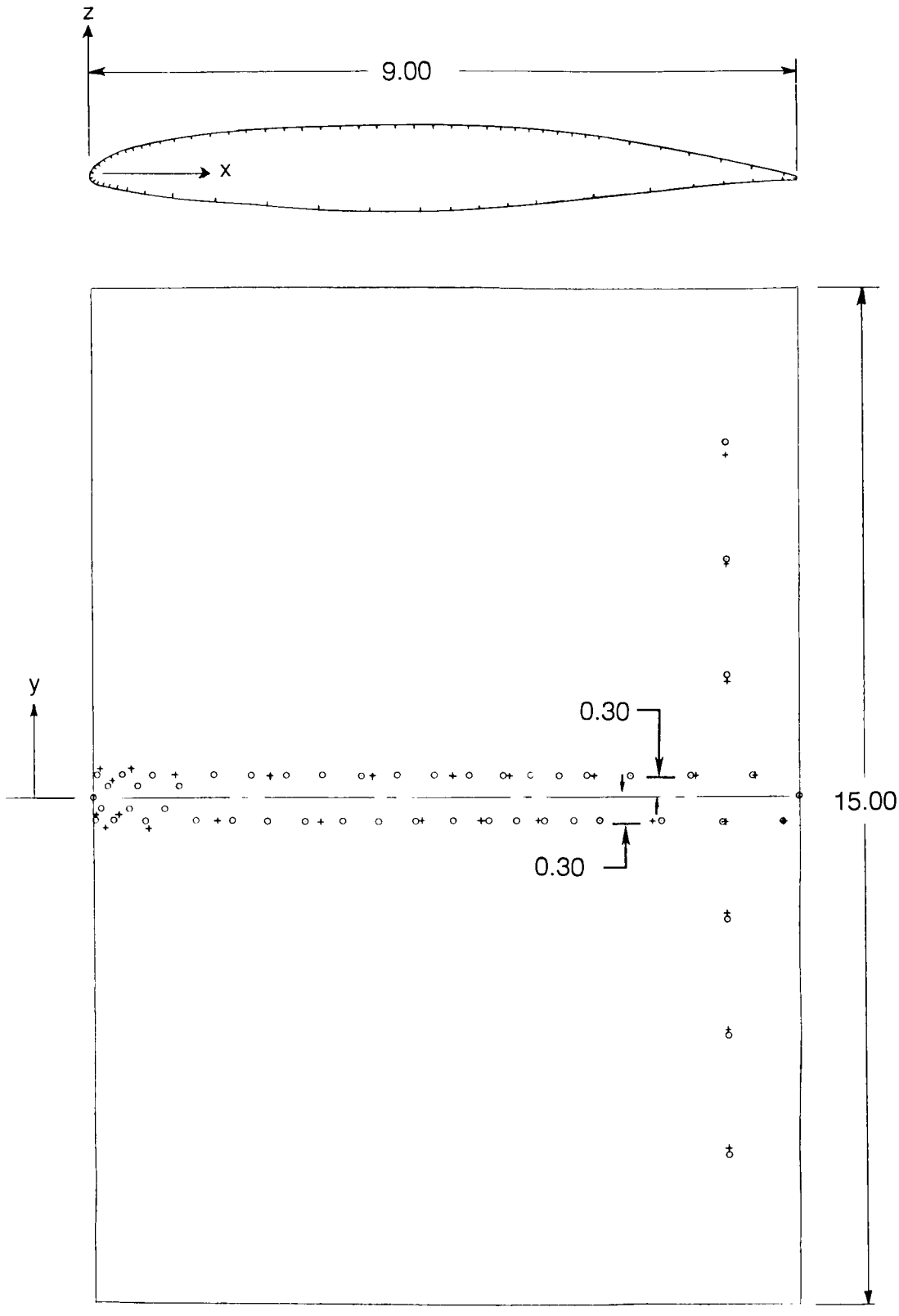

Figure 5. Layout of pressure orifice locations. All dimensions are in inches. Open symbols denote upper surface; "+" denotes lower surface.

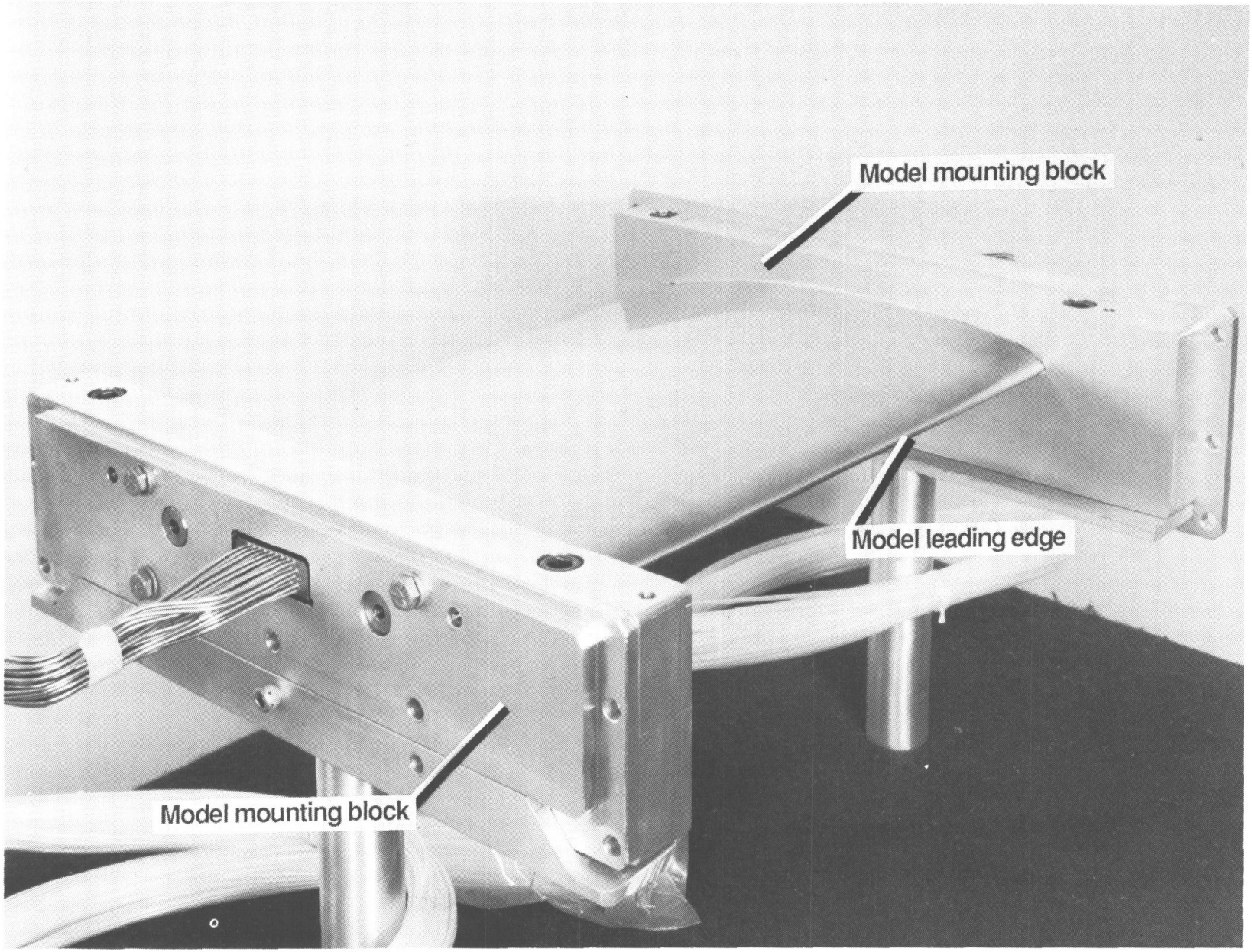

L-86-9833

Figure 6. Cast 10-2/DOA 2 airfoil model and turntable mounting blocks.

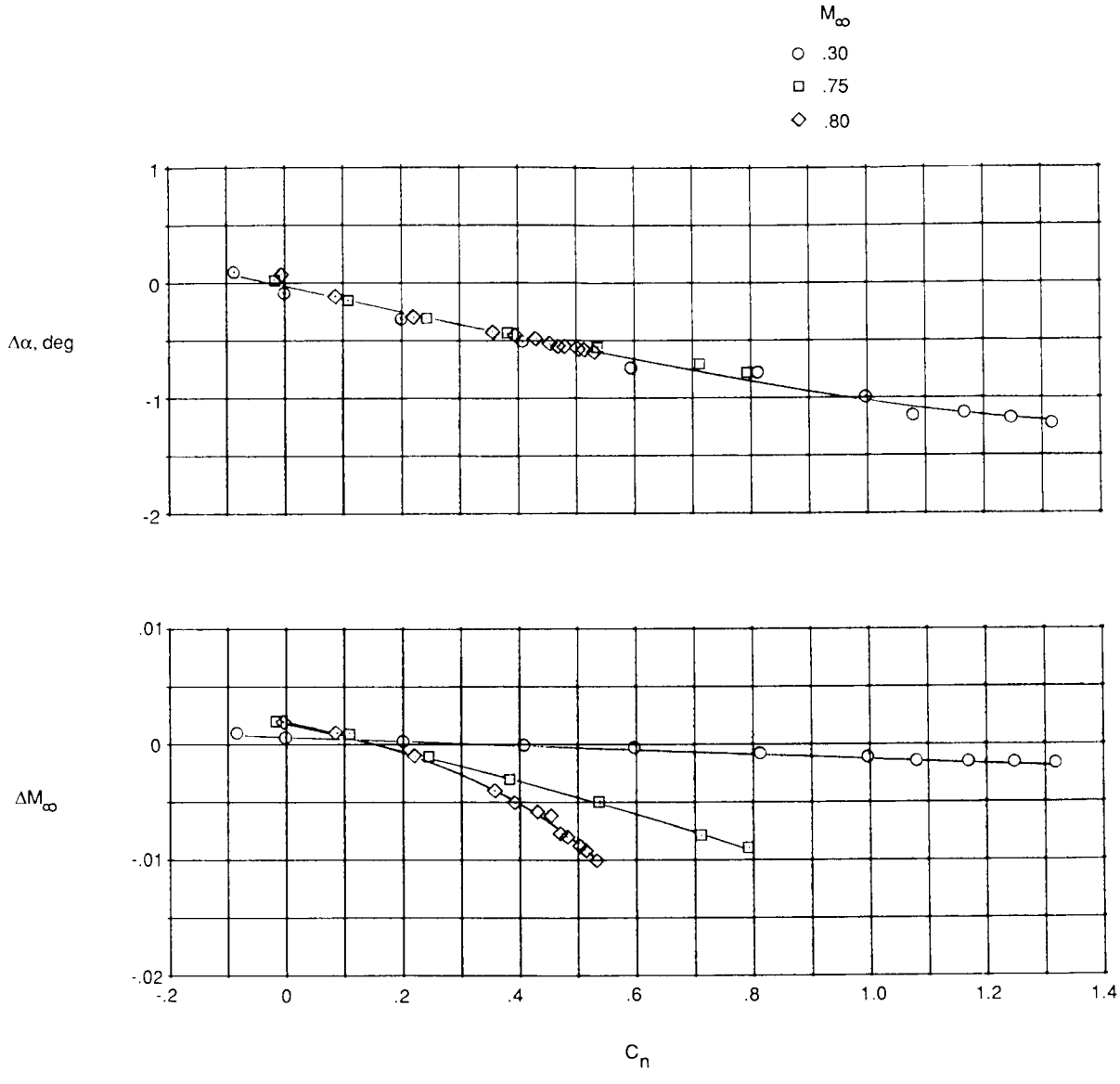

(a) HRNF tests.

Figure 7. Corrections applied to the results for top- and bottom-wall interference. $R_c = 10 \times 10^6$.

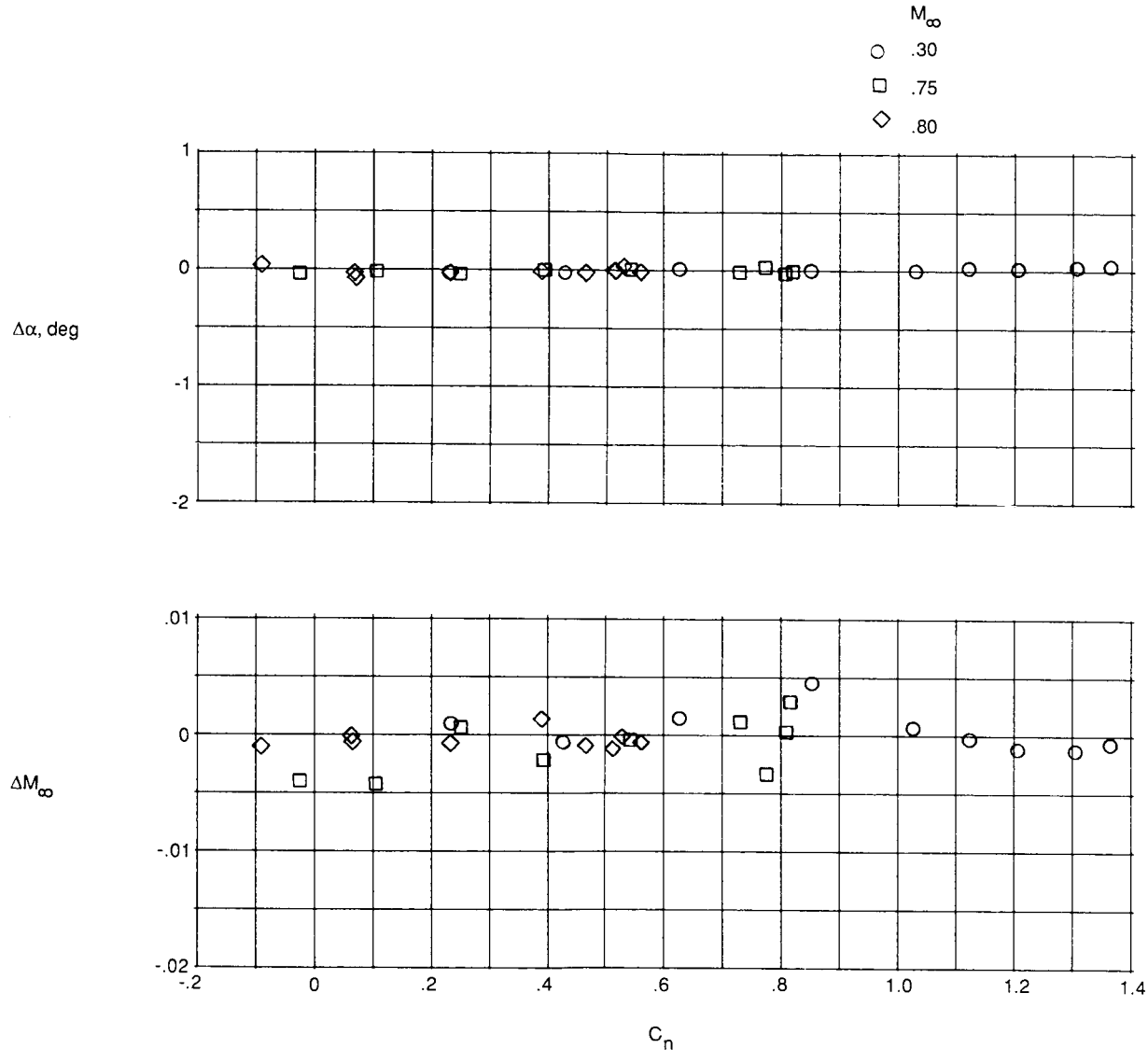

(b) 0.3-m TCT residual corrections.

Figure 7. Concluded.

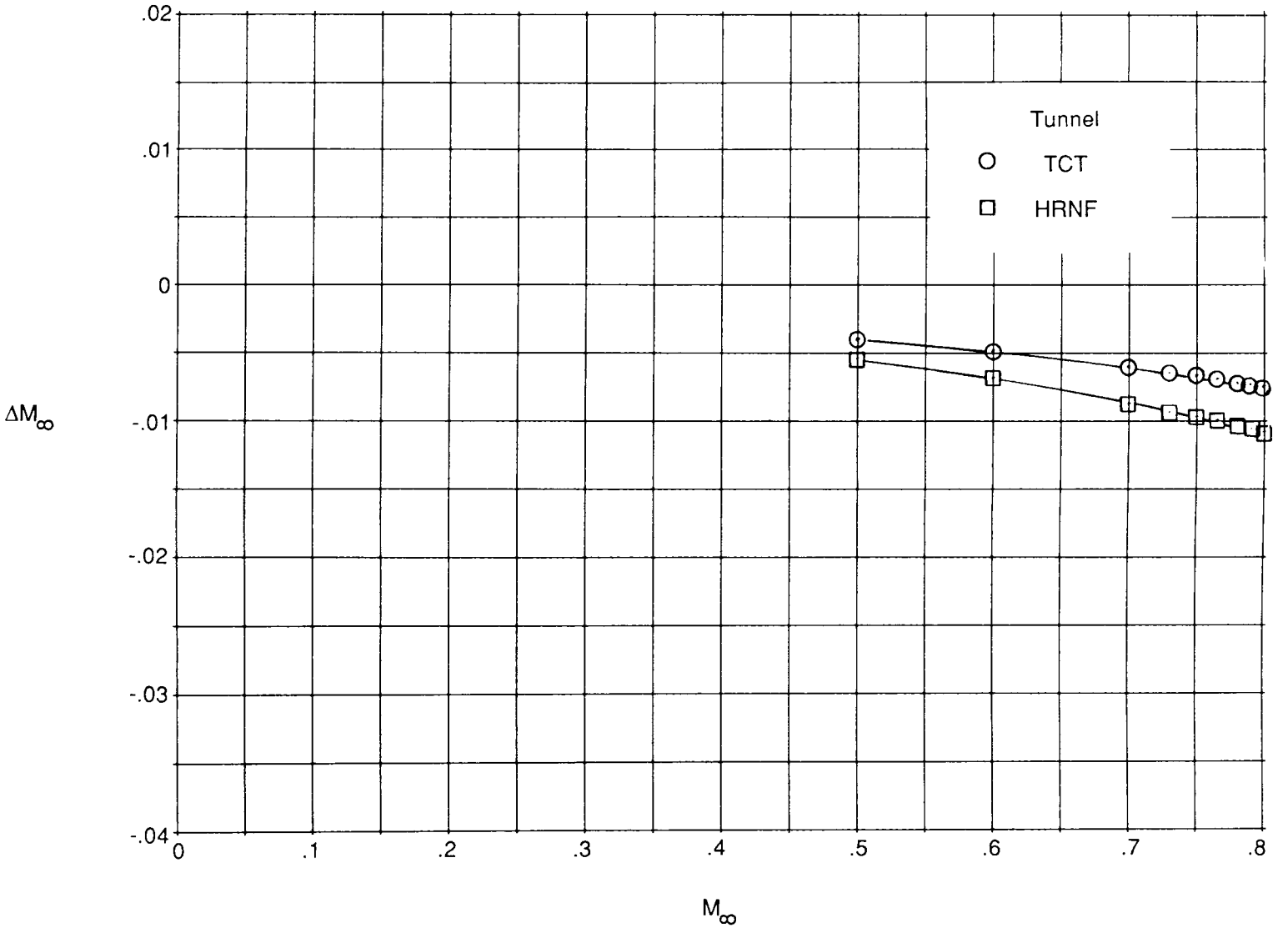

Figure 8. Computed corrections for sidewall interference. $R_c = 10 \times 10^6$.

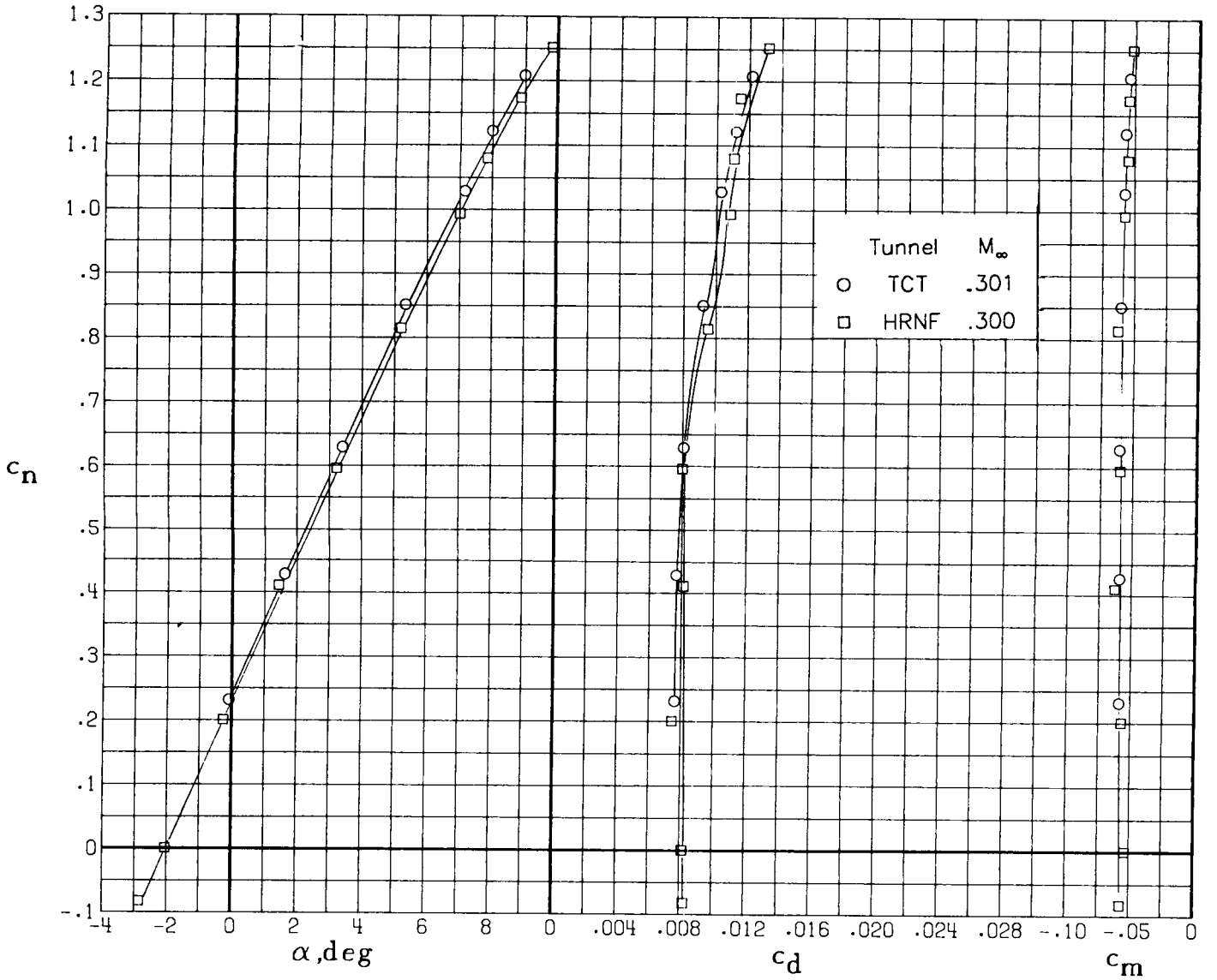

Figure 9. Comparison of 0.3-m TCT and HRNF baseline integrated force and moment coefficients for $R_c = 10 \times 10^6$.

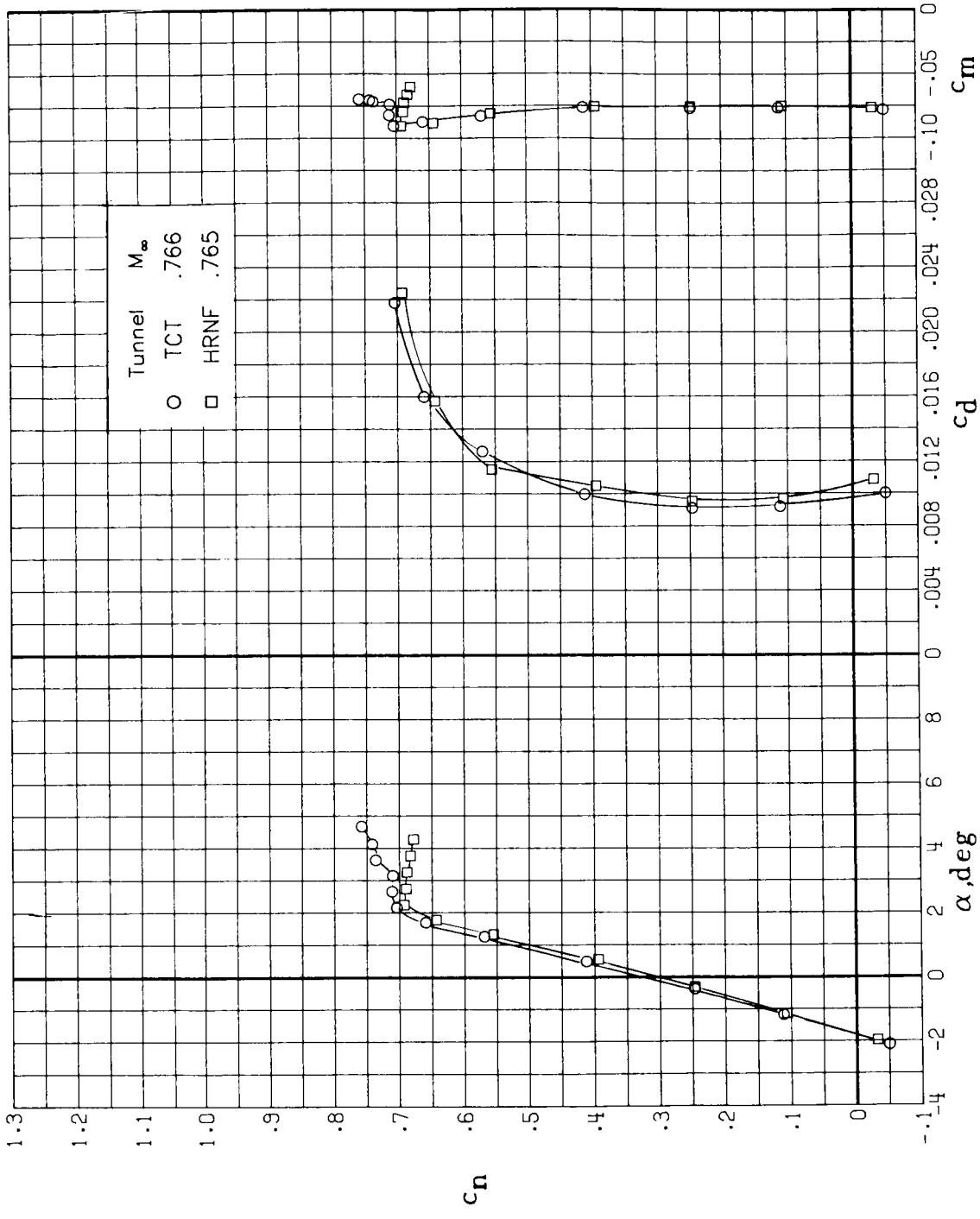

Figure 9. Continued.

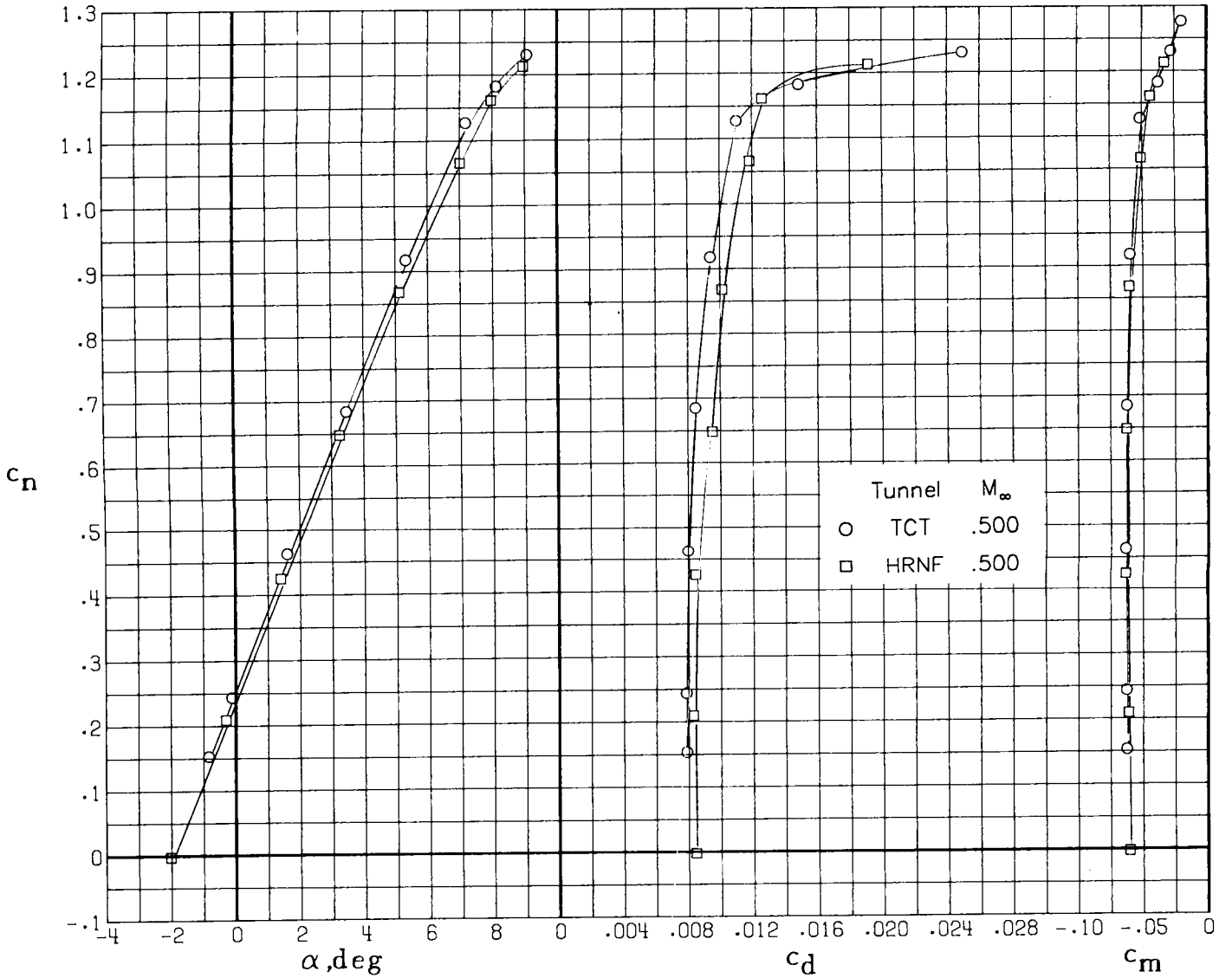

Figure 9. Continued.

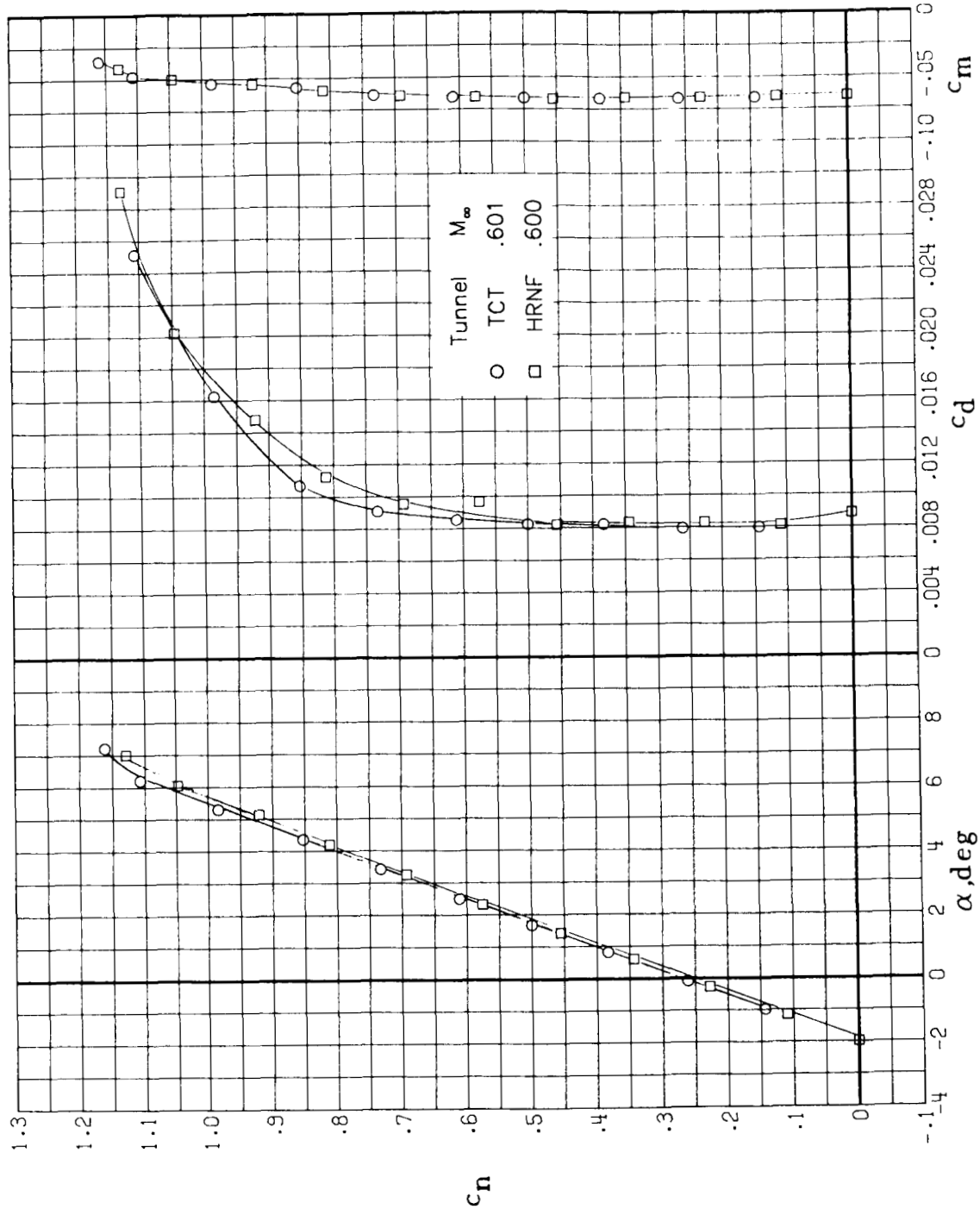

Figure 9. Continued.

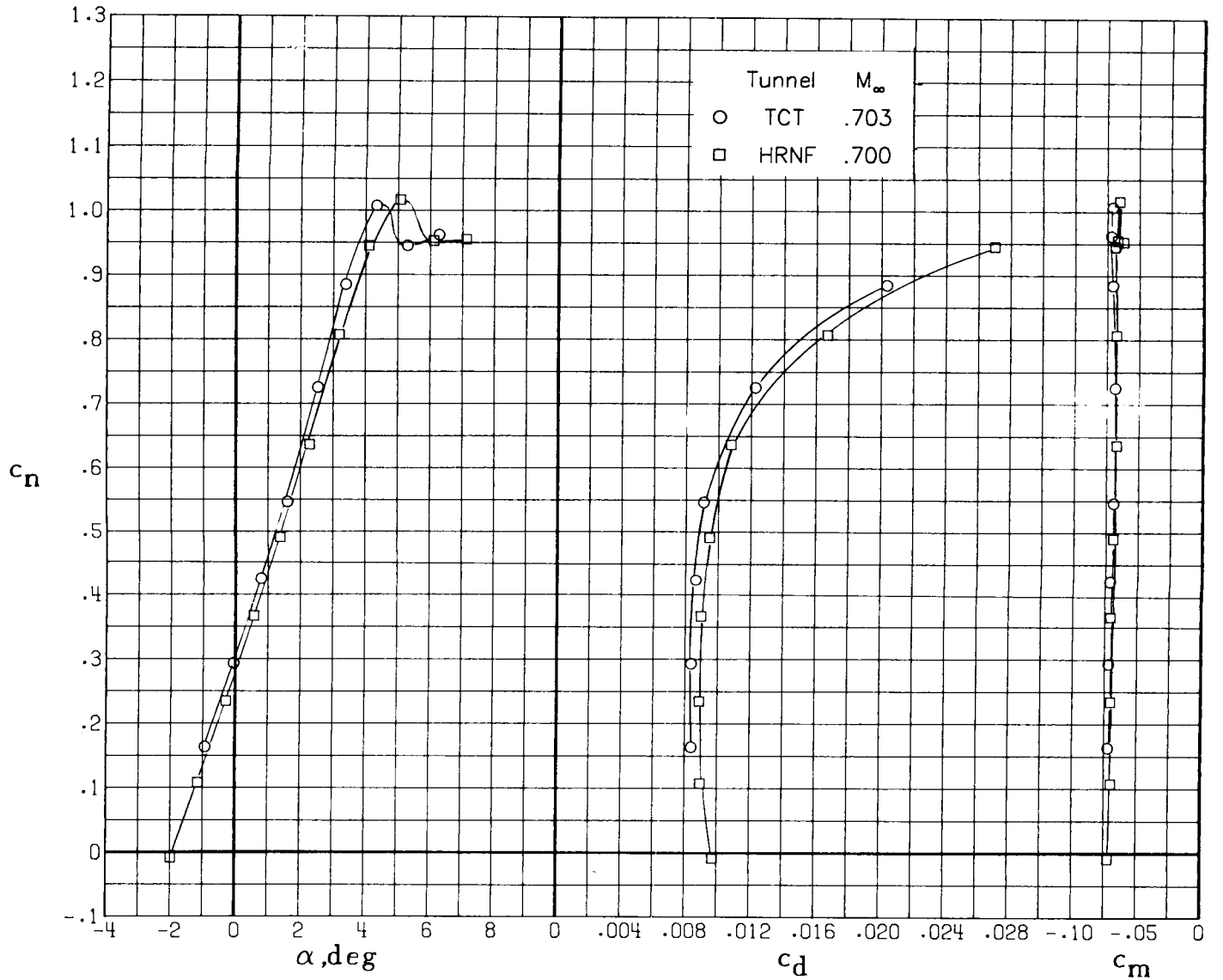

Figure 9. Continued.

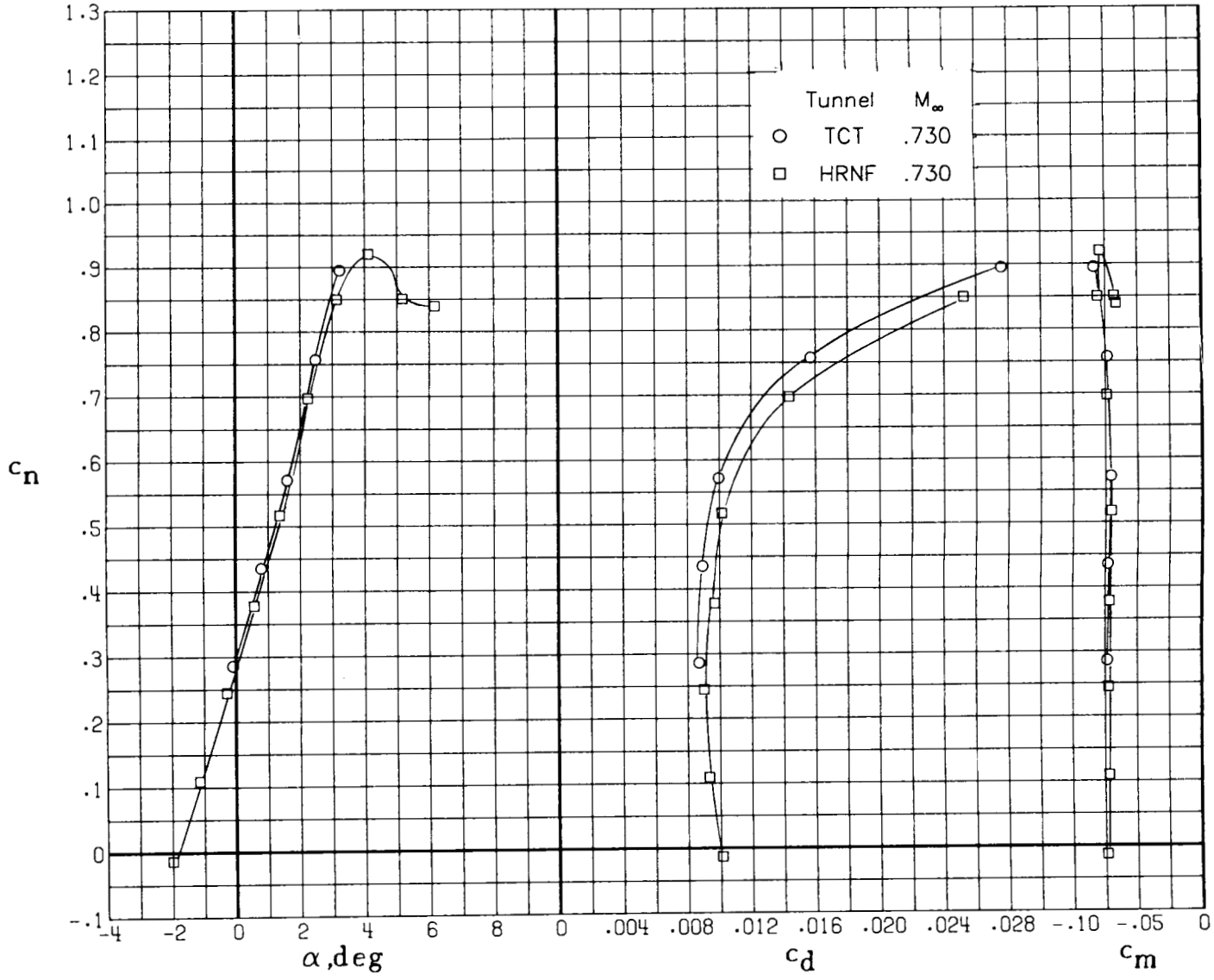

Figure 9. Continued.

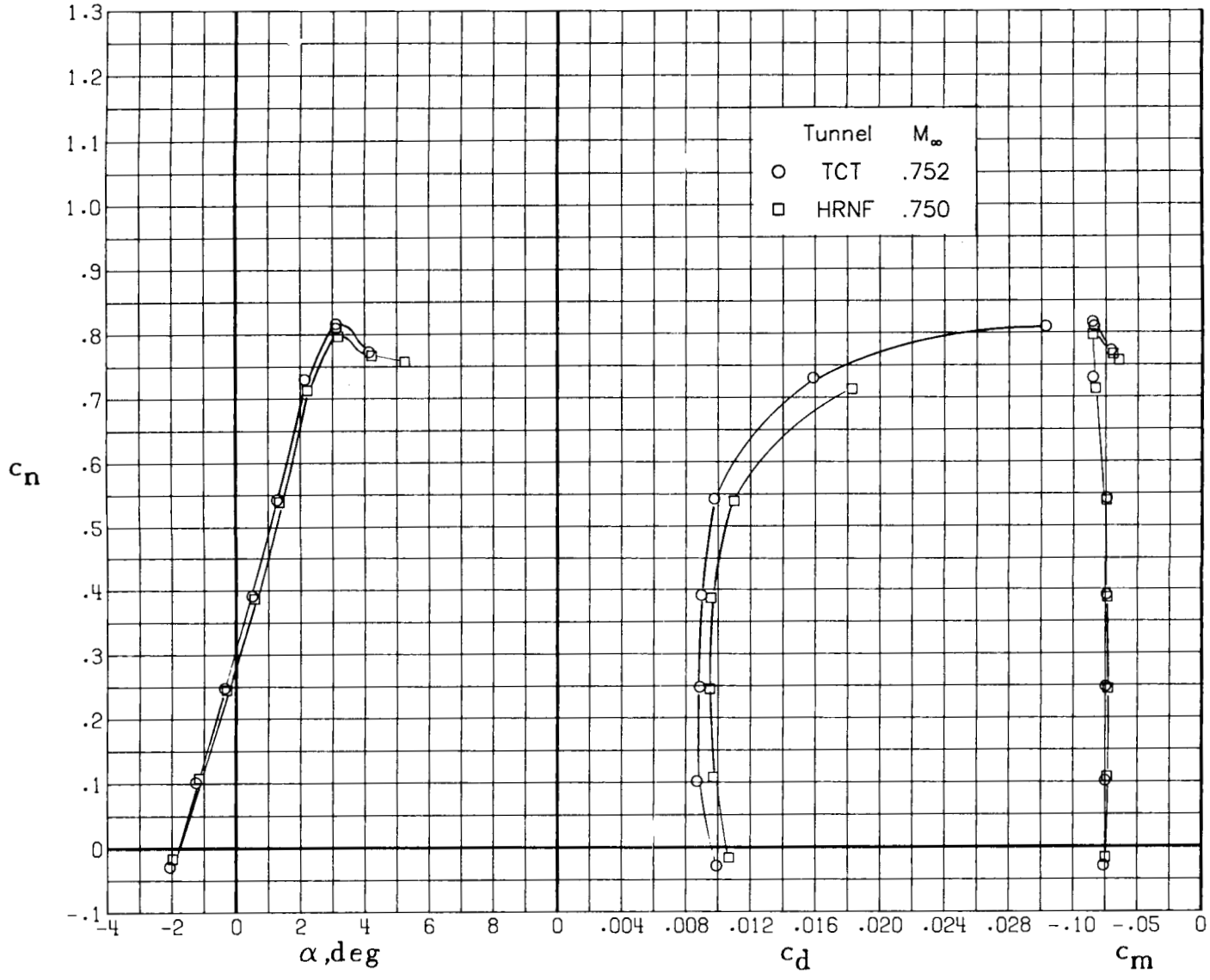

Figure 9. Continued.

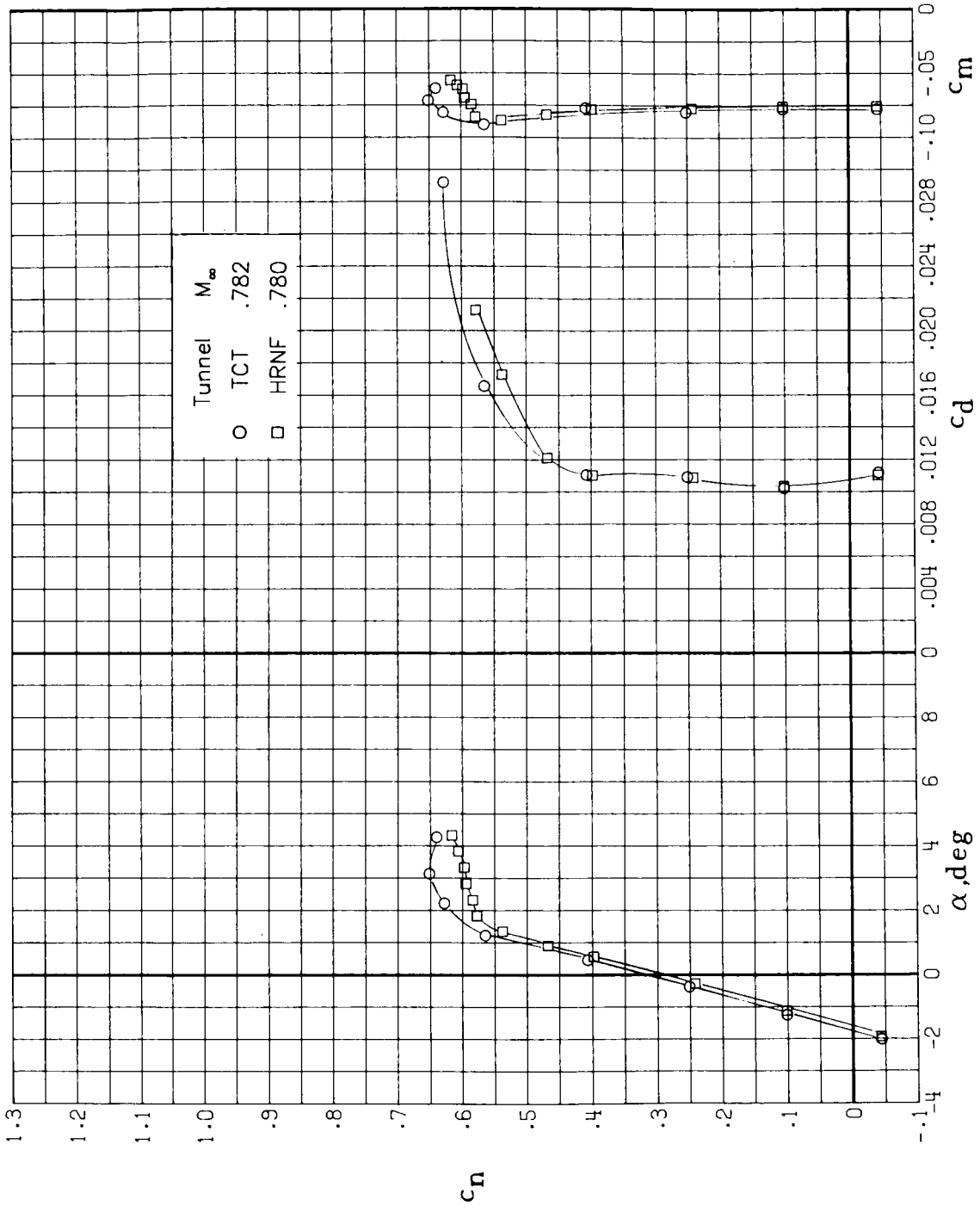

Figure 9. Continued.

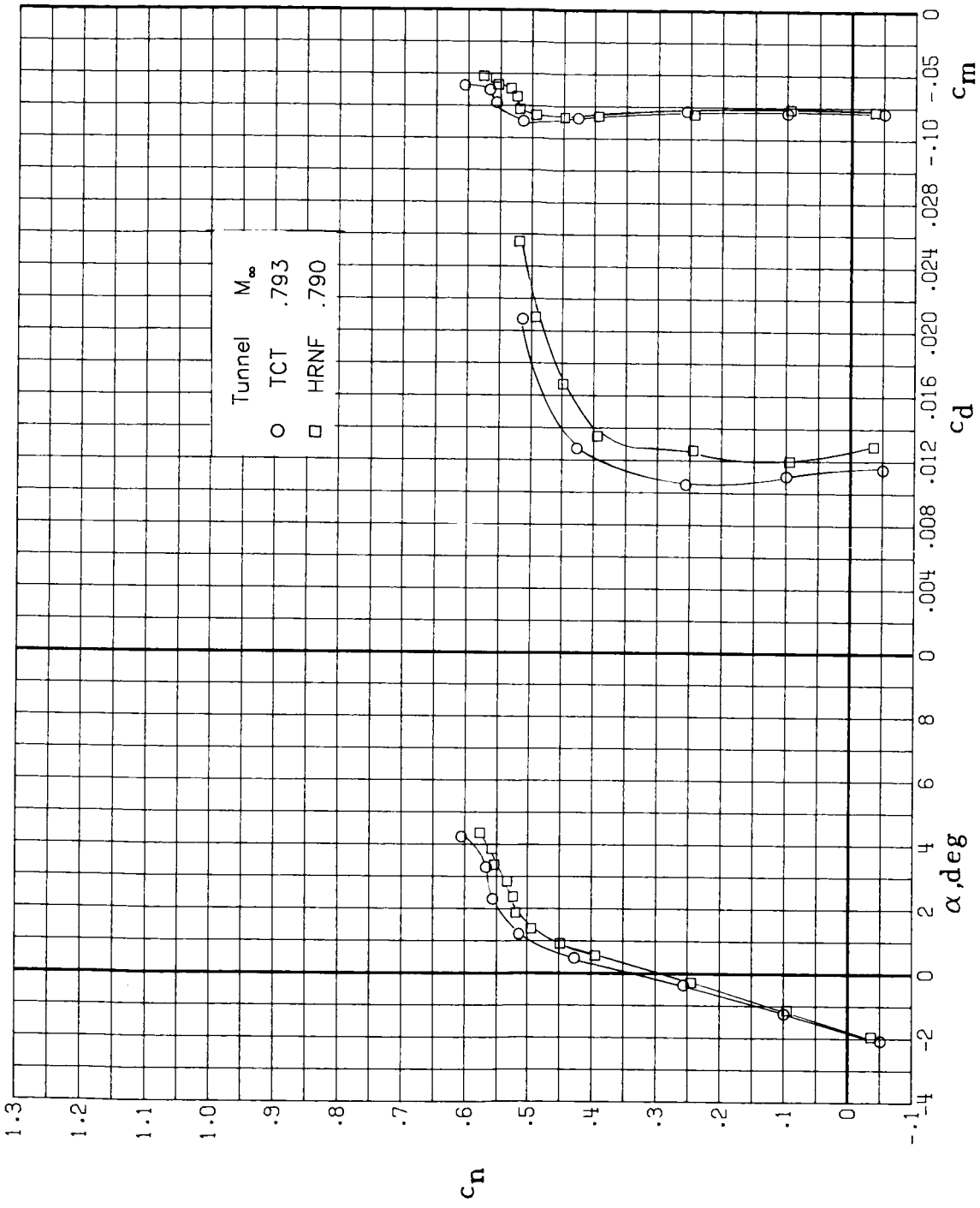

Figure 9. Continued.

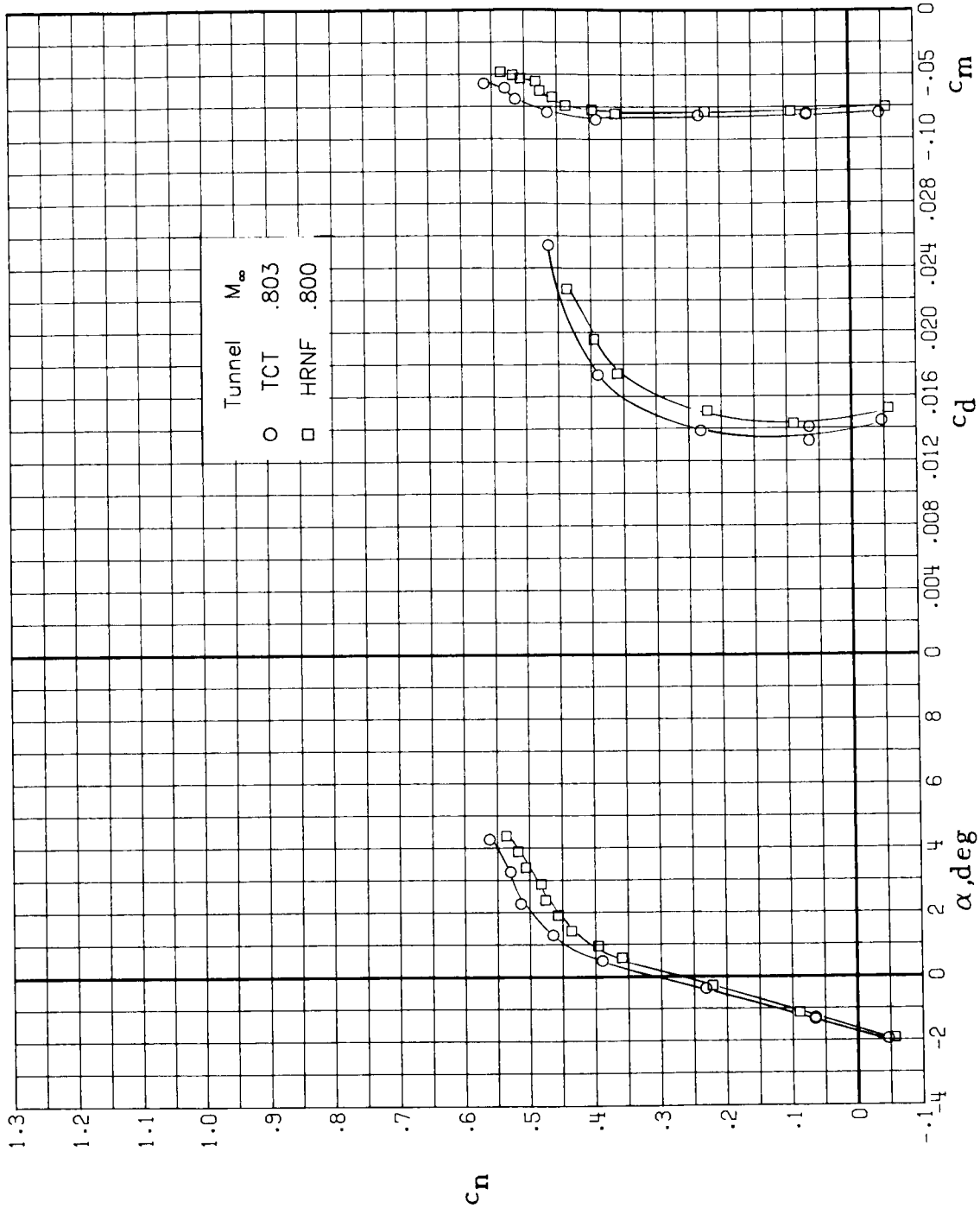

Figure 9. Concluded.

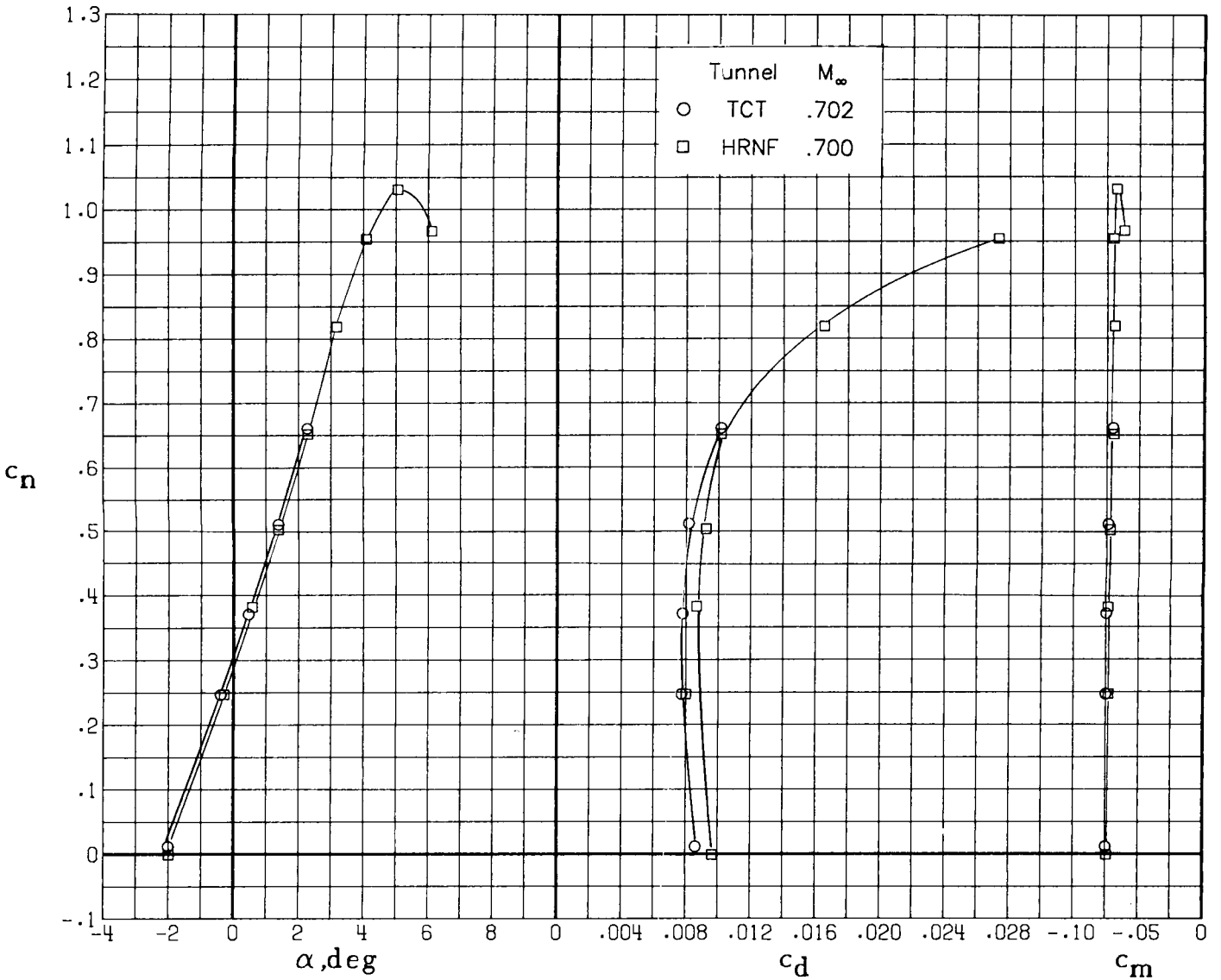

Figure 10. Comparison of 0.3-m TCT and HRNF baseline integrated force and moment coefficients for $R_c = 15 \times 10^6$.

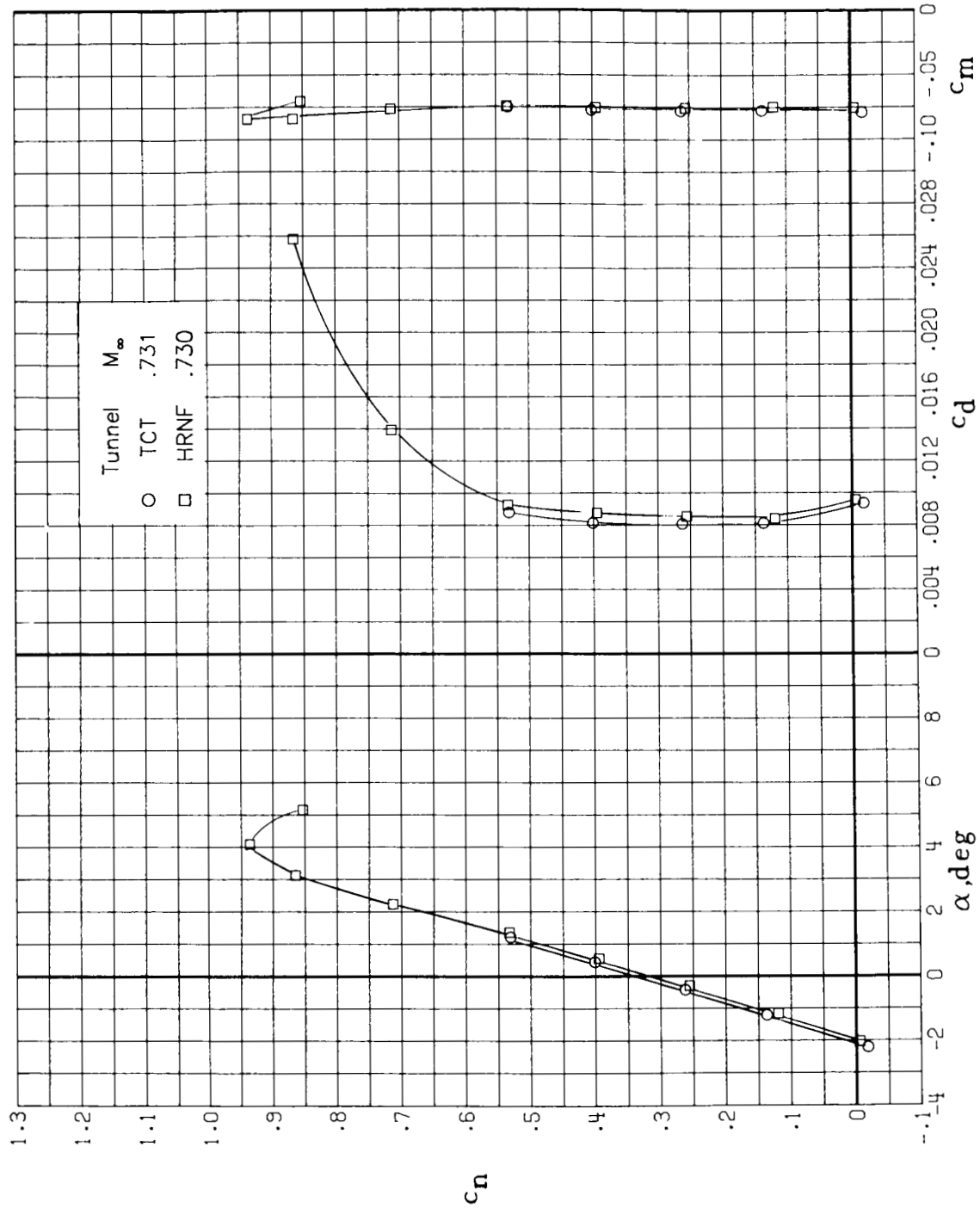

Figure 10. Continued.

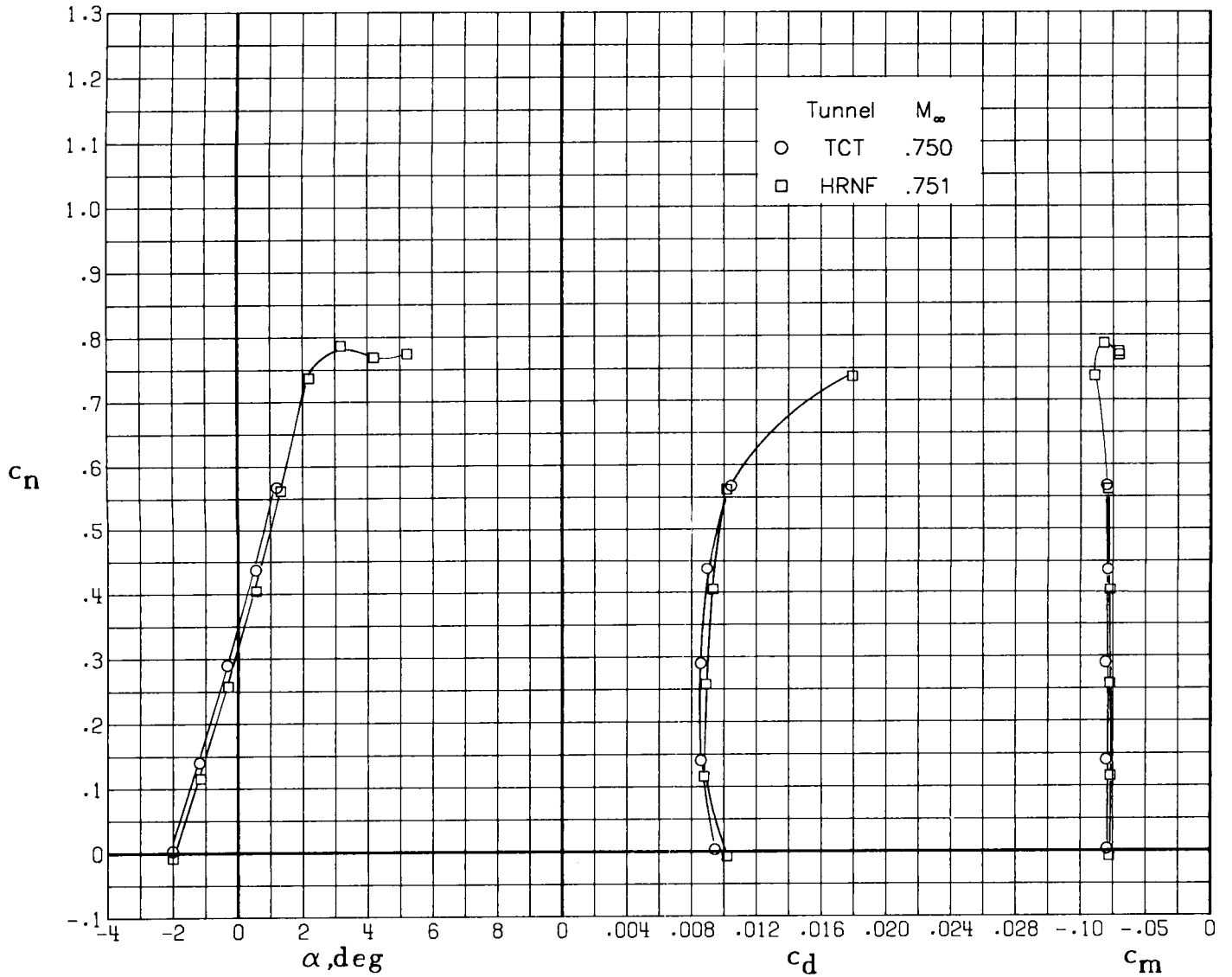

Figure 10. Continued.

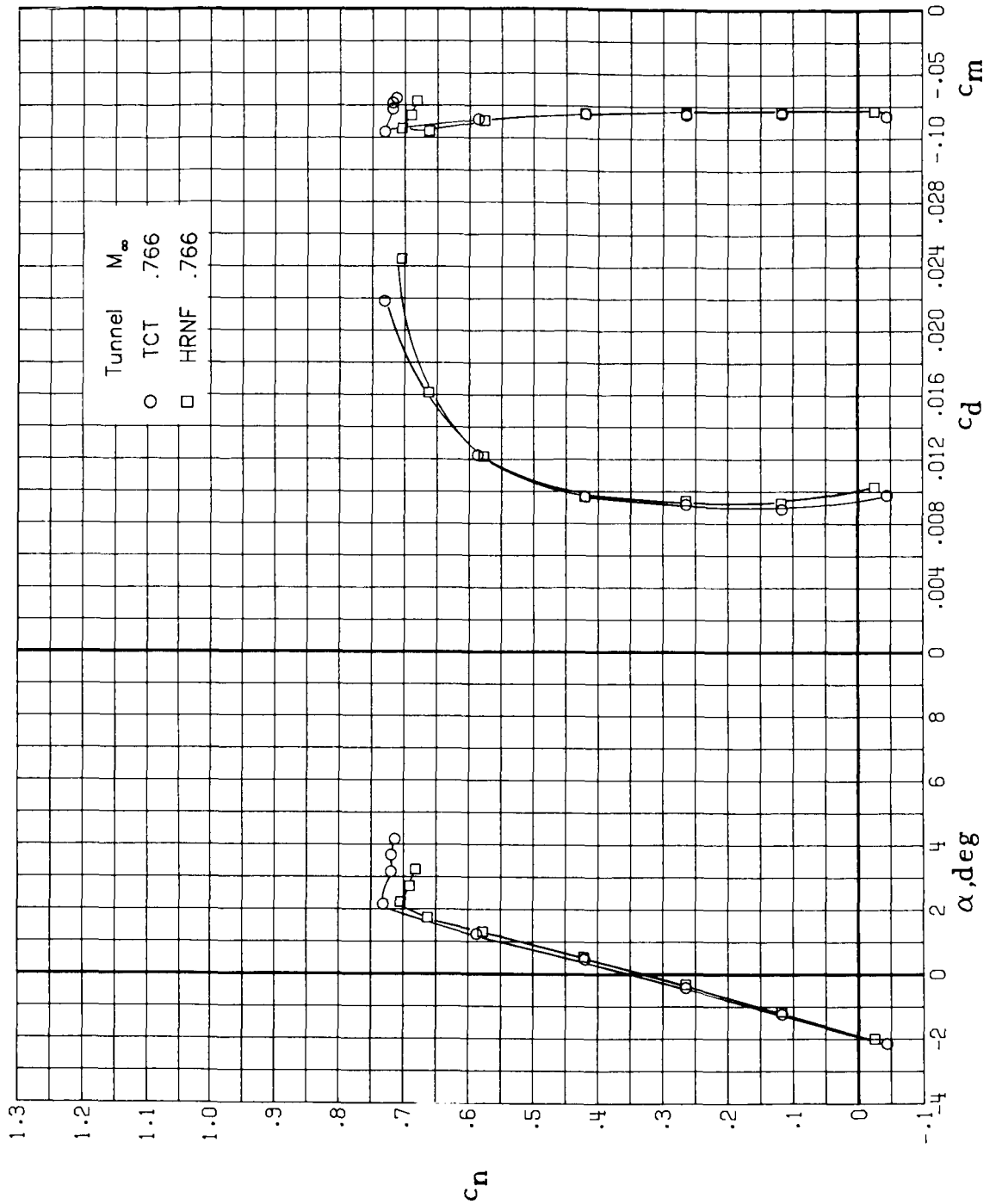

Figure 10. Continued.

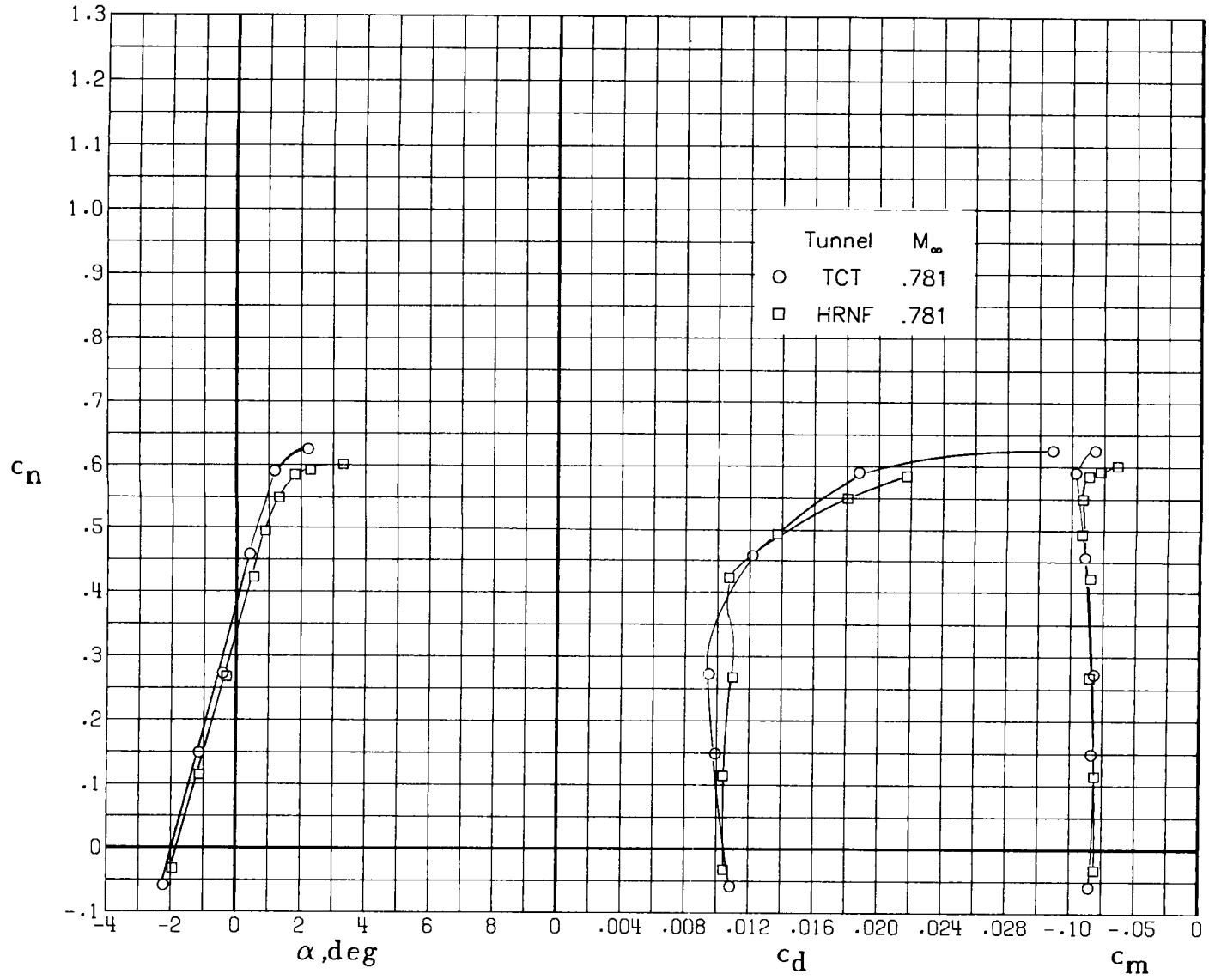

Figure 10. Continued.

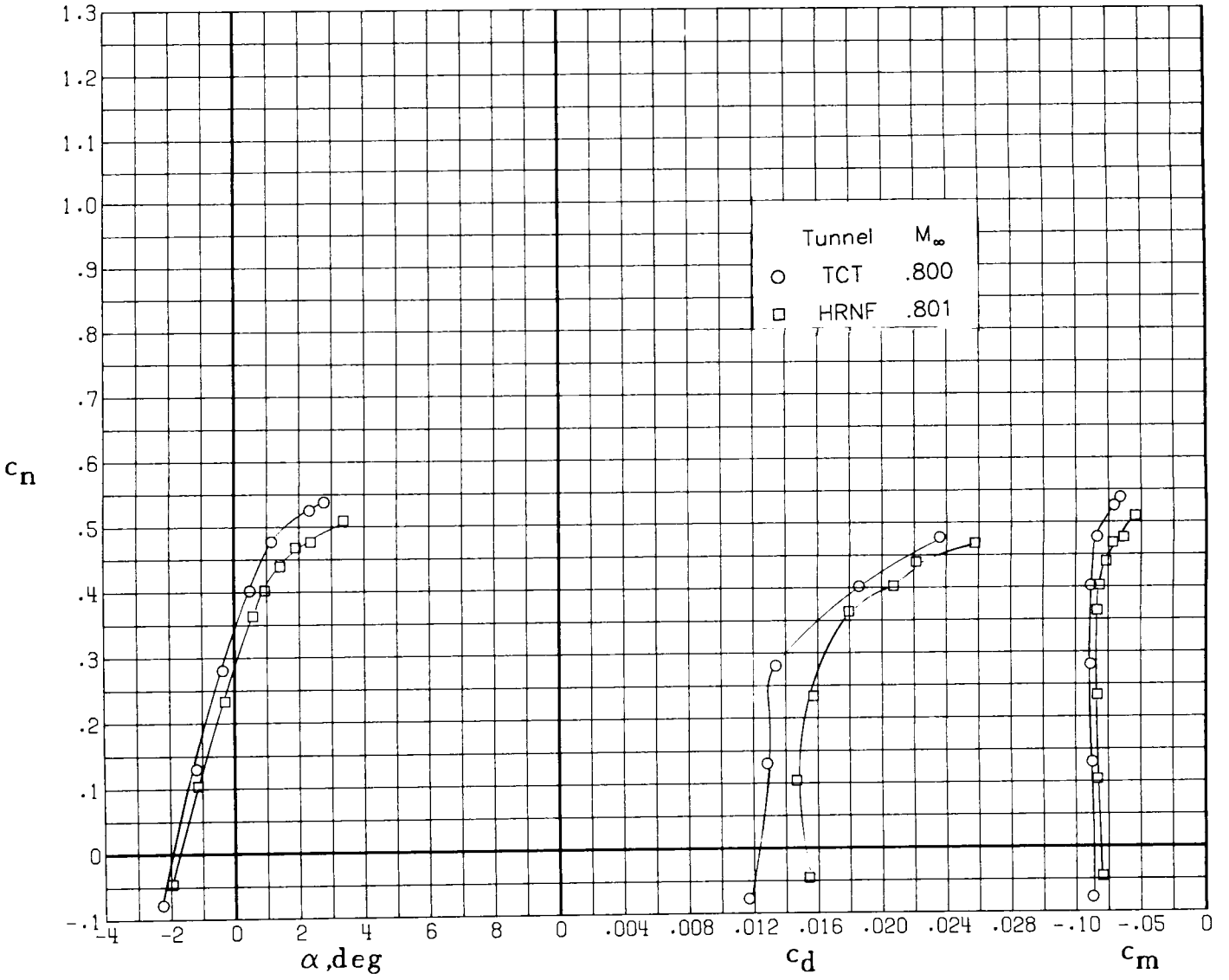

Figure 10. Concluded.

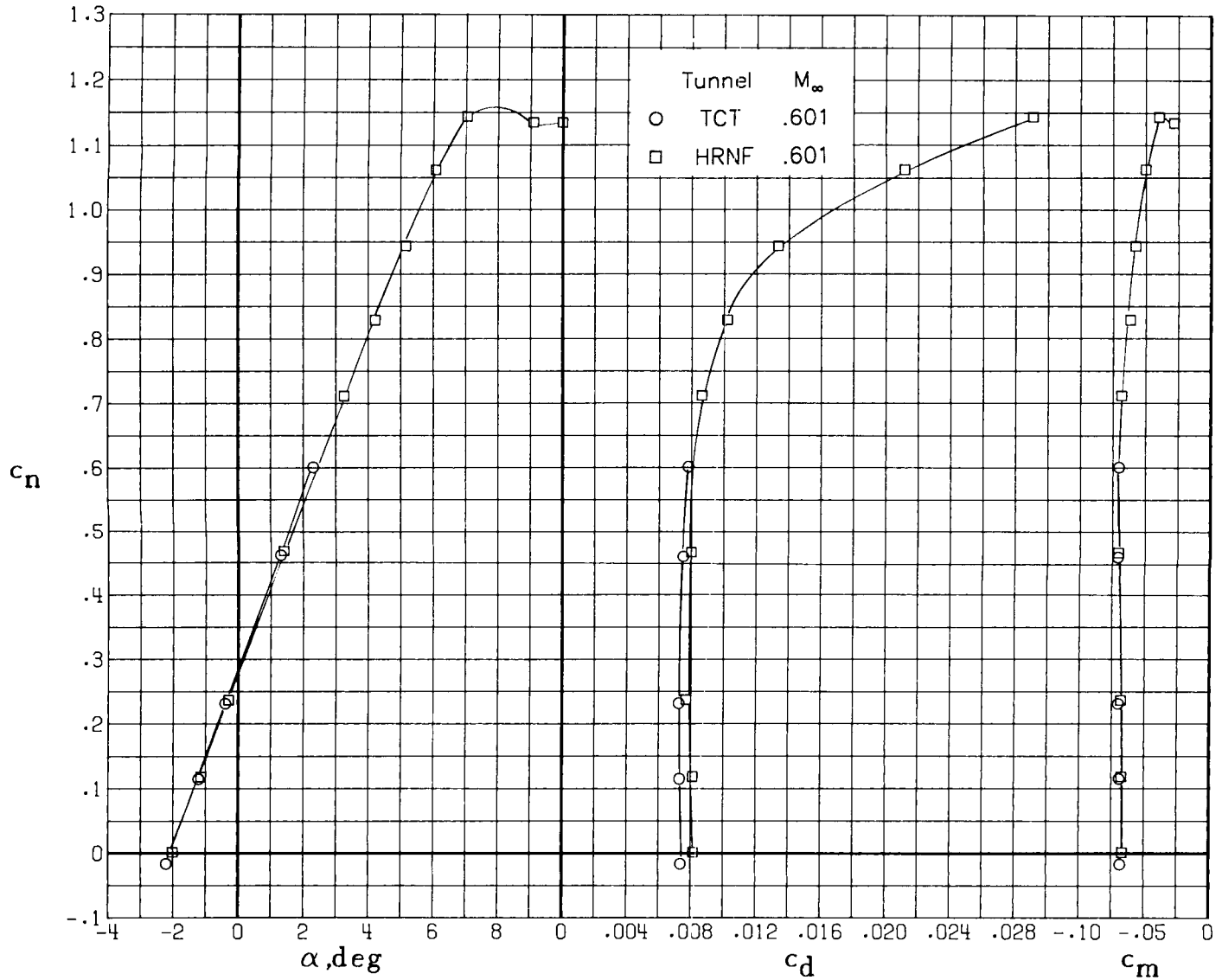

Figure 11. Comparison of 0.3-m TCT and HRNF baseline integrated force and moment coefficients for $R_c = 20 \times 10^6$.

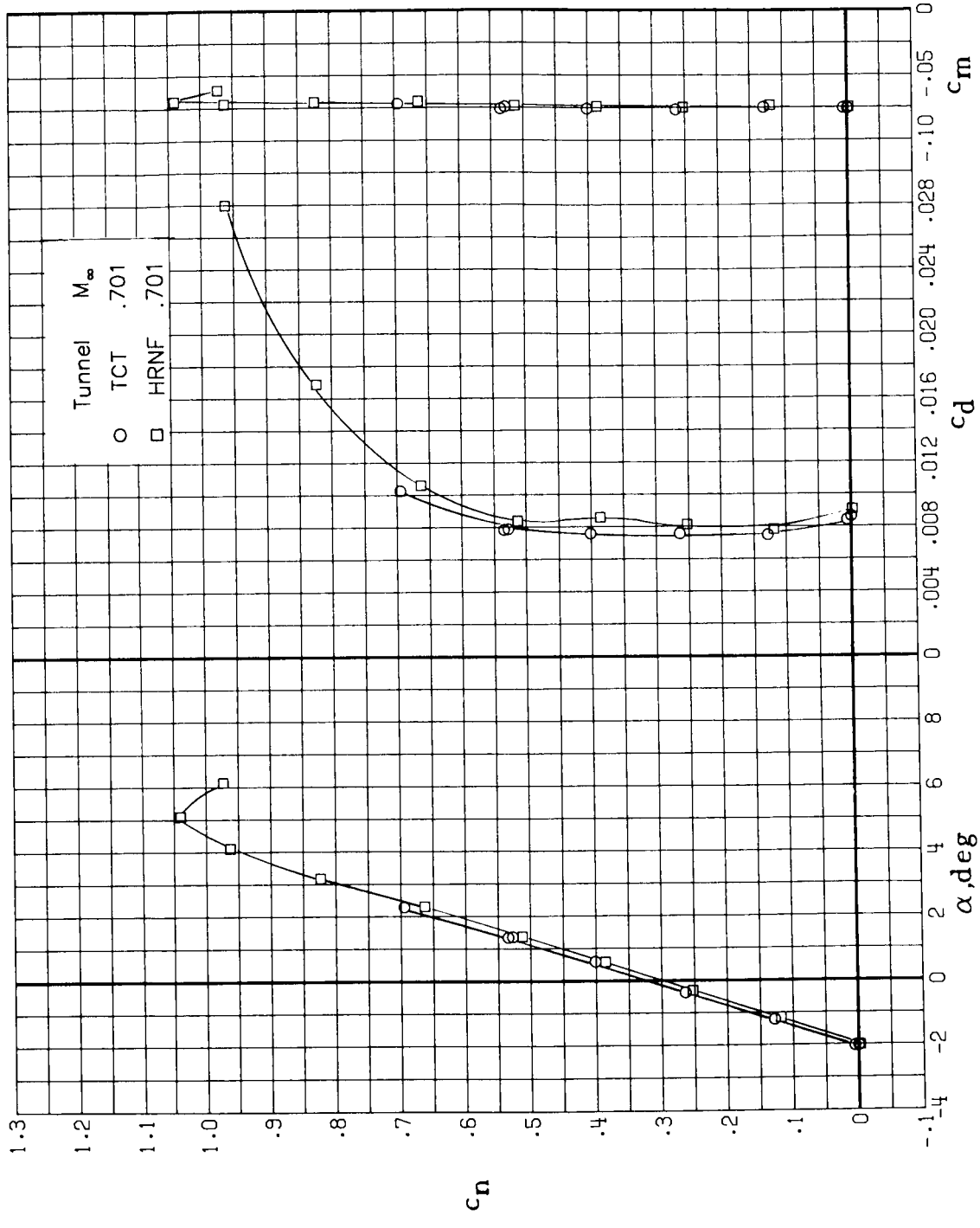

Figure 11. Continued.

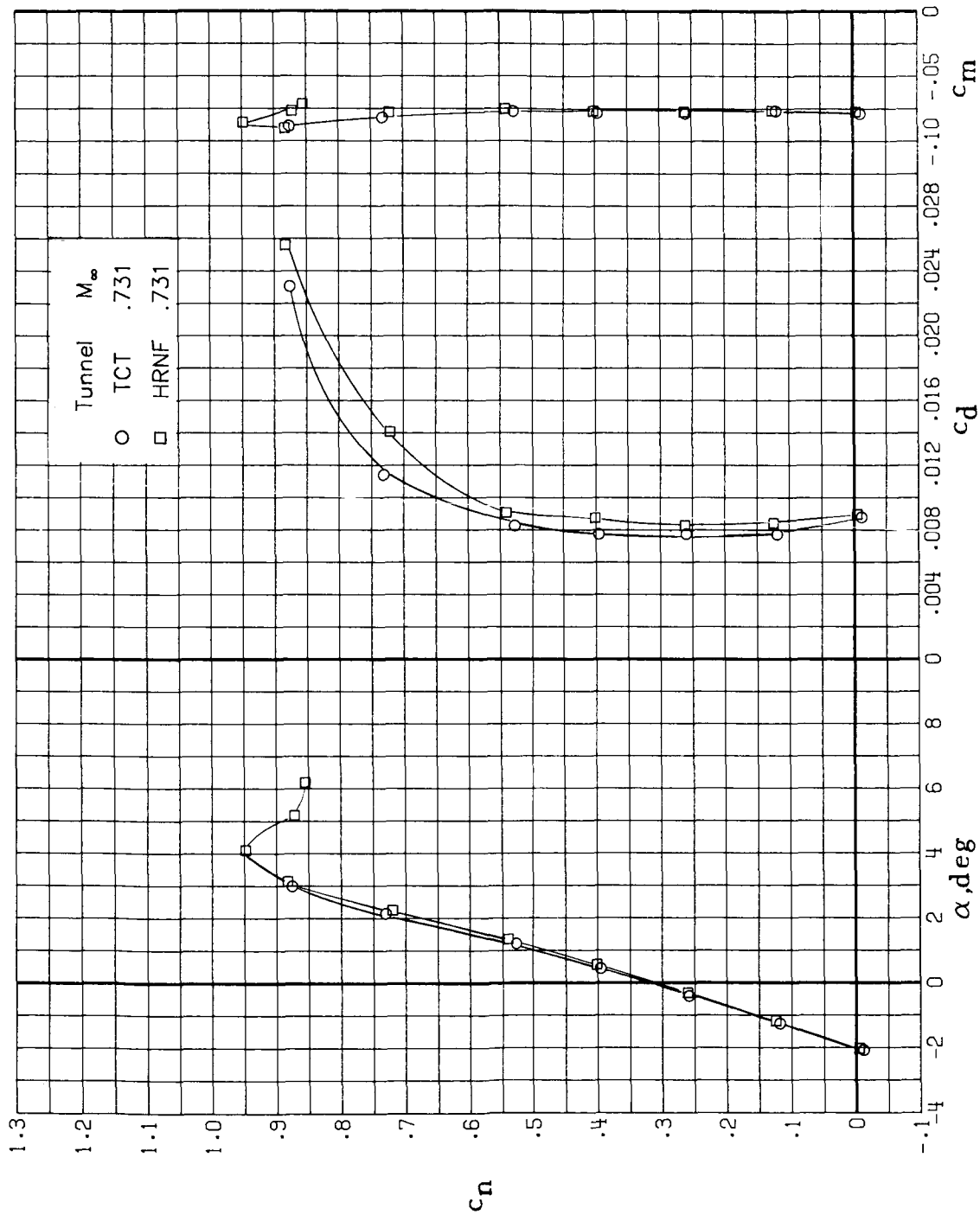

Figure 11. Continued.

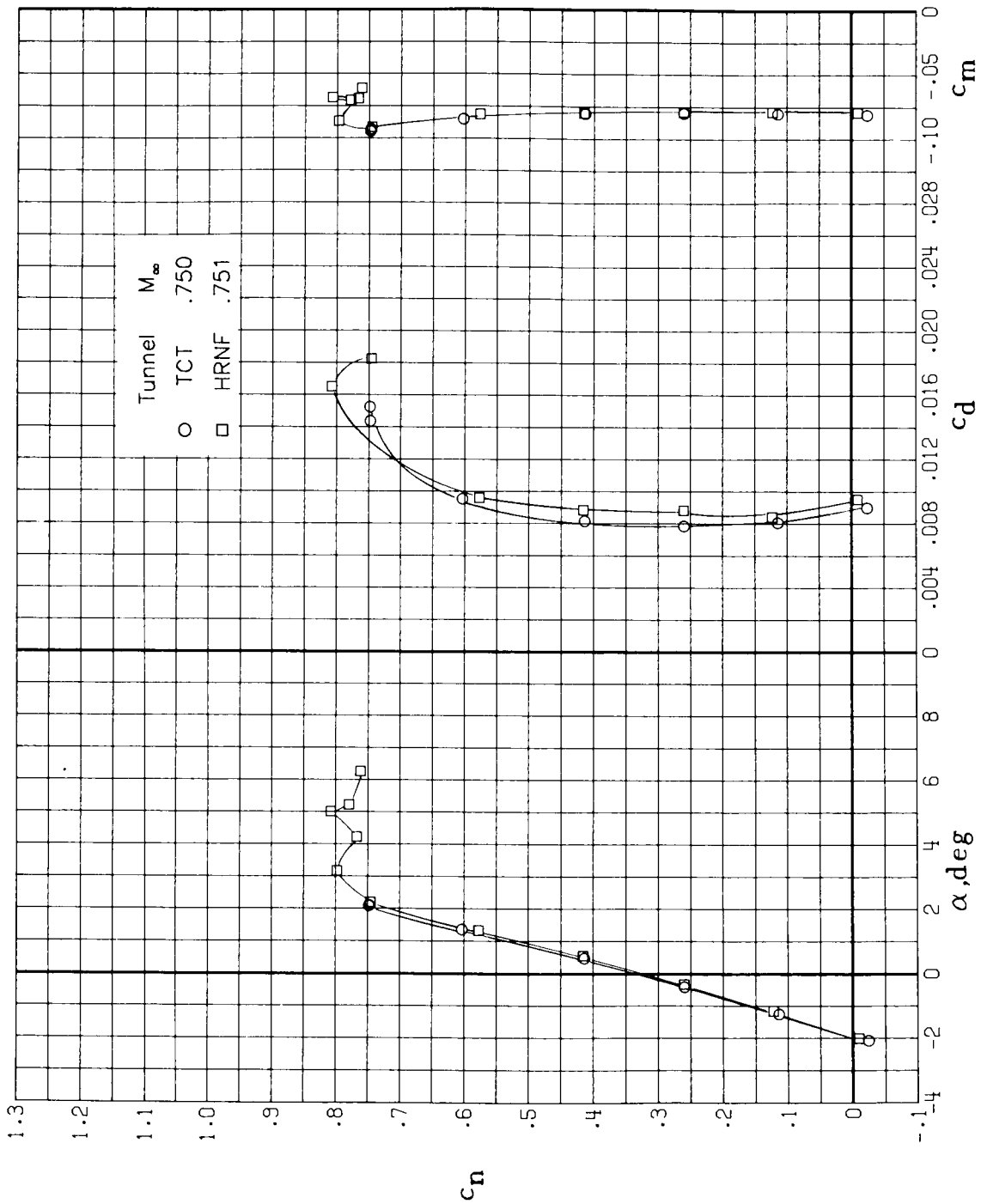

Figure 11. Continued.

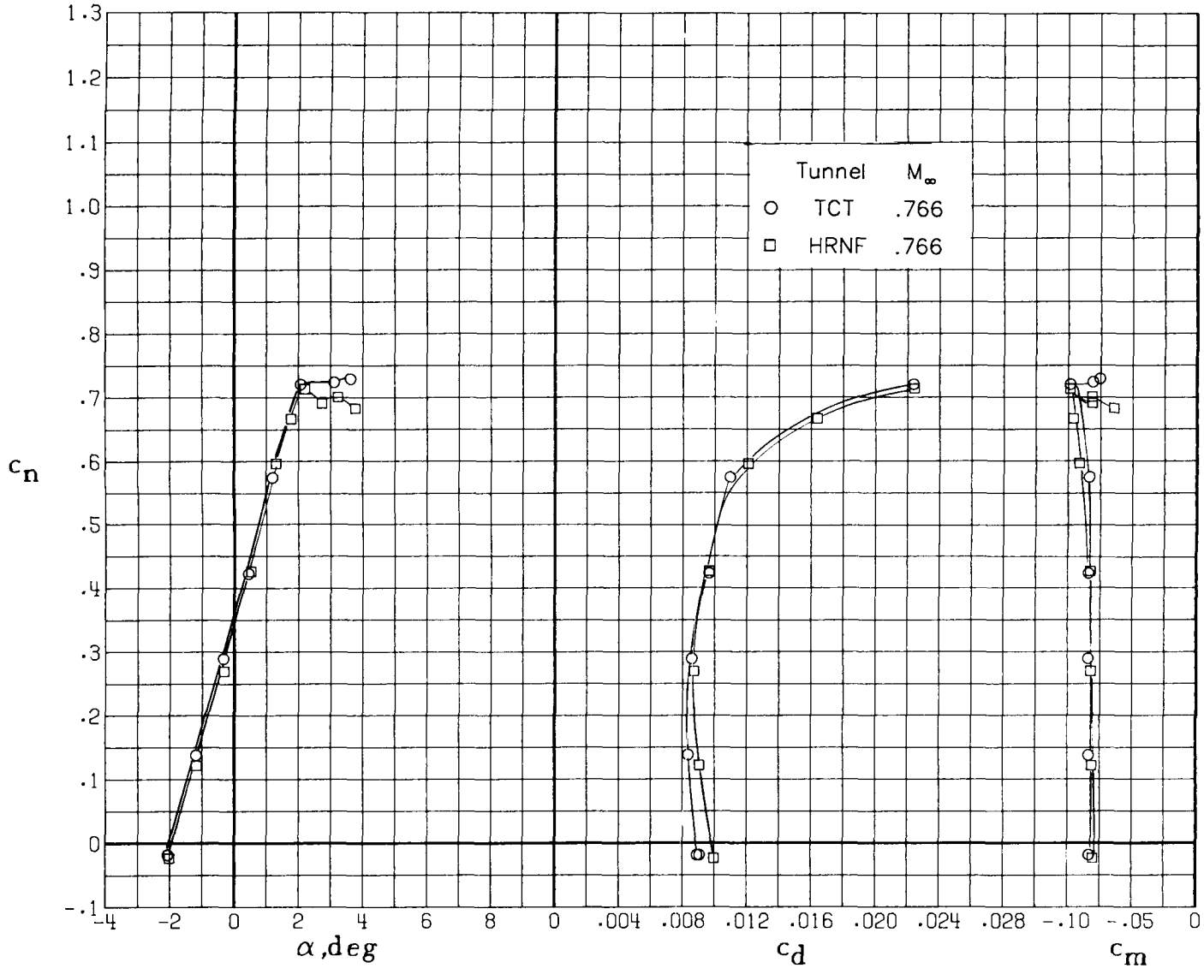

Figure 11. Continued.

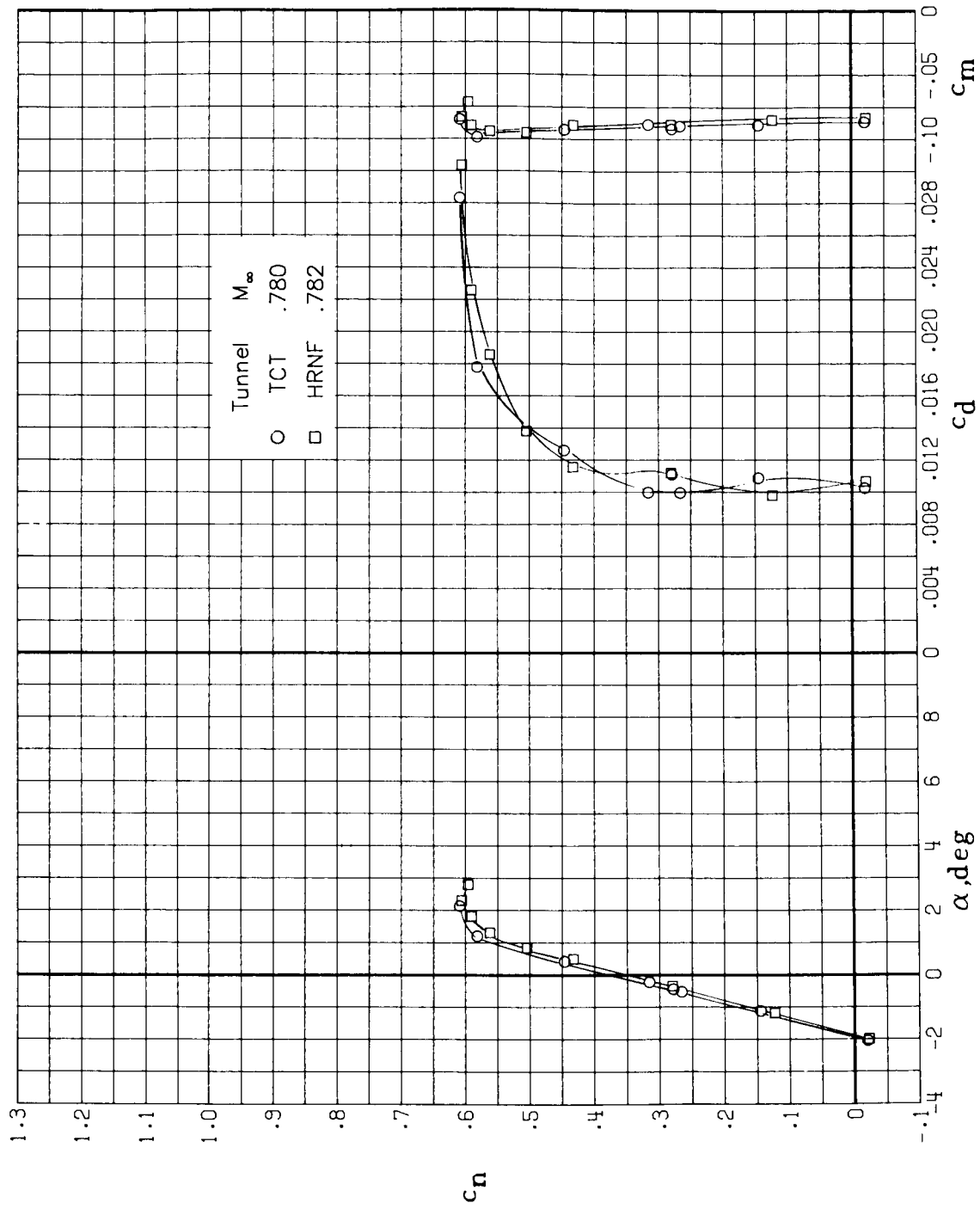

Figure 11. Continued.

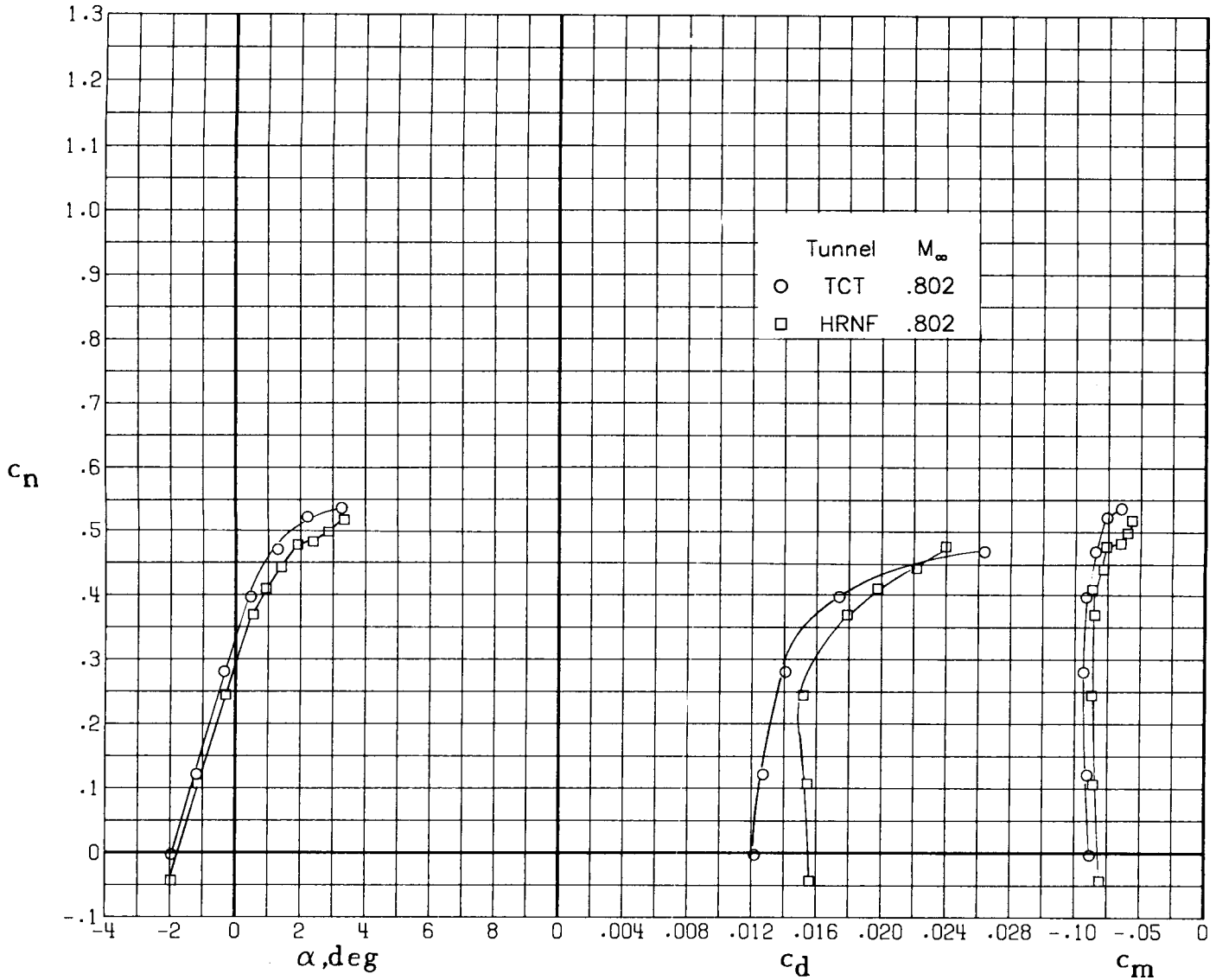

Figure 11. Concluded.

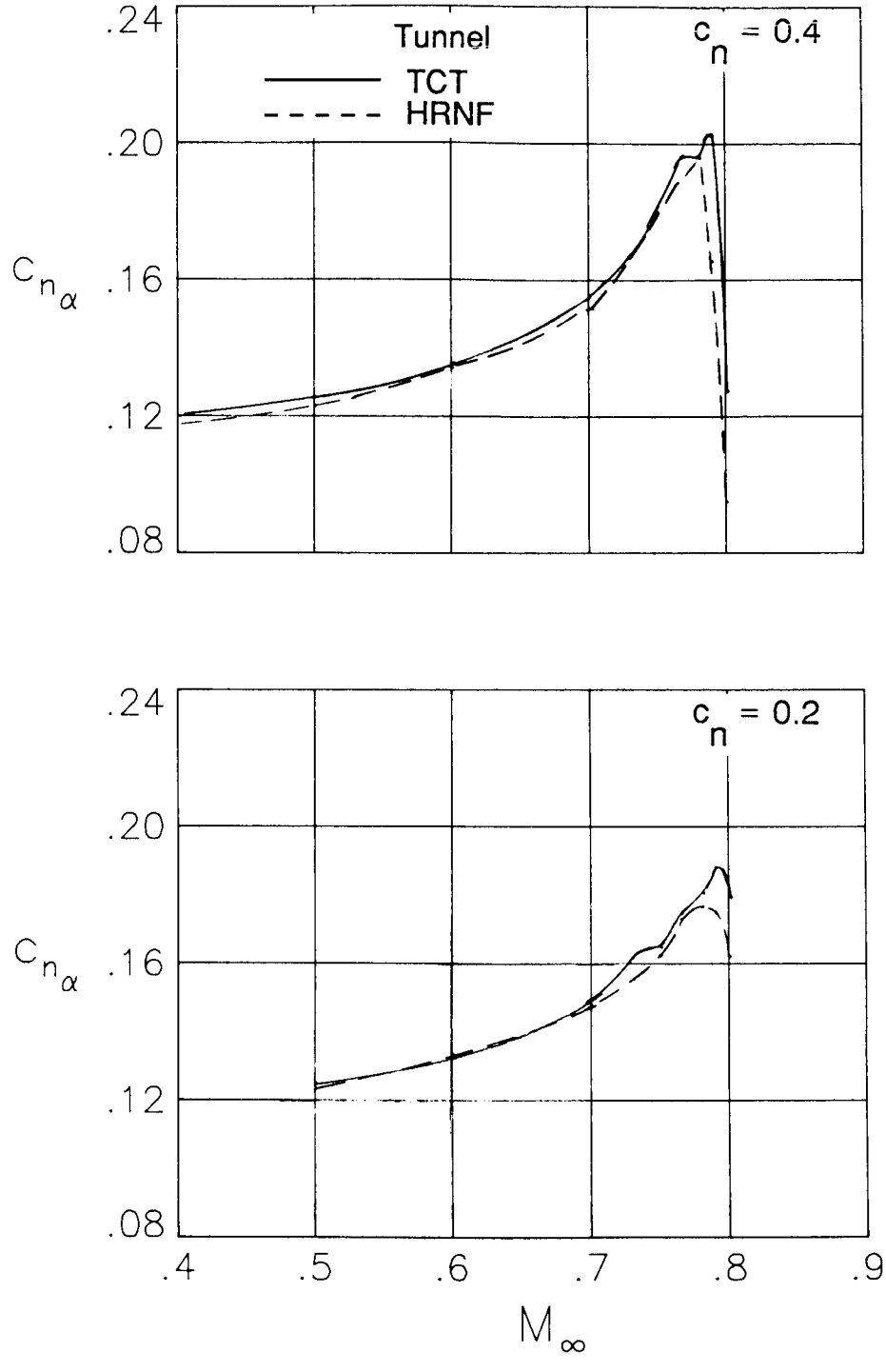

(a) $R_c = 10 \times 10^6$.

Figure 12. Comparison of 0.3-m TCT and HRNF baseline results for slopes of normal-force curves.

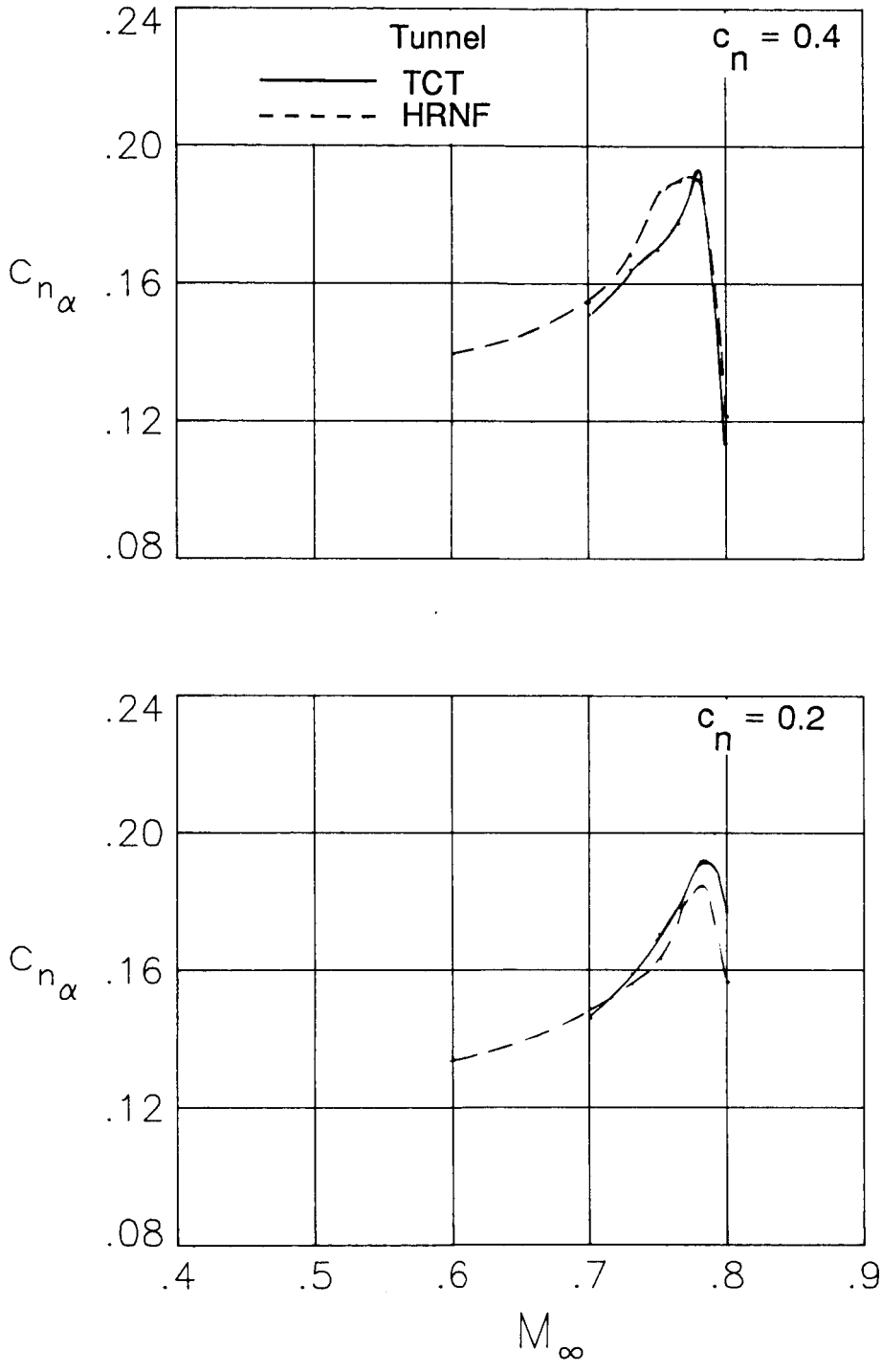

(b) $R_c = 15 \times 10^6$.

Figure 12. Continued.

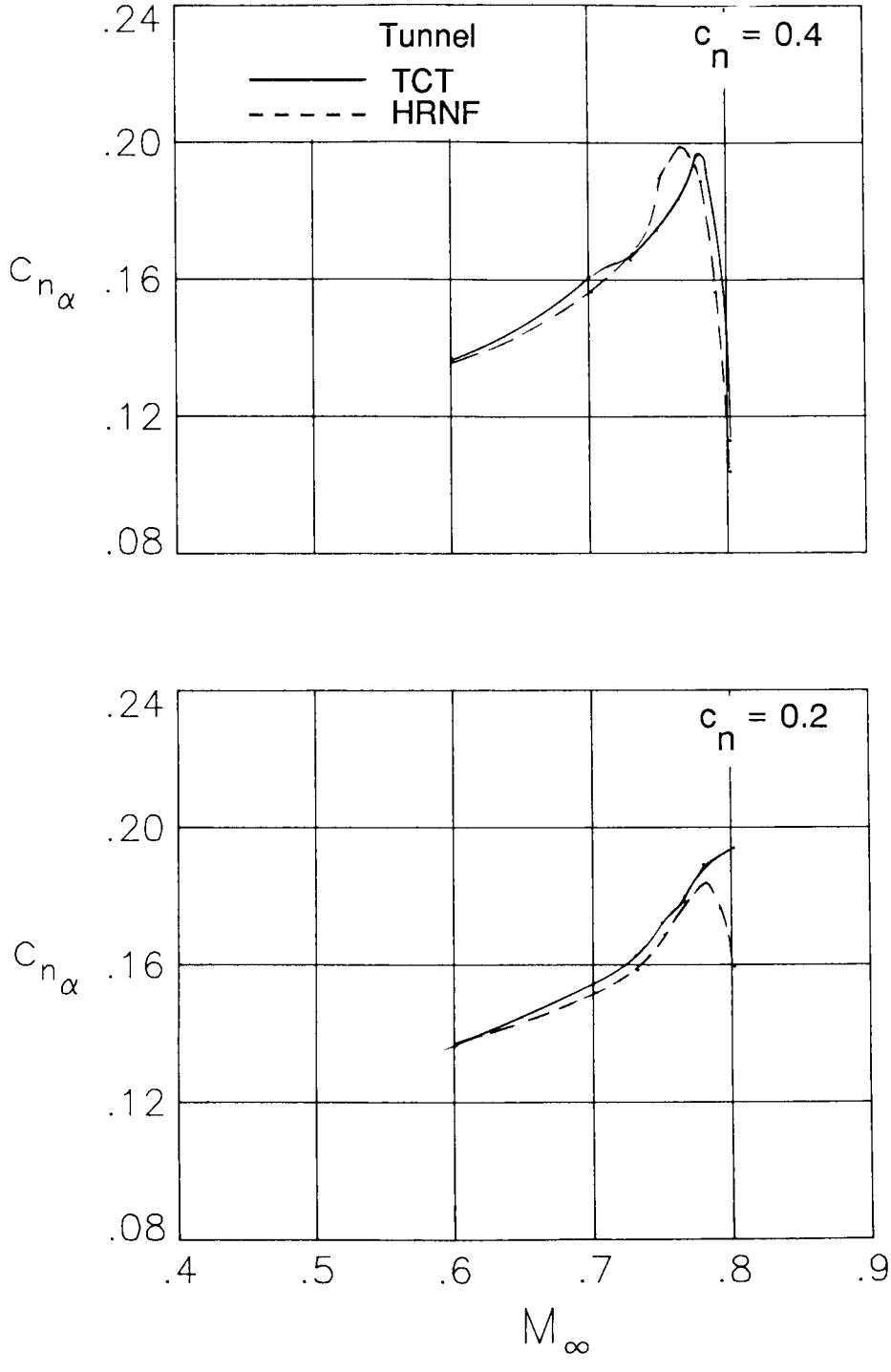

(c) $R_c = 20 \times 10^6$.

Figure 12. Concluded.

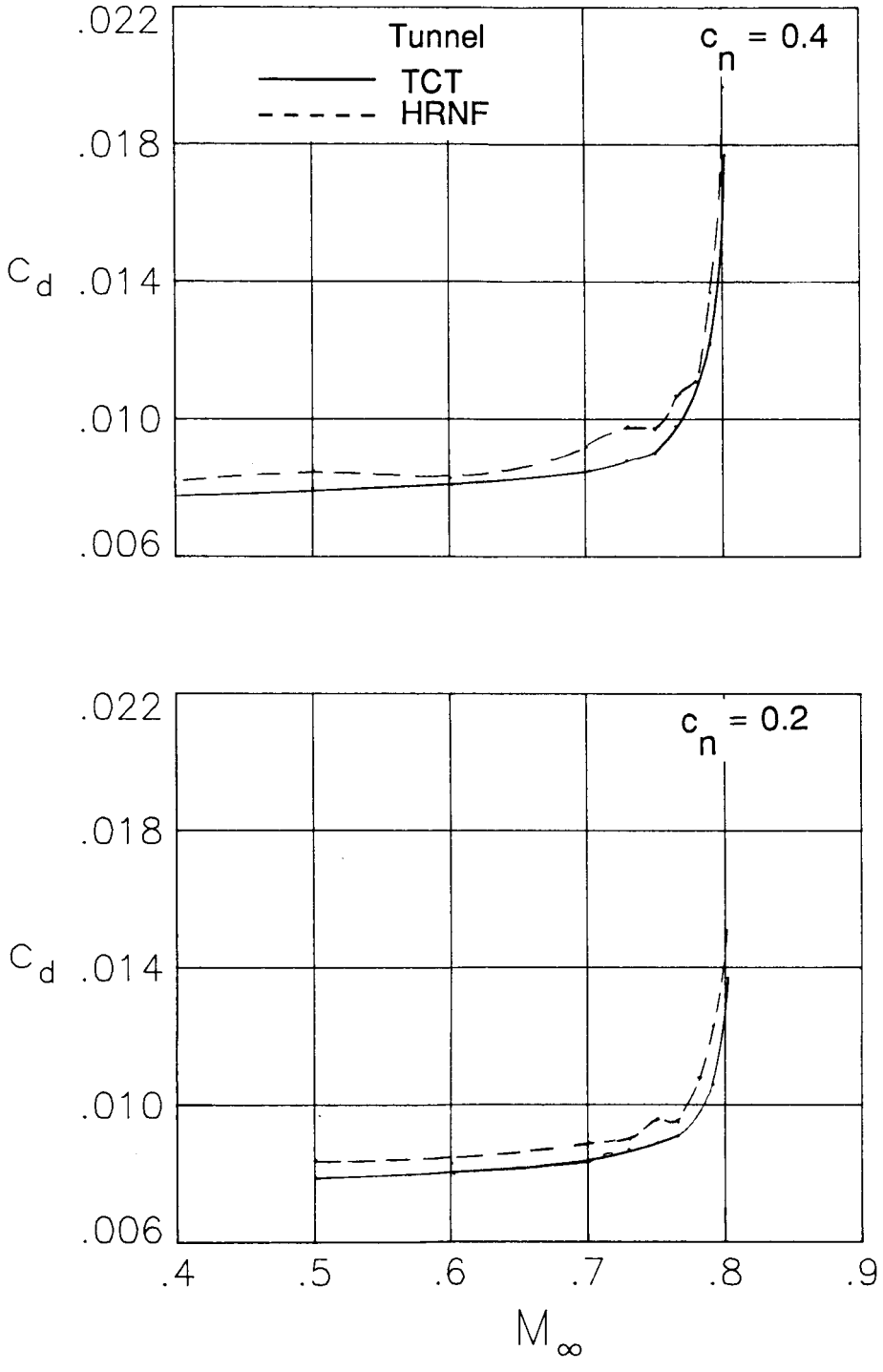

(a) $R_c = 10 \times 10^6$.

Figure 13. Comparison of 0.3-m TCT and HRNF baseline results for drag rise with Mach number.

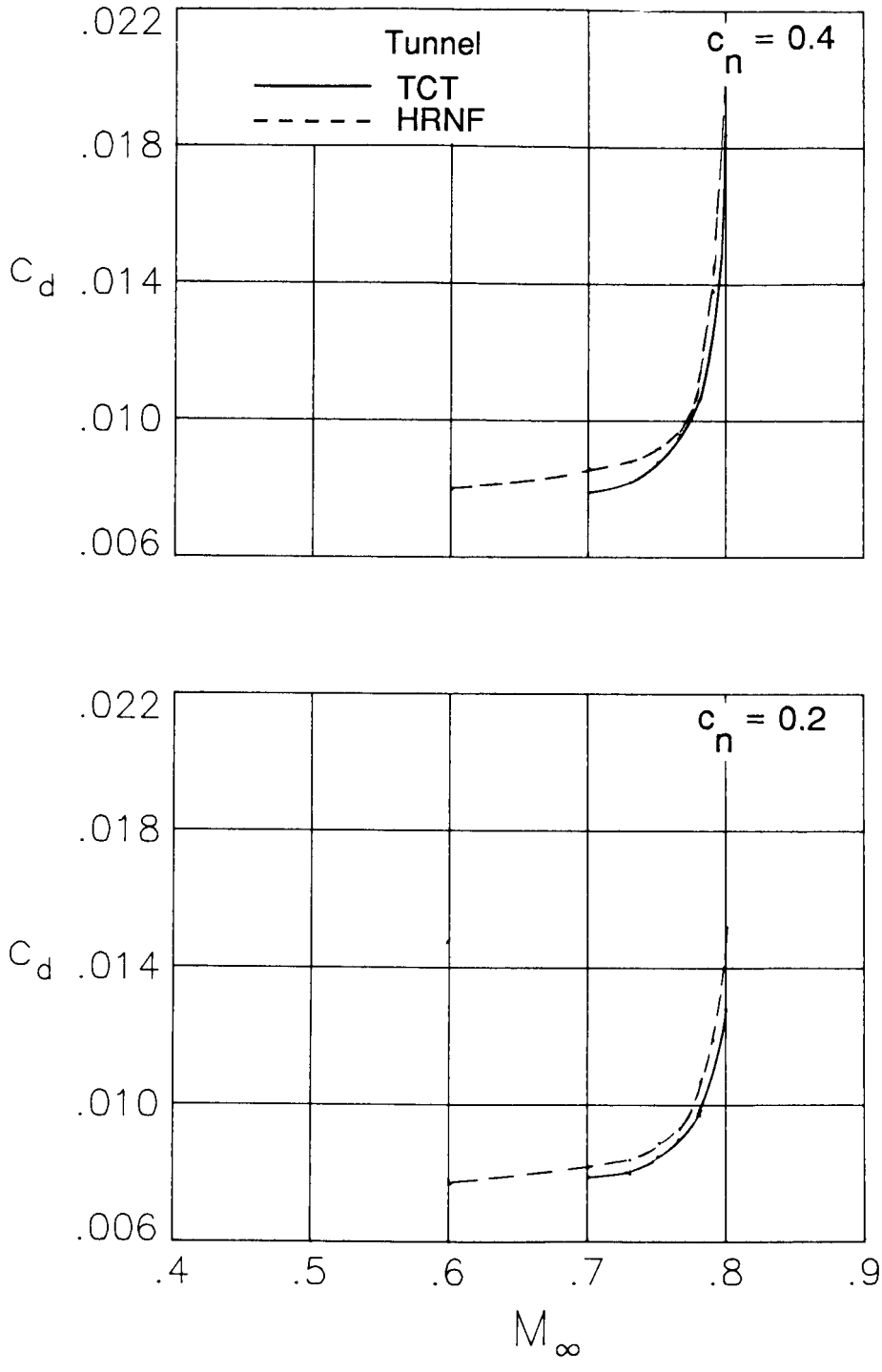

(b) $R_c = 15 \times 10^6$.

Figure 13. Continued.

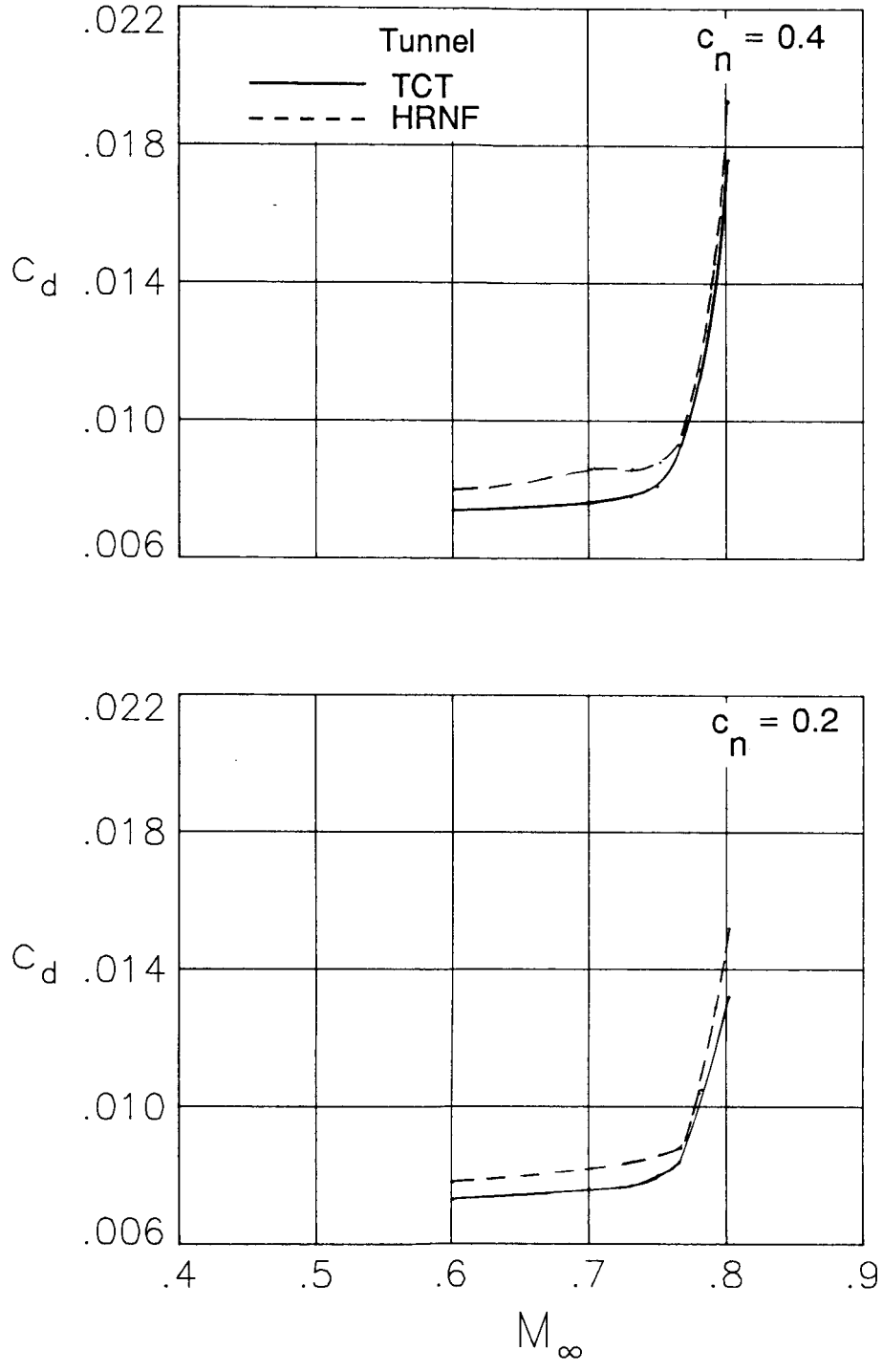

(c) $R_c = 20 \times 10^6$.

Figure 13. Concluded.

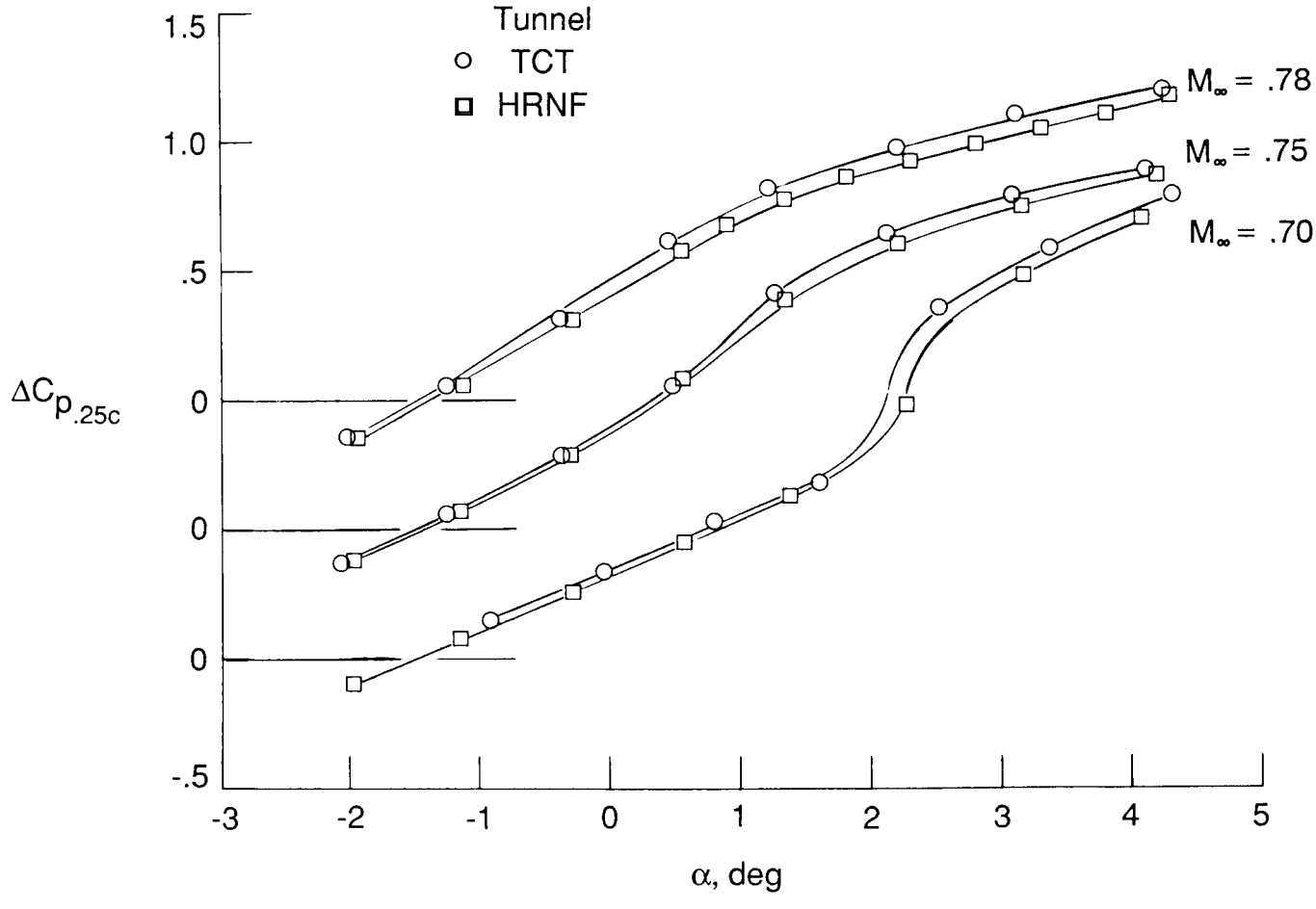

Figure 14. Comparison of 0.3-m TCT and HRNF baseline results for differential pressure coefficient at quarter-chord. $R_c = 10 \times 10^6$.

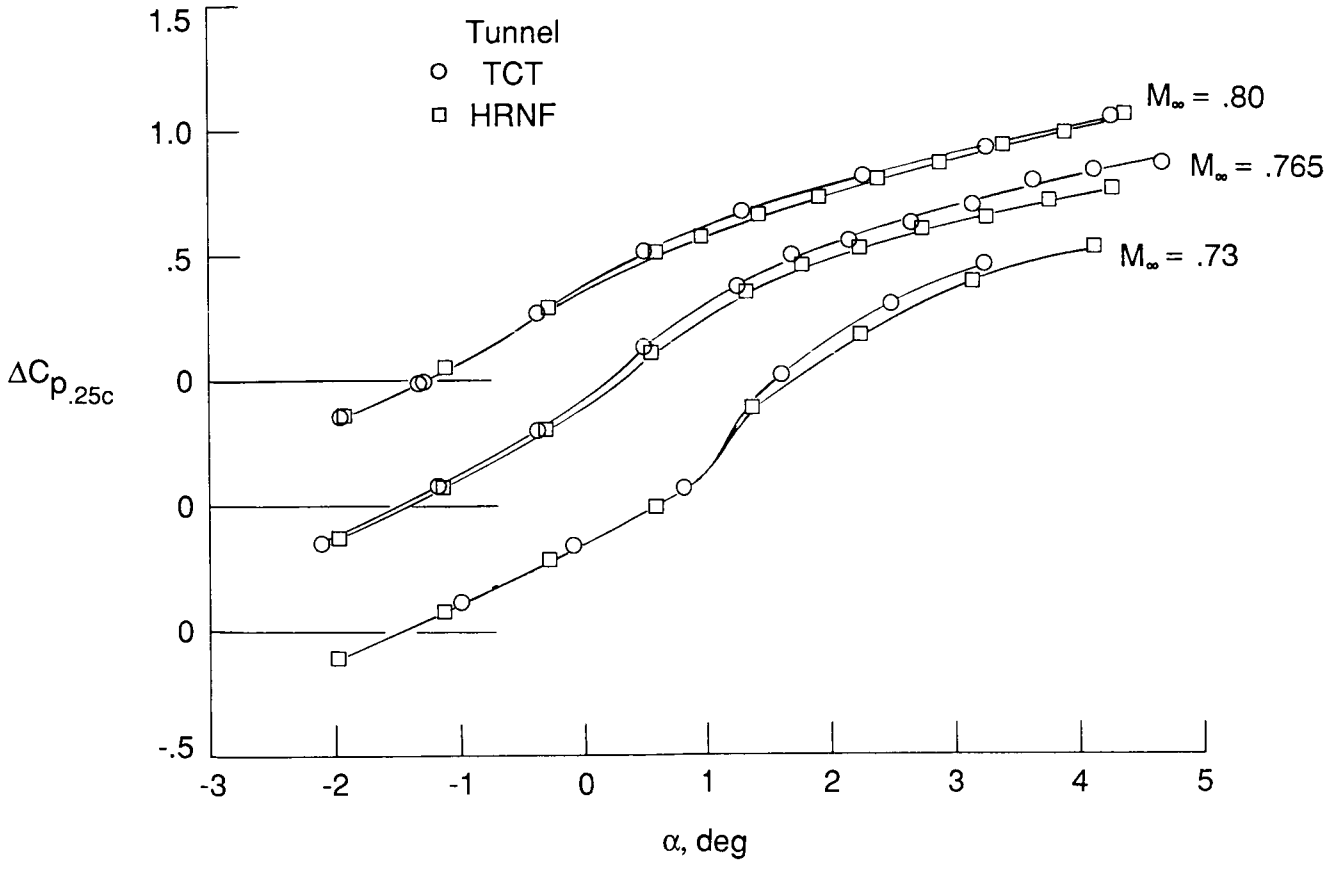

Figure 14. Concluded.

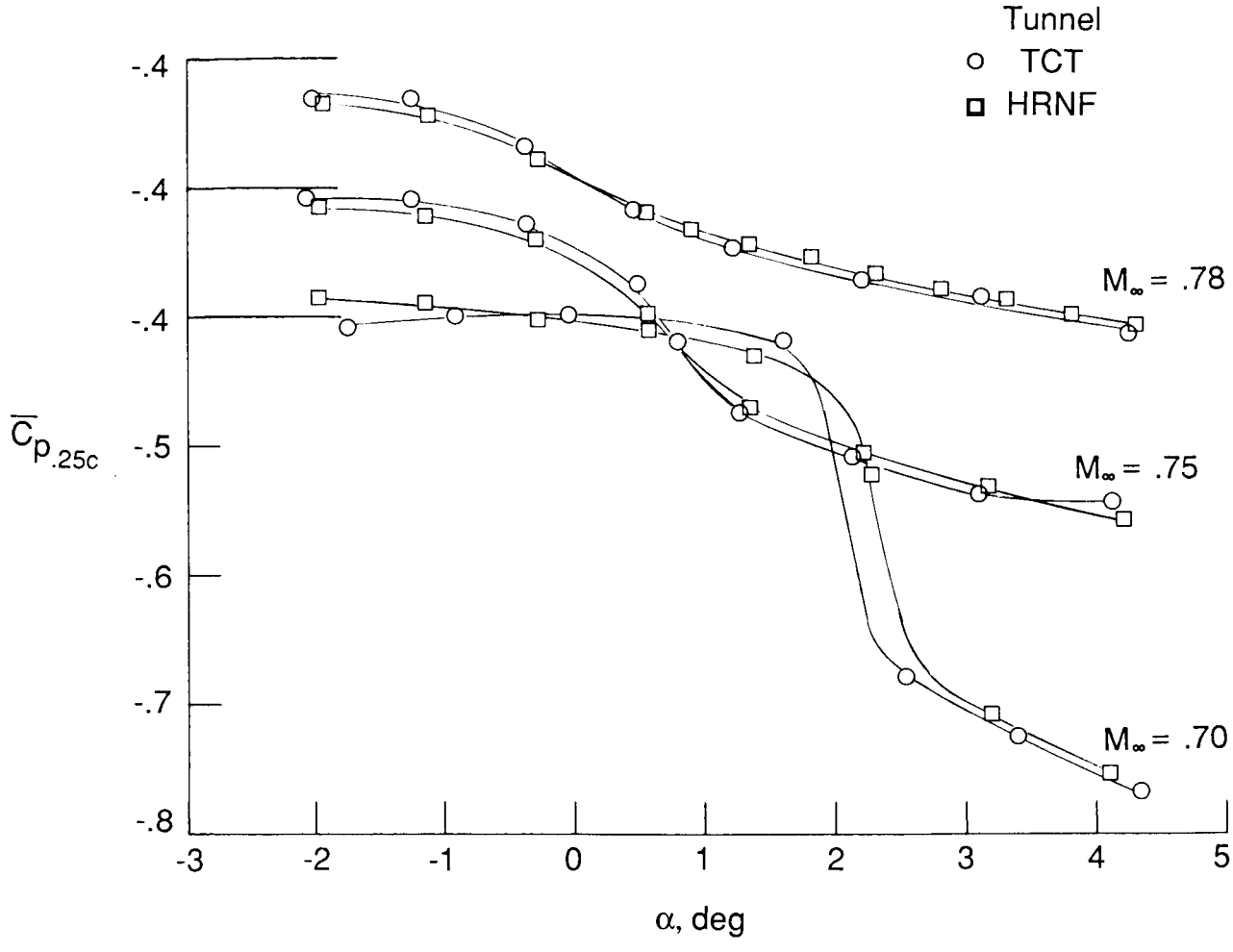

Figure 15. Comparison of 0.3-m TCT and HRNF baseline results for mean pressure coefficient at quarter-chord. $R_c = 10 \times 10^6$.

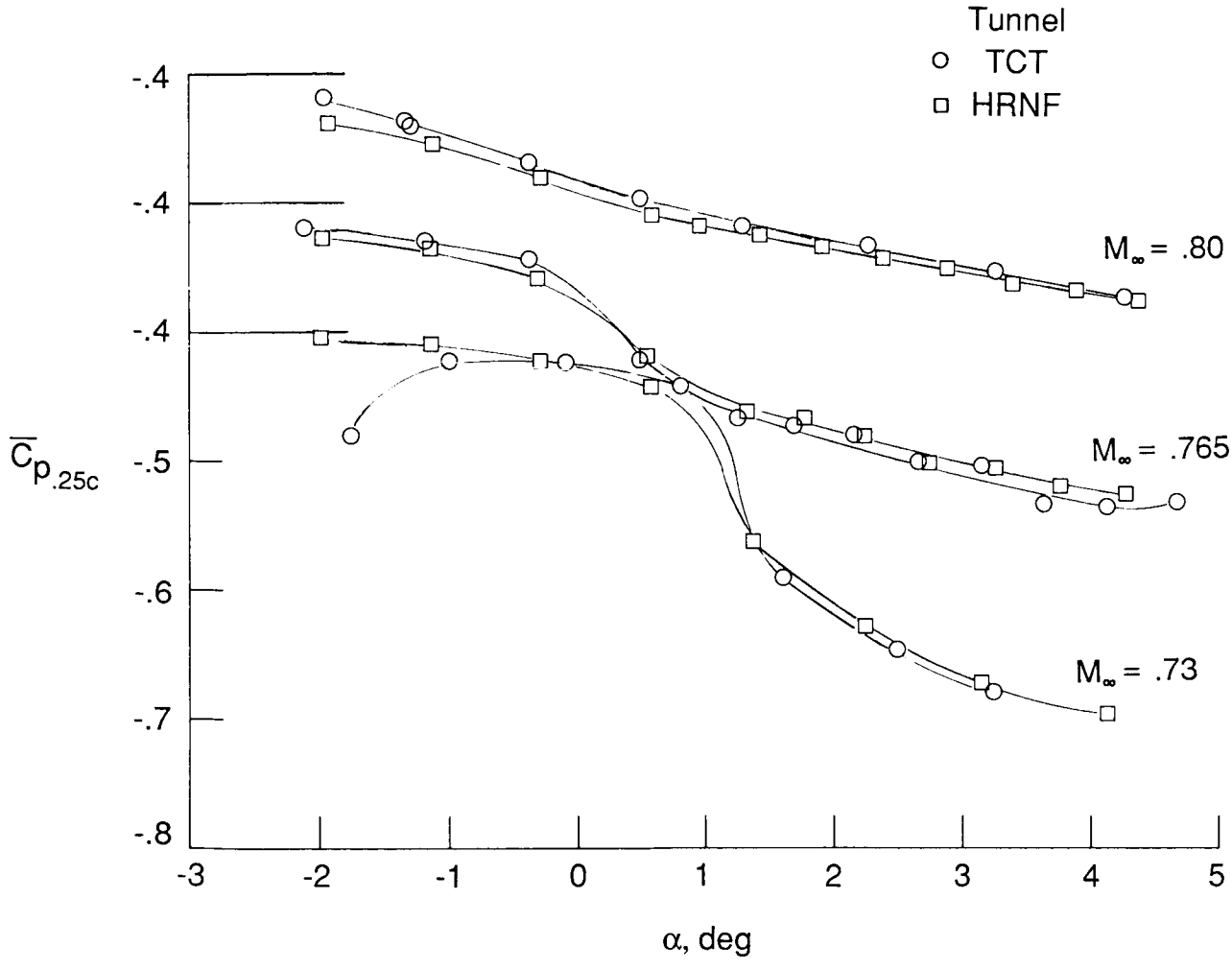

Figure 15. Concluded.

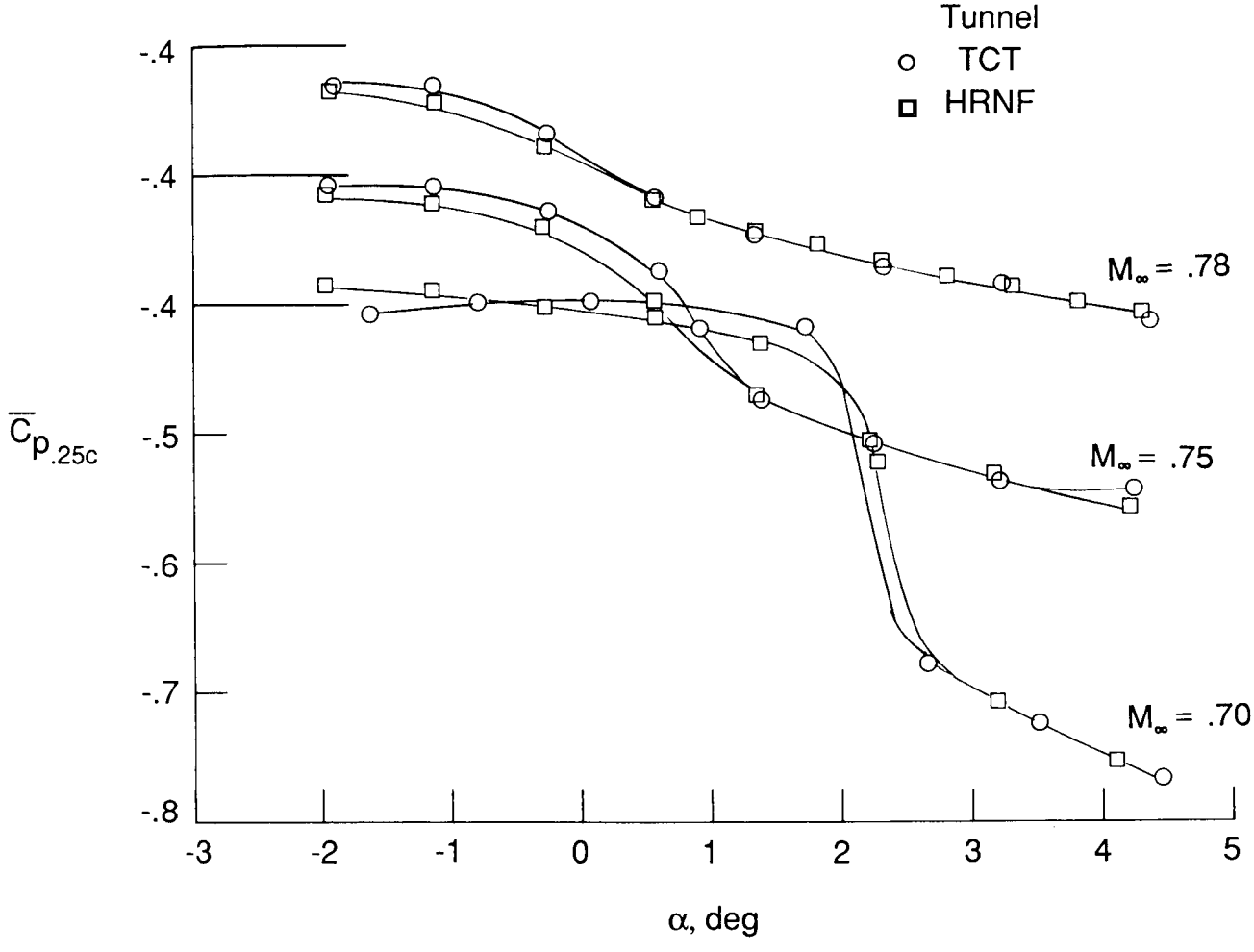

Figure 16. Comparison of 0.3-m TCT and HRNF baseline results for mean pressure coefficient at quarter-chord after TCT angle of attack increased by 0.12°. $R_c = 10 \times 10^6$.

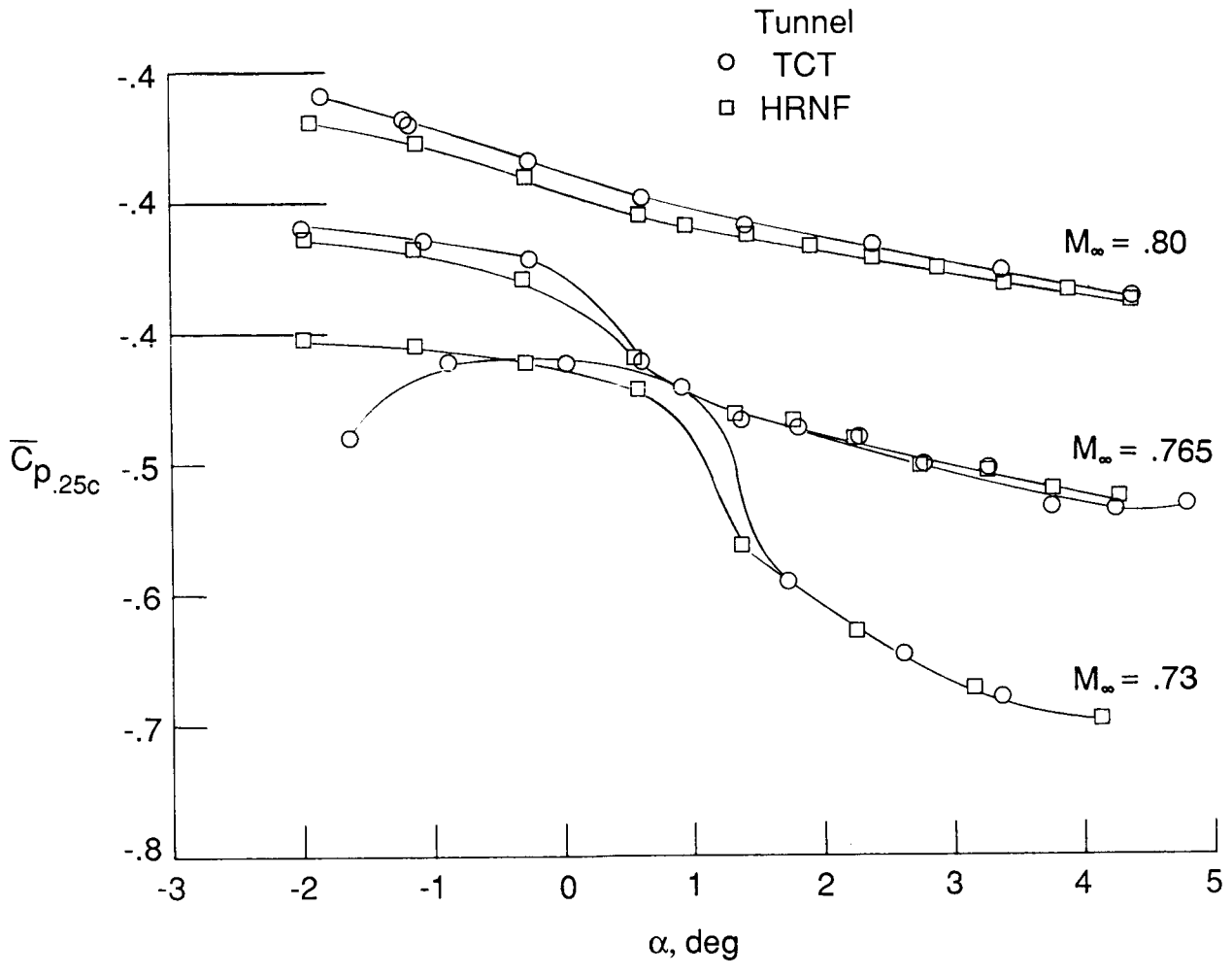

Figure 16. Concluded.

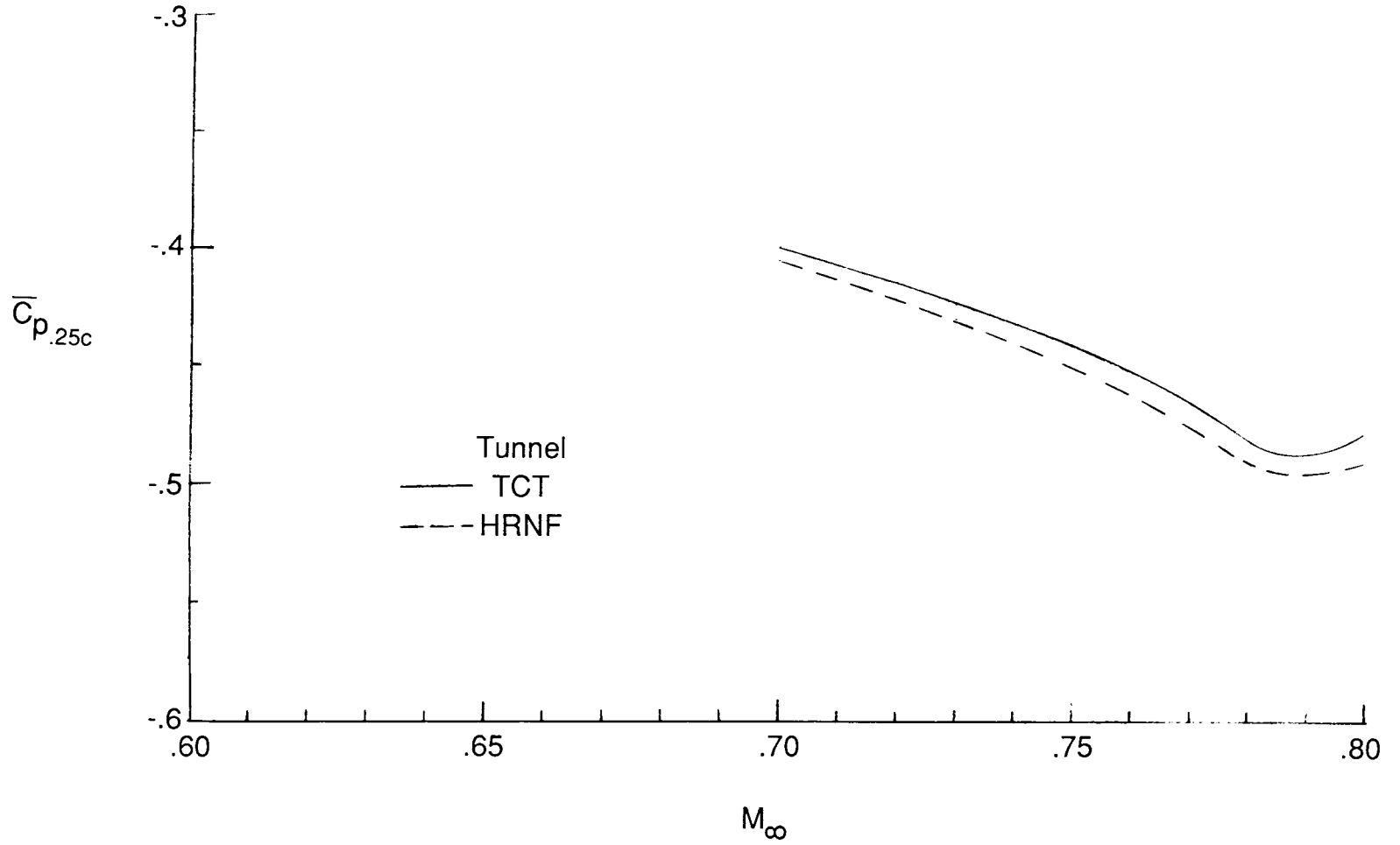

Figure 17. Variation of 0.3-m TCT and HRNF baseline results for mean pressure coefficient at quarter-chord with Mach number. The 0.3-m TCT angle of attack increased by 0.12°; $R_c = 10 \times 10^6$; $\alpha = 0°$.

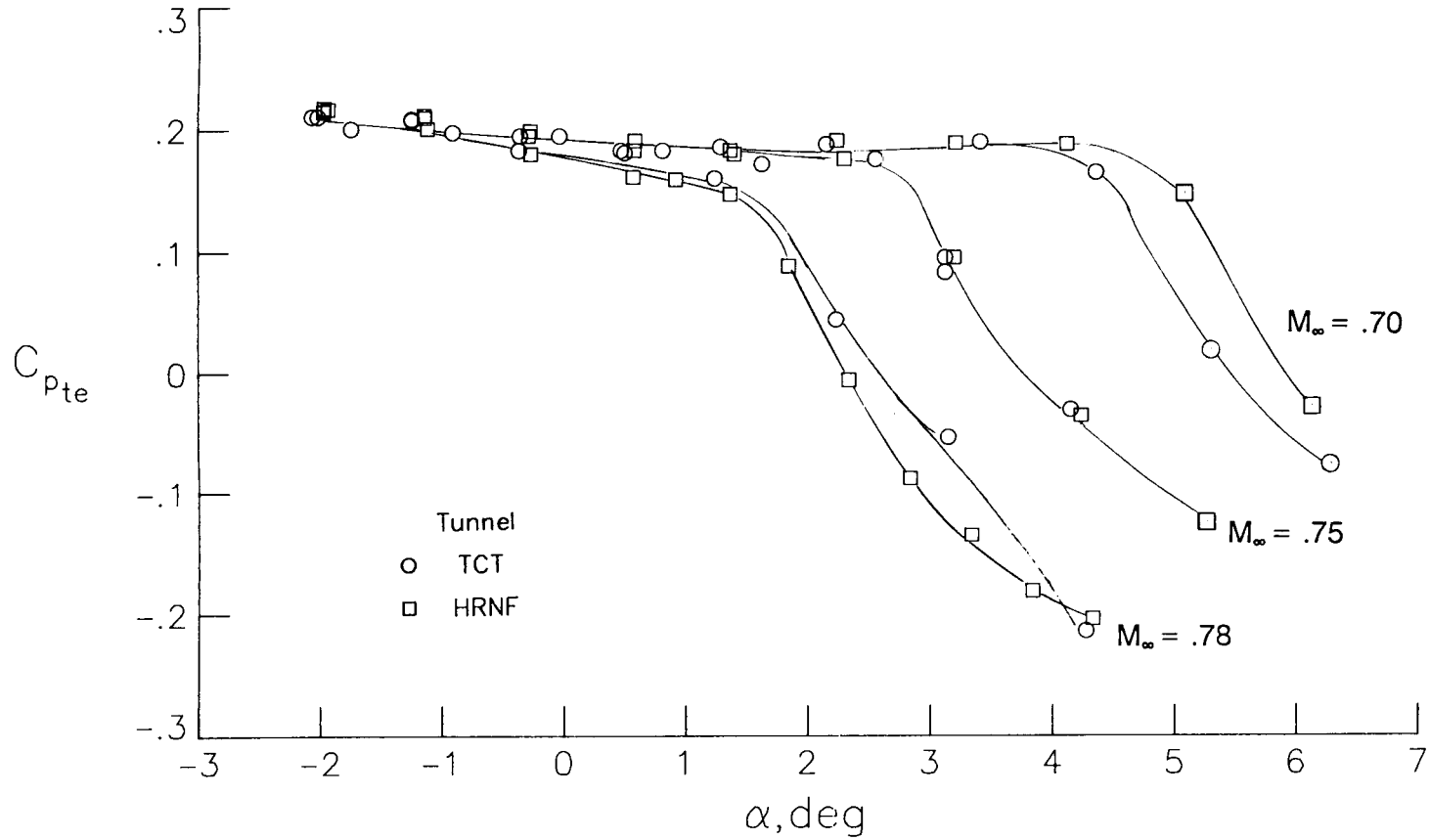

Figure 18. Comparison of 0.3-m TCT and HRNF baseline results for trailing-edge pressure coefficient. $R_c = 10 \times 10^6$.

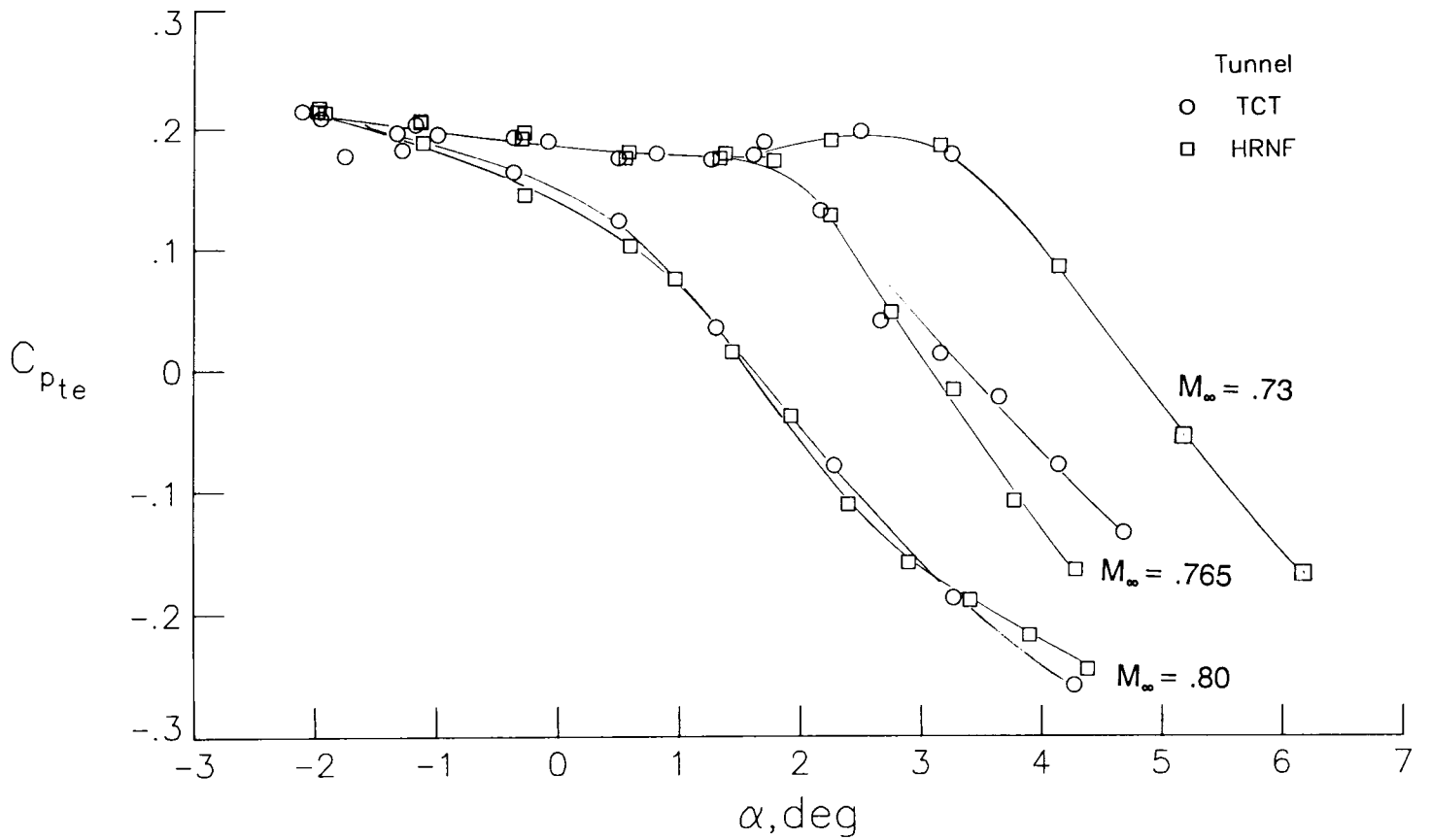

Figure 18. Concluded.

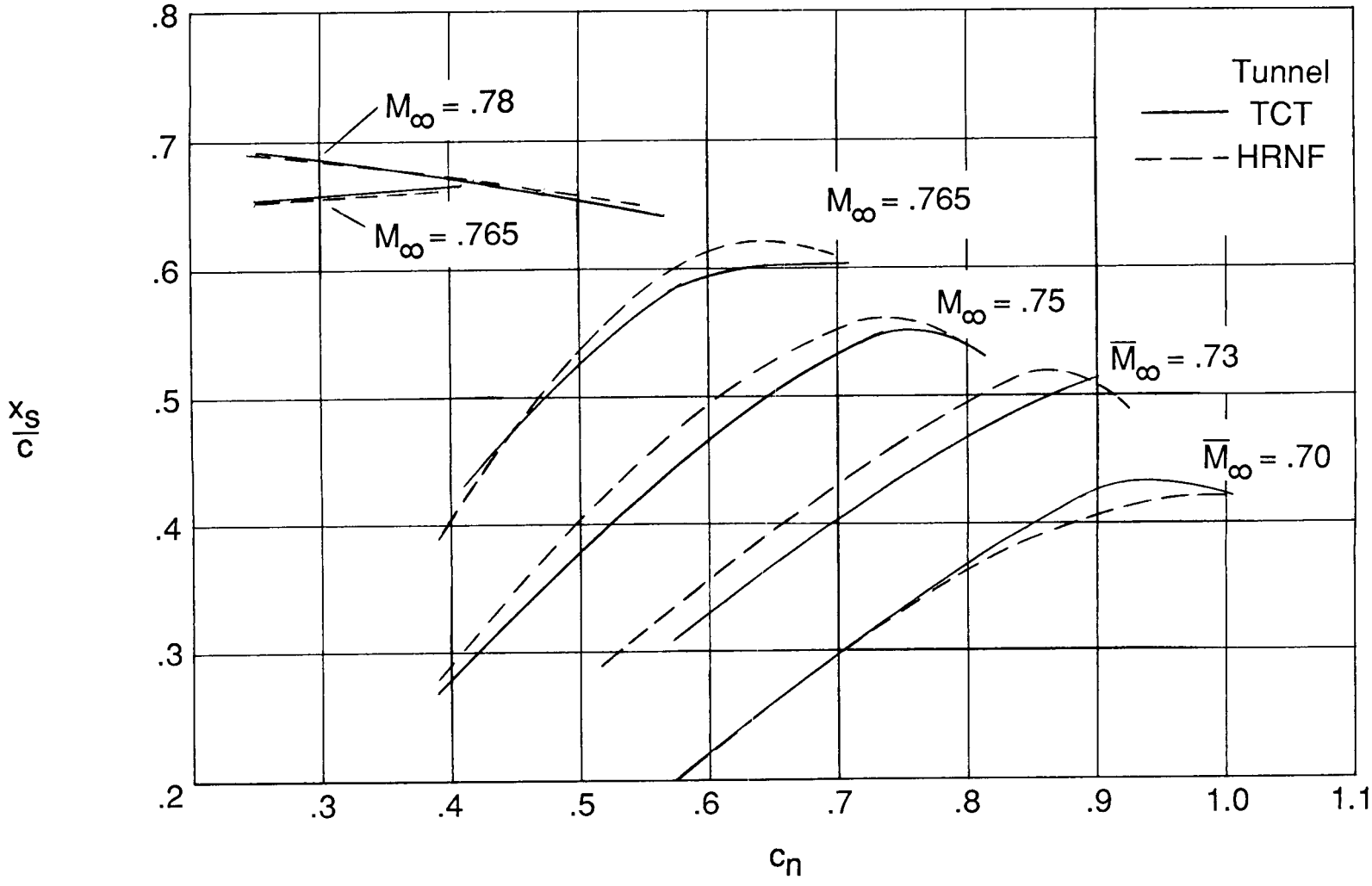

Figure 19. Comparison of 0.3-m TCT and HRNF baseline results for upper-surface shock position. $R_c = 10 \times 10^6$.

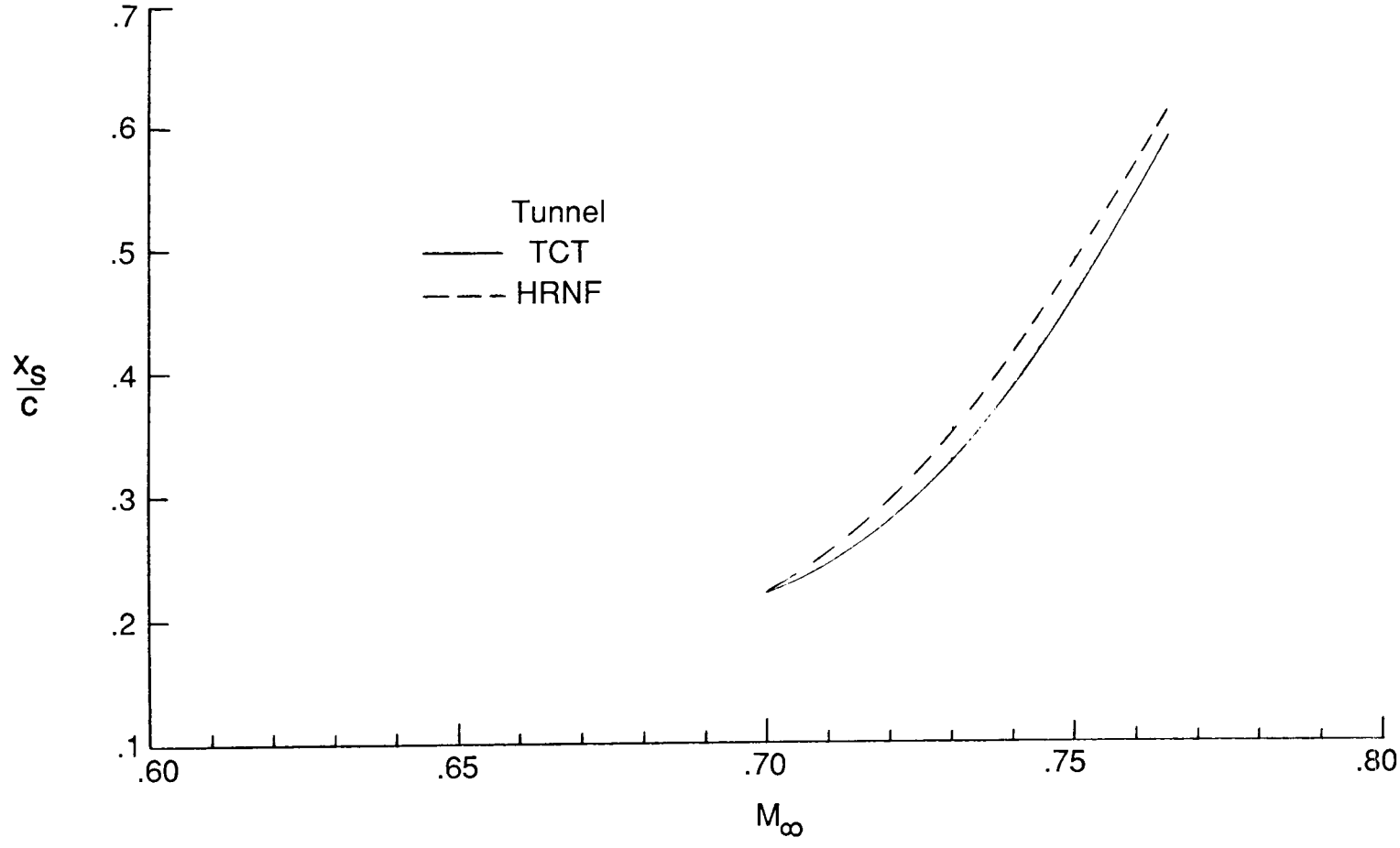

Figure 20. Variation of 0.3-m TCT and HRNF baseline results for upper-surface shock position with Mach number. $c_n = 0.6$; $R_c = 10 \times 10^6$.

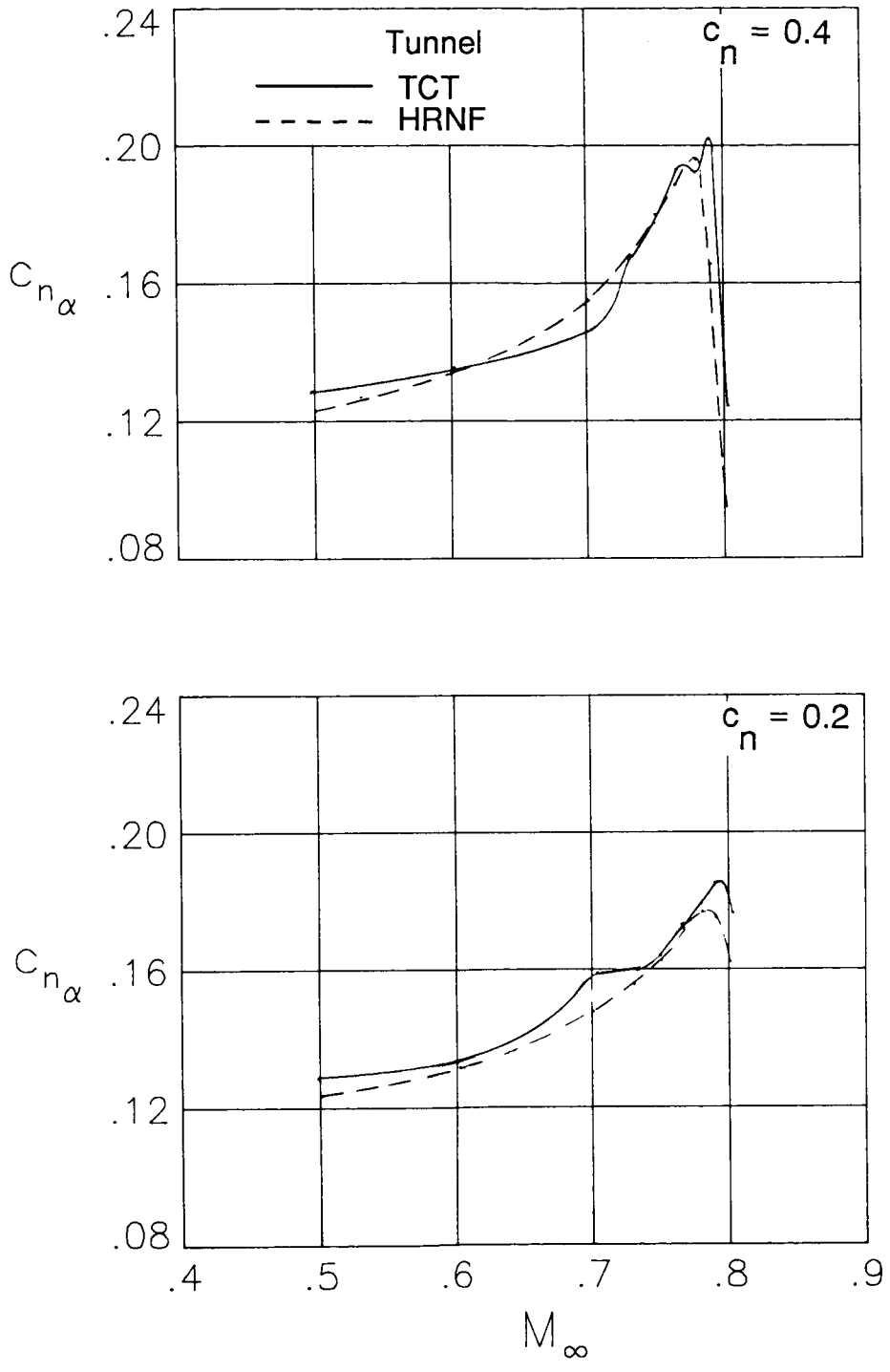

Figure 21. Comparison of 0.3-m TCT two-wall corrected results and HRNF baseline results for slopes of normal-force curves. $R_c = 10 \times 10^6$.

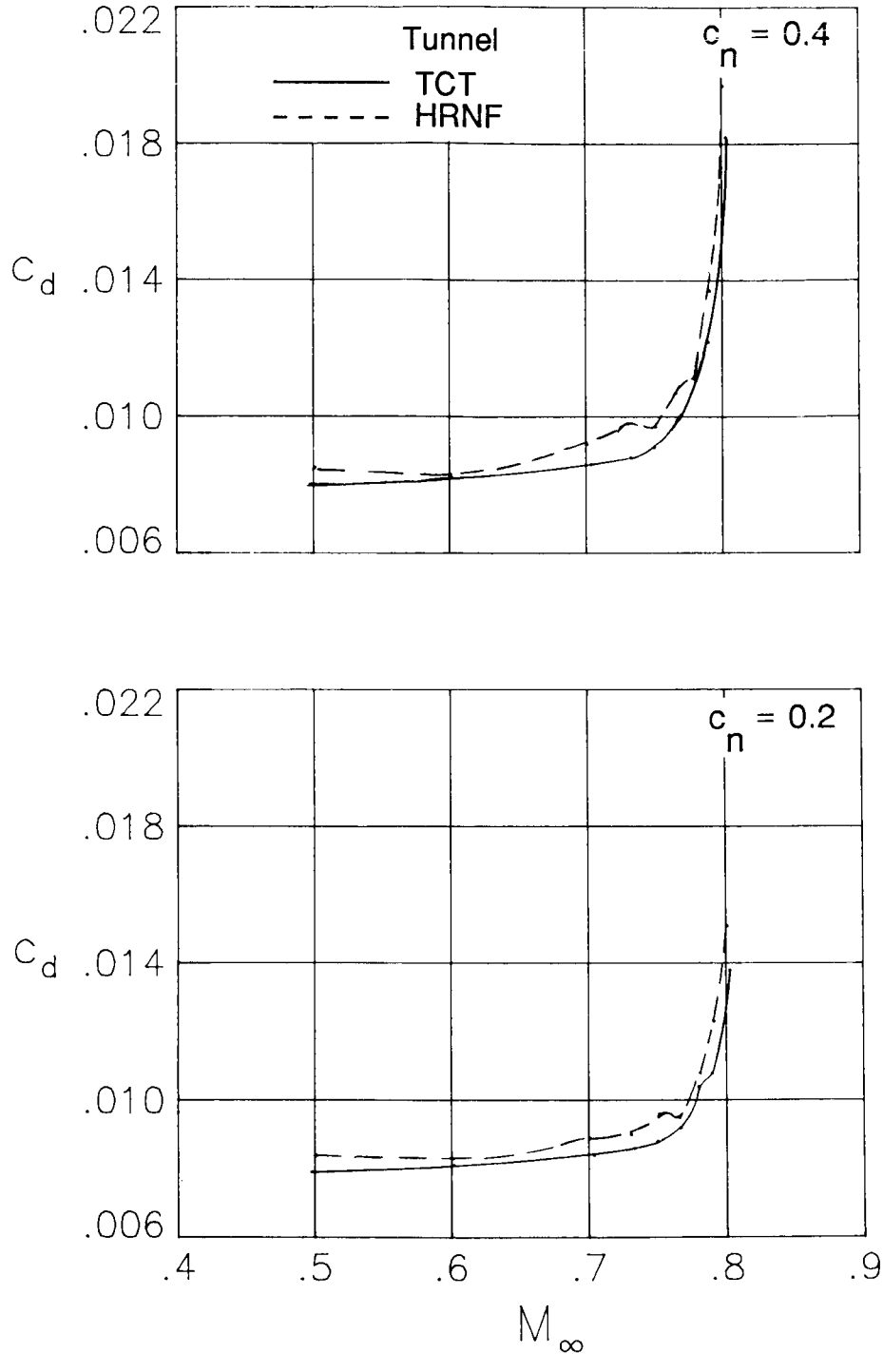

Figure 22. Comparison of 0.3-m TCT two-wall corrected results and HRNF baseline results for drag rise with Mach number. $R_c = 10 \times 10^6$.

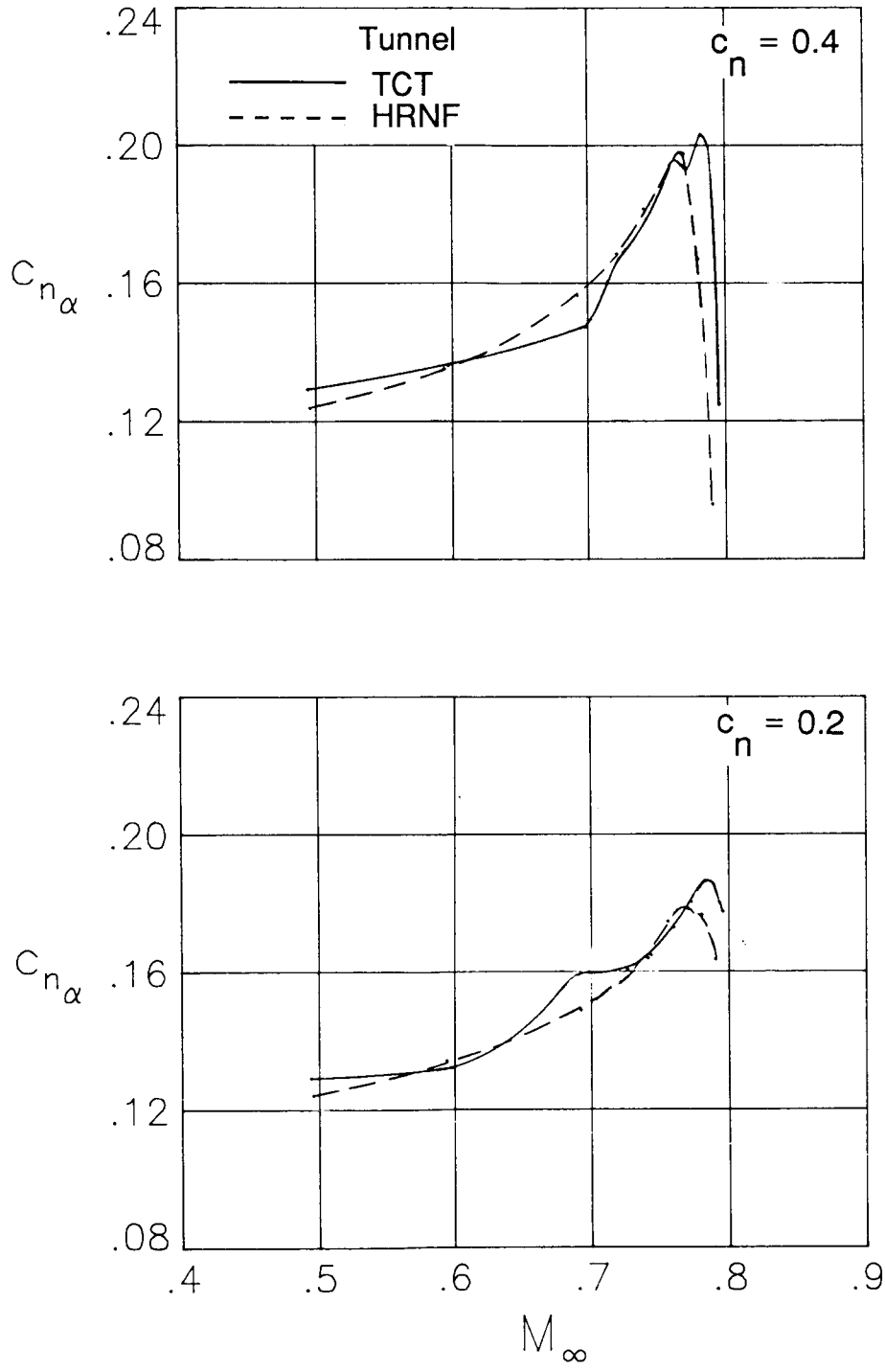

Figure 23. Comparison of 0.3-m TCT four-wall corrected results and HRNF four-wall corrected results for slopes of normal-force curves. $R_c = 10 \times 10^6$.

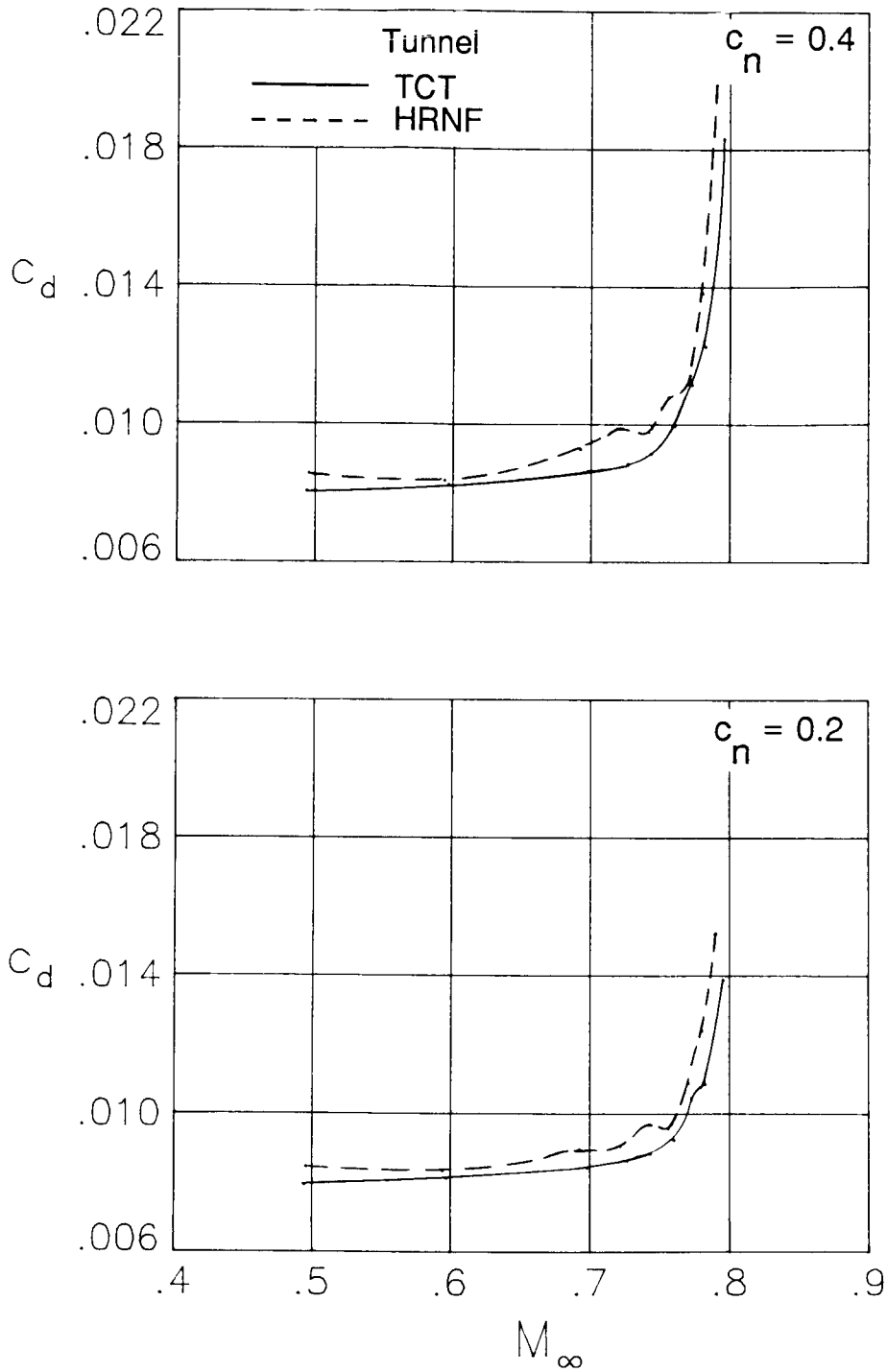

Figure 24. Comparison of 0.3-m TCT four-wall corrected results and HRNF four-wall corrected results for drag rise with Mach number. $R_c = 10 \times 10^6$.

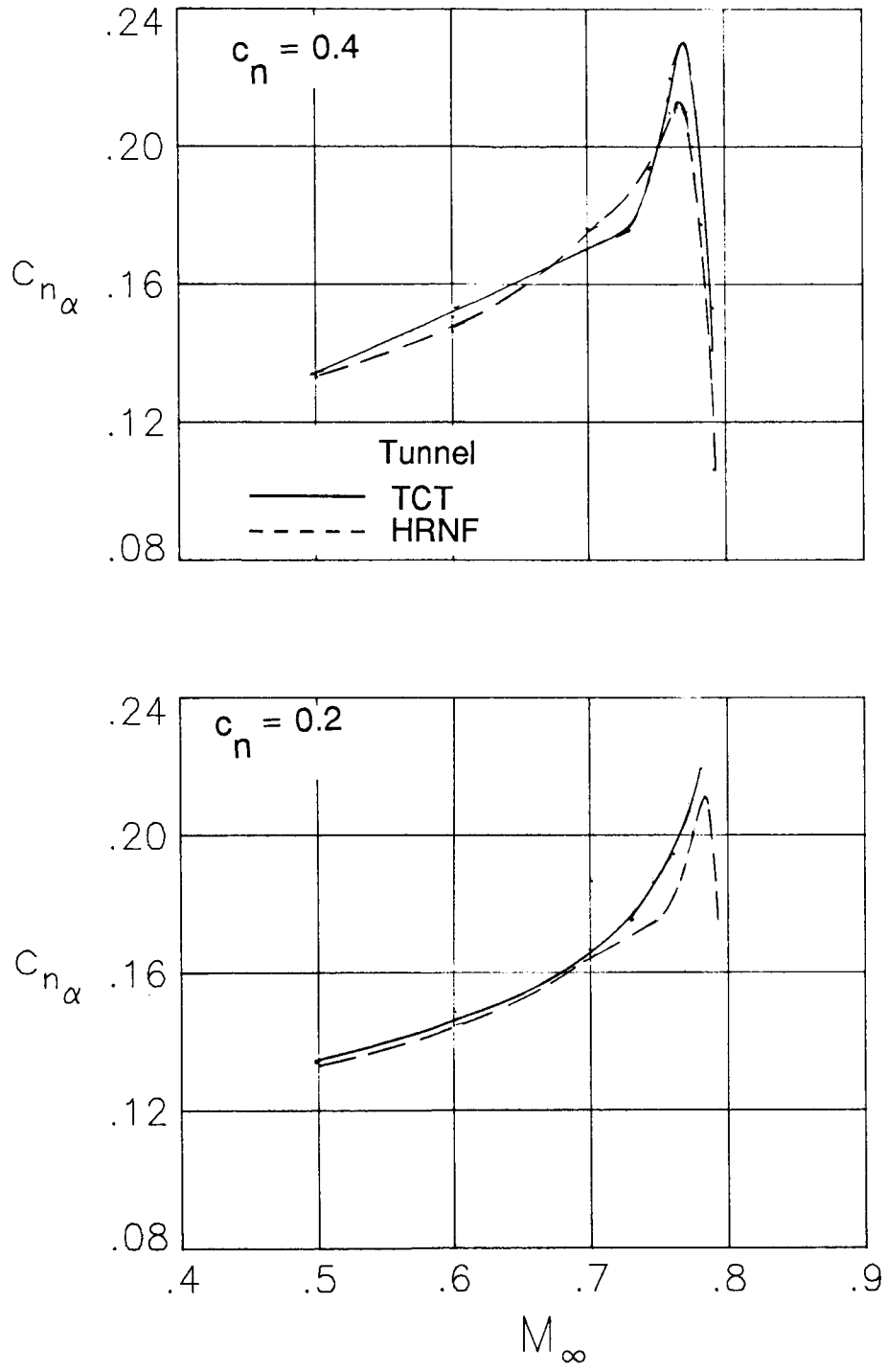

Figure 25. Comparison of 0.3-m TCT and HRNF unified, four-wall corrected results for slopes of normal-force curves. $R_c = 10 \times 10^6$.

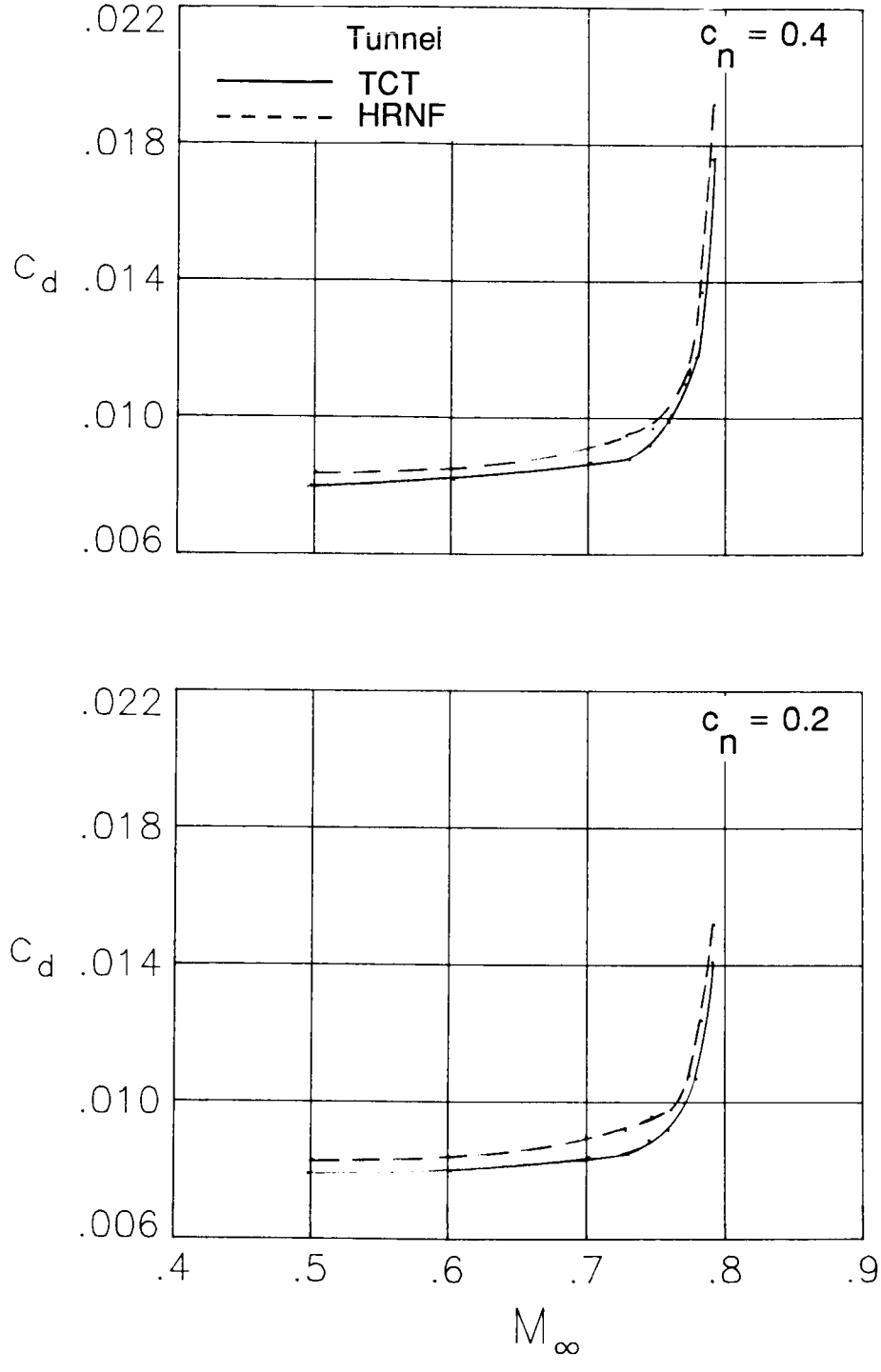

Figure 26. Comparison of 0.3-m TCT and HRNF unified, four-wall corrected results for drag rise with Mach number. $R_c = 10 \times 10^6$.

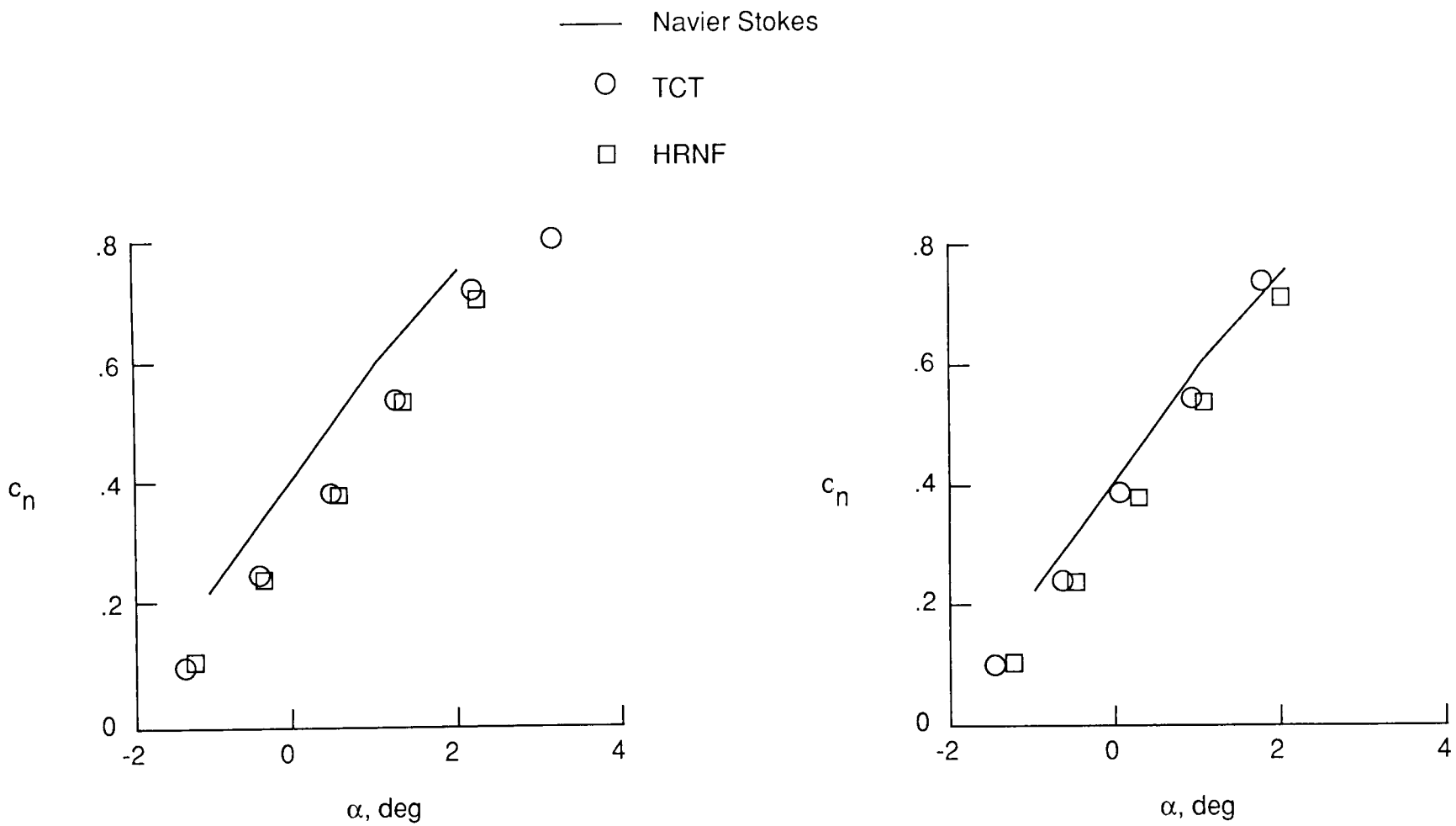

Figure 27. Comparison of experimental results and Navier-Stokes calculations. $M = 0.75$; $R_c = 10 \times 10^6$ (from ref. 19).

Comparisons of the chordwise pressure distributions at nearly the same normal-force coefficient and Mach number are presented in a "Supplement to NASA TP-3132."

Copies of this "Supplement to NASA TP-3132" will be furnished upon request. Requests for the supplement should be addressed to:

NASA Center for AeroSpace Information
P.O. Box 8757
Baltimore/Washington International Airport, Maryland 21240

Cut

- -

Date______________________

Please forward "Supplement to NASA TP-3132" to

____
Name of organization

____
Street number

____
City and State Zip code

Attention: ____
Name

____
Title

REPORT DOCUMENTATION PAGE

Form Approved
OMB No. 0704-0188

1. AGENCY USE ONLY *(Leave blank)*	2. REPORT DATE	3. REPORT TYPE AND DATES COVERED
	April 1992	Technical Paper

4. TITLE AND SUBTITLE
Comparison of a Two-Dimensional Adaptive-Wall Technique With Analytical Wall Interference Correction Techniques

5. FUNDING NUMBERS
WU 505-59-10-03

6. AUTHOR(S)
Raymond E. Mineck

7. PERFORMING ORGANIZATION NAME(S) AND ADDRESS(ES)
NASA Langley Research Center
Hampton, VA 23665-5225

8. PERFORMING ORGANIZATION REPORT NUMBER
L-16911

9. SPONSORING/MONITORING AGENCY NAME(S) AND ADDRESS(ES)
National Aeronautics and Space Administration
Washington, DC 20546-0001

10. SPONSORING/MONITORING AGENCY REPORT NUMBER
NASA TP-3132

11. SUPPLEMENTARY NOTES
Comparisons of the chordwise pressure distributions at nearly the same normal-force coefficient and Mach number are presented in a "Supplement to NASA TP-3132."

12a. DISTRIBUTION/AVAILABILITY STATEMENT
Unclassified Unlimited

Subject Category 02

12b. DISTRIBUTION CODE

13. ABSTRACT *(Maximum 200 words)*
A two-dimensional airfoil model has been tested in the adaptive-wall test section of the NASA Langley 0.3-Meter Transonic Cryogenic Tunnel (TCT) and in the ventilated test section of the National Aeronautical Establishment Two-Dimensional High Reynolds Number Facility (HRNF). The primary goal of the tests was to compare different techniques to account for wall interference: adaptive test section walls and classical, analytical corrections. Tests were conducted over a Mach number range from 0.3 to 0.8 at chord Reynolds numbers of 10×10^6, 15×10^6, and 20×10^6. The angle of attack was varied from about -2° up to stall. Movement of the top and bottom test section walls was used to account for the wall interference in the 0.3-m TCT tests and a classical analytical correction technique was used to account for the wall interference in the HRNF tests. The test results are in good agreement.

14. SUBJECT TERMS
Adaptive-wall test section; 2-D airfoil testing; Wall interference

15. NUMBER OF PAGES
70

16. PRICE CODE
A04

17. SECURITY CLASSIFICATION OF REPORT	18. SECURITY CLASSIFICATION OF THIS PAGE	19. SECURITY CLASSIFICATION OF ABSTRACT	20. LIMITATION OF ABSTRACT
Unclassified	Unclassified		

NSN 7540-01-280-5500

Standard Form 298(Rev. 2-89)
Prescribed by ANSI Std. Z39-18
298-102

NASA-Langley, 1992

National Aeronautics and
Space Administration
Code JTT
Washington, D.C.
20546-0001
Official Business
Penalty for Private Use, $300

BULK RATE
POSTAGE & FEES PAID
NASA
Permit No. G-27

AFSCLO
MS221

NASA

POSTMASTER: If Undeliverable (Section 158 Postal Manual) Do Not Return